



MINISTÉRIO DA CIÊNCIA, TECNOLOGIA, INOVAÇÕES E COMUNICAÇÕES
INSTITUTO NACIONAL DE PESQUISAS ESPACIAIS

sid.inpe.br/mtc-m21b/2016/05.12.04.17-TDI

SEA ICE STUDY AND ARCTIC POLAR AMPLIFICATION USING BESM MODEL

Fernanda Casagrande

Doctorate Thesis Course Graduate
in Earth System Science, guided by
Dr. Paulo Nobre, approved in may
25, 2016.

URL of the original document:

<http://urlib.net/8JMKD3MGP3W34P/3LLUKM5>

INPE
São José dos Campos
2017

PUBLISHED BY:

Instituto Nacional de Pesquisas Espaciais - INPE

Gabinete do Diretor (GB)

Serviço de Informação e Documentação (SID)

Caixa Postal 515 - CEP 12.245-970

São José dos Campos - SP - Brasil

Tel.:(012) 3208-6923/6921

Fax: (012) 3208-6919

E-mail: pubtc@inpe.br

**COMMISSION OF BOARD OF PUBLISHING AND PRESERVATION
OF INPE INTELLECTUAL PRODUCTION (DE/DIR-544):****Chairperson:**

Maria do Carmo de Andrade Nono - Conselho de Pós-Graduação (CPG)

Members:

Dr. Plínio Carlos Alvalá - Centro de Ciência do Sistema Terrestre (CST)

Dr. André de Castro Milone - Coordenação de Ciências Espaciais e Atmosféricas (CEA)

Dra. Carina de Barros Melo - Coordenação de Laboratórios Associados (CTE)

Dr. Evandro Marconi Rocco - Coordenação de Engenharia e Tecnologia Espacial (ETE)

Dr. Hermann Johann Heinrich Kux - Coordenação de Observação da Terra (OBT)

Dr. Marley Cavalcante de Lima Moscati - Centro de Previsão de Tempo e Estudos Climáticos (CPT)

Silvia Castro Marcelino - Serviço de Informação e Documentação (SID) **DIGITAL**

LIBRARY:

Dr. Gerald Jean Francis Banon

Clayton Martins Pereira - Serviço de Informação e Documentação (SID)

DOCUMENT REVIEW:

Simone Angélica Del Ducca Barbedo - Serviço de Informação e Documentação (SID)

Yolanda Ribeiro da Silva Souza - Serviço de Informação e Documentação (SID)

ELECTRONIC EDITING:

Marcelo de Castro Pazos - Serviço de Informação e Documentação (SID)

André Luis Dias Fernandes - Serviço de Informação e Documentação (SID)



MINISTÉRIO DA CIÊNCIA, TECNOLOGIA, INOVAÇÕES E COMUNICAÇÕES
INSTITUTO NACIONAL DE PESQUISAS ESPACIAIS

sid.inpe.br/mtc-m21b/2016/05.12.04.17-TDI

SEA ICE STUDY AND ARCTIC POLAR AMPLIFICATION USING BESM MODEL

Fernanda Casagrande

Doctorate Thesis Course Graduate
in Earth System Science, guided by
Dr. Paulo Nobre, approved in may
25, 2016.

URL of the original document:

<http://urlib.net/8JMKD3MGP3W34P/3LLUKM5>

INPE
São José dos Campos
2017

Cataloging in Publication Data

Casagrande, Fernanda.

C261s Sea ice study and Arctic polar amplification using BESM model / Fernanda Casagrande. – São José dos Campos : INPE, 2017.
xx + 69 p. ; (sid.inpe.br/mtc-m21b/2016/05.12.04.17-TDI)

Thesis (Doctorate in Earth System Science) – Instituto Nacional de Pesquisas Espaciais, São José dos Campos, 2016.

Guiding : Dr. Paulo Nobre.

Título em Português: Estudo do gelo marinho e da amplificação polar no Ártico com modelo BESM .

1. Sea ice. 2. Coupled climate models. 3. Global climate change.
4. Brazilian earth system model. 5. polar amplification. I.Title.

CDU 551.326.7:551.58(98)



Esta obra foi licenciada sob uma Licença [Creative Commons Atribuição-NãoComercial 3.0 Não Adaptada](https://creativecommons.org/licenses/by-nc/3.0/).

This work is licensed under a [Creative Commons Attribution-NonCommercial 3.0 Unported License](https://creativecommons.org/licenses/by-nc/3.0/).

Aluno (a): **Fernanda Casagrande**

Título: "ESTUDO DO GELO MARINHO E DA AMPLIFICAÇÃO POLAR NO ÁRTICO COM O MODELO BESM".


Aprovado (a) pela Banca Examinadora
em cumprimento ao requisito exigido para
obtenção do Título de **Doutor(a)** em
Ciência do Sistema Terrestre

Dr. Ronald Buss de Souza



Presidente / INPE / Santa Maria - RS

Dr. Paulo Nobre



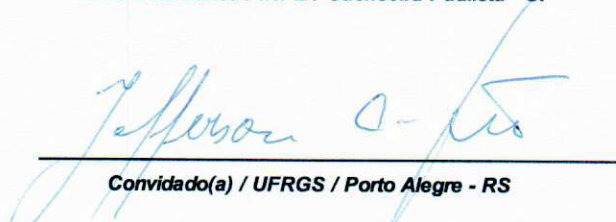
Orientador(a) / INPE / Cachoeira Paulista - SP

Dr. Vinicius Buscioli Capistrano



Membro da Banca / INPE / Cachoeira Paulista - SP

Dr. Jefferson Cardia Simões



Convidado(a) / UFRGS / Porto Alegre - RS

Dr. Ricardo de Camargo



Convidado(a) / IAG/USP / São Paulo - SP

Este trabalho foi aprovado por:

maioria simples

unanimidade

(In Portuguese)

*“Dedico aos grandes doutores da minha vida, meus pais Jaime Campagnolo
Casagrande e Zeni F. Nogueira Casagrande”*

ACKNOWLEDGEMENTS

(In Portuguese)

Mais um ciclo se encerra e ainda resta muito a fazer.....

Agradeço primeiramente a meus pais Zeni e Jaime Casagrande que sempre estiveram presentes mesmo quando a distância era grande e que seguramente são os que mais compartilham da minha alegria. Por ser exemplo de força, conduta e perseverança. Essa conquista é de vocês, pois eu não chegaria tão longe se não tivesse vocês me carregando no colo nos momentos que me faltaram pernas. A tia Evita (Eva Nogueira) pelo amor e incentivo dedicado à distância.

A meu irmão e colega de CCST Leandro Casagrande o qual pude compartilhar diversas experiências nessa jornada, pelo seu apoio, amizade e parceria. Ao meu irmão Henrique Casagrande (meu negrinho), pela sua amizade, parceria e companheirismo mesmo quando a distancia era grande.

Meus sinceros agradecimentos ao meu orientador Dr. Paulo Nobre por me receber como orientador no INPE, pelos ensinamentos científicos, incentivo e valorosas sugestões para melhorar a tese. Meu respeito e admiração pelo seu amor, dedicação e comprometimento com a ciência. Agradeço especialmente por ter sido paciente frente ao meu anseio em ver as regiões polares além das simulações numéricas.

Ao Dr. Ronald B. Souza, que me colocou nessa piscina gelada (literalmente) e a quem serei eternamente grata. Obrigada por acreditar no meu potencial e sempre se fazer presente mesmo longe. Patrão, a ti minha gratidão, respeito, admiração e amizade.

Aos meus queridos amigos e colegas do INPE: Alan, Etienne, Aline, Fernanda (Tocaia), Chiquita, Vagner, Guilherme, Carol, Wendell, Raquel, André, Sandro, Val. Valeu por tudo!

Aos meus queridos amigos da mansão Foster: Catarina, Marcelo (Frango), Cae, Elaine, Vivi e Ana Carol que fizeram meus dias em Cachoeira Paulista mais divertidos e tranquilos.

Aos meus colegas de laboratório GMAO pelo excelente convívio e valorosas discussões que enriqueceram o meu trabalho.

Aos professores da PG-CCST que participaram da minha formação científica e aos funcionários do INPE, em especial á Angela Arado.

Ao CNPq pela bolsa concedida.

Aos membros da Banca examinadora pela pronta disponibilidade em analisar este trabalho e valorosas contribuições para melhorar o documento final.

Enfim, a todos que de algum modo fizeram parte desse caminho.

ABSTRACT

Important international reports and a significant number of scientific publications have reported on the abrupt decline of the Arctic sea ice, polar amplification and its impact on the Global Climate System. In this thesis, we evaluate the ability of the Brazilian Earth System Model (BESM) to represent the Arctic sea ice and sensitivity to the atmospheric Carbon dioxide (CO₂) forcing. We used decadal simulations (1980-2012), future scenarios with Representative Concentration Pathway RCP 4.5 and RCP 8.5 (2006-2100) and quadrupling of the atmospheric CO₂ concentration (2006-2300). We validated our results with satellite observations and compared them to Coupled Model Intercomparison Project, Phase 5 (CMIP5) for the same numerical experiment designs. BESM results for the Arctic sea ice seasonal cycle are consistent with CMIP5 models and observations. However, almost all models tend to overestimate sea ice extent (SIE) in March compared to observations. The correct evaluation of minimum record of sea ice, in terms of time, spatial and area remains a limitation in Coupled Global Climate Models (CGCM). Looking to spatial patterns, we found a systematic model error in September sea ice cover between the Beaufort Sea and East Siberia for most models. Future scenarios show a decrease in SIE as response to an increase in radiative forcing due to the increase of greenhouse gases concentration for all models. From the year 2045 onwards, all models show a dramatic shrinking in sea ice and consequent expansion of ice-free conditions at the end of the melting season. The projected future sea ice loss is explained by the combined effects of both: the amplified warming in northern hemisphere high latitudes and climate feedbacks. The quadrupling of CO₂ concentration numerical experiment shows the amplified warming at high latitudes as response to CO₂ forcing with strongest warming in winter (DJF) and Autumn (SON). The Polar warming is linked with changes in SIE and Sea Ice Thickness (SIT). The albedo sea ice feedback reinforces the polar warming with marked contributions from April to August.

Keywords: Sea ice, Coupled Climate Models, Global climate change, Brazilian Earth System Model, Polar Amplification

ESTUDO DO GELO MARINHO E DA AMPLIFICAÇÃO POLAR NO ÁRTICO COM O MODELO BESM

RESUMO

Importantes relatórios internacionais e um expressivo número de publicações científicas têm reportado sobre o abrupto declínio do gelo marinho Ártico, amplificação polar e seus impactos no sistema climático global. Nessa tese nós analisamos a habilidade do Modelo Brasileiro do Sistema Terrestre (BESM) em representar o gelo marinho Ártico e sensibilidade ao forçamento radiativo de Dióxido de Carbono (CO₂), usando simulações decenais (1980-2012), cenários futuros usando Caminhos Representativos de Concentração RCP 4.5 e RCP 8.5 (2006-2100) e quadruplicando a concentração de CO₂ (2006-2300). Nós validamos nossos resultados utilizando as observações de satélites e comparando com o Projeto de Intercomparação de Modelos Acoplados, Fase 5 (CMIP5) para o mesmo experimento numérico. Os resultados do BESM para o ciclo sazonal são consistentes com os modelos do CMIP5 e observações. No entanto, a maioria dos modelos tende a superestimar a extensão do gelo marinho (SIE) em Março comparado às observações. A correta análise do mínimo registrado de gelo marinho em termos de padrão temporal, espacial e área continua sendo uma limitação nos Modelos Climáticos Globais Acoplados (CGCM). Avaliando o padrão espacial, nós encontramos um erro sistemático na cobertura de gelo marinho em Setembro entre o mar de Beaufort e Leste da Sibéria para a maioria dos modelos. Os cenários futuros mostram uma diminuição do gelo marinho como resposta ao aumento do forçamento radiativo devido ao aumento na concentração dos gases do efeito estufa para todos os modelos. A partir do ano de 2045, todos os modelos mostram um encolhimento drástico no gelo marinho e consequente aumento das condições de oceano livre de gelo no final da estação de derretimento. As projeções futuras de retração de gelo marinho são explicadas por efeitos combinados: Aquecimento amplificado em altas latitudes norte e os processos de retroalimentação climáticos. O experimento numérico quadruplicando a concentração de CO₂ mostra amplificado aquecimento em altas latitudes como resposta ao forçamento radiativo do CO₂, com aquecimento mais intenso no verão (DJF) e outono (SON). O aquecimento polar está relacionado com mudanças na extensão de gelo marinho e espessura do gelo marinho (SIT). O processo de retroalimentação albedo gelo marinho reforça o aquecimento polar com acentuadas contribuições de Abril até Agosto.

Palavras chave: Gelo marinho, Modelos Climáticos Acoplados, Mudanças Climáticas Globais, Modelo Brasileiro do Sistema Terrestre, Amplificação Polar.

LIST OF FIGURES

Figure 2.1 Coupled ocean-atmosphere-sea ice interactions scheme, climate feedbacks and local effects in Arctic region.	7
Figure 2.2. Arctic Ocean Circulation Scheme. Blue arrows show cold, relatively fresh water and red arrows show warm, salty water that has entered the system from the North Atlantic.	10
Figure 2.3. (Left) Global, northern and southern hemisphere air surface temperatures anomalies ($^{\circ}\text{C}$), based on HadCRU ¹ data for the period from 1960 to 2015. (Right) Global SAT anomalies in 2015 using observational data set, relative to the 1981-2010 base period.	12
Figure 2.4. The ESGF node at INPE/CPTEC.	17
Figure 2.5. Schematic representation of the three-layer sea ice model. The four prognostic variables are: snow layer thickness (h_s), the ice layer thickness (h_i), the upper ice layer Temperatures (T1) and the lower ice layer Temperatures (T2). The sea ice bottom temperature is fixed at T_f (freezing temperature of seawater). T_s is the temperature of ice or snow and is determined from the surface energy balance. K_i is the thermal conductivity of sea ice. Source: Winton (2000)	21
Figure 3.1. Climatology of SIE (1980 to 2010) in the northern hemisphere simulated by BESM-OA V2.3, CMIP5 models and observations.	25
Figure 3.2. Difference between BESM-OA2.3 simulations and observations for LongwaveUp (red line) and LongwaveDown (black line) from 1980 to 2010. The observation data are from International Satellite Cloud Climatology Project (ISCCP) Global Radiative Flux Data Products (ZHANG 2004). Available in: http://isccp.giss.nasa.gov/projects/flux.html	25
Figure 3.3. Taylor diagram of September, March and climatological annual cycle of SIE for the period 1980-2012. The x-axis and y-axis are the standard deviation normalized. The correlation coefficient between observations and each model is given by the azimuthal position. The centered RMS difference between simulated and observed is proportional to their distance one from another	27
Figure 3.4. Arctic study area and September SIC Climatology (1980-2010) from satellite observations (shaded colors). Dark gray and orange lines refer to the 2007 and 2012 minimum events respectively.	29
Figure 3.5. Difference between model simulations and observations for September SIC climatologic average from 1980 to 2010. BESM-OA V2.31, GFDL-CM2.1 (upper), CanCM4 and MPI-ESM-LR (middle), HadCM3 and NCAR-CCSM4 (bottom). Positive (negative) value depicted in red (blue) represent areas where the model overestimates (underestimates) sea ice concentration values.	30

Figure 3.6. Difference between model simulations and observations for March SIC climatologic average from 1980 to 2010. BESM-OA V2.31, GFDL-CM2.1 (upper), CanCM4 and MPI-ESM-LR (middle), HadCM3 and NCAR-CCSM4 (bottom). Positive (negative) value depicted in red (blue) represent areas where the model overestimates (underestimates) sea ice concentration values.....	31
Figure 3.7. Arctic sea ice extent time series of September from 1980 to 2014 for CMIP5 models and observational data.	33
Figure 3.8. Spatial distribution of SIE average (left) and lowest values of September SIE found between 1980 to 2010, (right), for all CMIP5 models evaluated in this work.....	35
Figure 3.9. Time series of modeled Arctic SIE in September and March from 2006 to 2100, using Representative Concentration Pathways RCP4.5 (solid lines) and RCP8.5 (dash lines). Black lines are the satellite observations and gray lines refer to the control run of the BESM-OA V2.3.....	37
Figure 3.10. Surface Anomalies Temperature (SAT) and Total Cloud Cover (right) from January 2006 to December 2100 for BESM-OA V2.3 and BESM-OA V2.5 For SAT, the red lines represent the average for latitudes between 75°N to 90°N. Green and blue lines are for latitudes between 45°N to 75°N and 25°N to 45°N, respectively. Latitudes between 0°N to 90°N are represented by the black lines.	39
Figure 4.1. Zonal mean surface temperature (K) for the last 30 years of quadrupling atmospheric CO ₂ numerical experiment compared to the last 30 years of the piControl run for the following models: BESM-OA V2.5 (top left), NCAR-CCSM4 (top right), GFDL-ESM-LR (bottom left) and MPI-ESM-LR (bottom right) in winter (DJF) represented by blue lines, spring (MAM) represented by black lines, summer (JJA) represented by red lines and autumn (SON) represented by green lines.	42
Figure 4.2. Spatial differences of surface temperature between 4 X CO ₂ and piControl numerical experiments, considering only the last 30 years of each simulation in BESM-OA V2.5 annual (top) and for seasonal cycle (below) in the BESM-OA V2.5, NCAR-CCSM4, GFDL-ESM-LR and MPI-ESM-LR for winter (DJF), spring (MAM), summer (JJA) and autumn (SON).	43
Figure 4.3. Seasonal cycle at northern high latitudes (70°N-90°N) of surface air temperature (°C), Albedo, SIE and SIT for the last 30 years of the quadrupling atmospheric CO ₂ numerical experiment compared to the last 30 years of the piControl run, using BESM-OA V2.5.....	47
Figure 4.4. Seasonal cycle at northern high latitudes (70°N-90°N) of heat fluxes (sum of sensible and latent fluxes) and Freshwater Fluxes (Precipitation – Evaporation) for the last 30 years of quadrupling atmospheric CO ₂ numerical experiment compared to the last 30 years of the piControl run, using BESM-OA V2.5.	48
Figure 4.5. Climate feedbacks in BESM V2.5 for northern high latitudes (70°N-90°N). Black line represent albedo feedback while red and green line represent water vapour feedback for LW and SW respectively.	50

LIST OF TABLES

Table 3.1. CMIP5 main characteristics.....	19
--	----

LIST OF ABBREVIATIONS

AGCM	Atmospheric General Circulation Model
AMOC	Atlantic Meridional Overtuning Circulation
BESM	Brazilian Earth System Model
BESM-OA	Brazilian Earth System Model coupled Ocean- Atmosphere
CGCM	Coupled Global Climate Models
CMIP	Coupled Model Intercomparison Project
CMIP3	Coupled Model Intercomparison Project, Phase 3
CMIP5	Coupled Model Intercomparison Project, Phase 5
CO ₂	Carbon dioxide
CPTEC	Center for Weather Forecasting and Climate Research
E	Evaporation
ESGF	Earth System Grid Federation
ESM	Earth System Model
GHG	Greenhouse Gas
IGBP	International Geosphere Biosphere Program
INPE	National Institute for Space Research
IPCC	Intergovernmental Panel on Climate Change
ISCCP	International Satellite Cloud Climatology Project
MOM4p1	Modular Ocean Model version 4p1
NASA	National Aeronautics and Space Administration
NCEP-NCAR	National Centers for Environmental Prediction
NOAA	National Oceanic and Atmospheric Administration
NSIDC	National Snow and Ice Data Center
OGCM	Oceanic General Circulation Model
P	Precipitation

PCMDI Program for Climate Model Diagnostics and Intercomparison

R Runoff

RCP Representative Concentration Pathway

SAT Surface Air Temperature

SIC Sea Ice Concentration

SIE Sea Ice Extent

SIS Sea Ice Simulator

SIT Sea Ice Thickness

SSM/I Special Sensor Microwave Imager

SST Sea Surface Temperature

WGCM Working Group on Coupled Models

WRCP World Climate Research Program

CONTENTS

	<u>Page</u>
1 INTRODUCTION.....	1
2 THEORICAL BACKGROUND.....	5
2.1 Sea ice characteristics	5
2.2 Polar Amplification and climate feedbacks mechanisms	11
2.3 Coupled Model Intercomparison Project	15
2.4 Data source.....	17
2.4.1 BESM-OA Model	19
3 ARCTIC SEA ICE: DECADEAL SIMULATIONS AND FUTURE SCENARIOS USING BESM-OA.....	23
3.1 Seasonal Cycle	23
3.2 Spatial Pattern	27
3.3 Minimum of Sea Ice Extent	32
3.4 Future Projection of Arctic Sea Ice.....	35
3.5 Surface Anomalies Temperatures	38
4 POLAR AMPLIFICATION OF CLIMATE CHANGE	41
4.1 Polar amplification.....	41
4.2 Coupled ocean-atmosphere-sea ice processes	45
5 FINAL REMARKS.....	51
REFERENCES.....	55
ANEXO A	69

1 INTRODUCTION

Sea ice formed by freezing seawater in Polar Oceans is an important component of Earth's Climate System because it regulates the energy exchange between the ocean and atmosphere, affects the heat redistribution between high and low latitudes and by the effect in climate sensitivity through the climate feedback mechanisms. The nature of sea ice is highly interdisciplinary since its changes may affect weather and climate, ecosystems, life and human activities in diverse ways.

An expressive number of reports and scientific publications have warned about the effects of ongoing and projected climate change in the Arctic sea ice. Over the last few decades, the Arctic sea ice has diminished faster than forecasted and is unprecedented in the past 1.5 millennia (STROEVE et al., 2012; KINNARD et al., 2011; STROEVE et al., 2007). The Arctic sea ice cover reached the smallest extent ever recorded in the satellite era (since 1979) during the summers of 2007 and 2012, reaching a minimum extent of 4.2×10^6 km² and 3.4×10^6 km², respectively (STROEVE et al., 2012; KINNARD et al., 2011). Sea ice age and thickness also have decreased rapidly resulting in a sea ice more sensitive to dynamic and thermodynamic forcing (STROEVE et al., 2012; PEROVICH, 2011). Recent studies suggest that severe winters in northern continents, hot summer extremes in mid-latitudes and flooding in Eurasia are linked to the Arctic sea ice loss (TANG et al., 2013; SCREEN, 2013; COHEN et al., 2012; ACIA, 2005).

There is an agreement among scientists about the link between Arctic sea ice loss and global warming as a response to atmospheric CO₂ forcing (DOESCHER et al., 2014; HOLLAND; BITZ, 2003). The Arctic sea ice retreat accelerates the warming through feedback mechanisms. According to Holland and Bitz (2003) the range of simulated polar warming is from 1.5 to 4.5 times the global mean warming. This is known as Arctic Amplification and it is a response to increase in Greenhouse Gas Concentration (GHC).

In addition to the role of the sea ice in the climate system, the dynamics and geographical distribution of sea ice cover is also essential for human activities such as navigation, oil exploration and fishery (MEIER et al., 2014; ACIA, 2005). According

to Meier et al (2014) and Cochran et al (2013) changes in Arctic threaten the infrastructure, health and safety of the Arctic indigenous people as well as present a significant risk to local marine biodiversity.

The physical processes involving the coupled ocean-atmosphere-sea ice system at high latitudes and polar amplification are currently considered a hot topic in climate change research and still lack conclusive answers. In fact, the scientific community still doesn't know exactly how Arctic sea ice loss will affect the global climate system. The main sources of uncertainties in global climate models are linked to feedback mechanisms and associated with changes in sea ice, radiation, clouds and water vapor (EYRING et al., 2015; DOESCHER et al., 2014; PITHAN; MAURTSEN, 2014).

However, even with their inherent uncertainties and limitations, Global Climate Models are powerful tools for investigating the complex interactions at high latitudes and to provide future scenarios to guide decision makers, governments and communities. Therefore, advance in climate modeling is needed to provide the most reliable simulation possible, to prepare the society to the effects of enhanced Arctic warming as well as to understand the impacts of Arctic change in the global climate system.

In a recent issue of Nature Journal, Whiteman et al (2013) suggested that sea ice changes will affect all nations, not just those in the world's far north, so all countries should be concerned about changes that are happening in the Arctic region.

In Brazil, a collective effort between several researchers and institutions, lead by the National Institute for Space Research (INPE), originated the Brazilian Earth System Model (BESM). The BESM project aims to build a multidisciplinary research framework with the intent to understand the causes of global climate change and their impacts on society (NOBRE et al., 2013). The BESM model project also intent to contribute to the Program for Climate Model Diagnostics and Intercomparison (PCMDI) with short-term and long-term simulations as well as to provide futures scenarios of climate change (NOBRE et al., 2013).

Motivated by the importance of Arctic sea ice in the global climate system, this study makes use of BESM-OA (Brazilian Earth System Model coupled Ocean-

Atmosphere) simulations to investigate the Arctic sea ice changes and polar amplification of climate change.

The goal of this work is to investigate changes in Arctic sea ice and the polar amplification using the BESM-OA model as well as intercomparing BESM results with other CMIP5 models.

The hypothesis of this work is: Sea ice decrease due to efficiency of feedback mechanism involving coupled ocean-atmosphere-sea ice. The scientific questions addressed are: (1) Are the Global Climate Models able to reproduce present-day sea ice changes? (2) What are the responses of sea ice and the polar amplification to atmospheric CO₂ forcing in the global climate models including BESM-OA?

To respond those questions, we used two versions of the BESM-OA (with different cloud microphysics scheme and surface layer scheme), CMIP5 models outputs and satellite data. We used three numerical experiment categories following Taylor (2012) Protocol: (1) Decadal simulations (1960-2035); (2) Future Scenarios with RCP 4.5 and RCP 8.5 (2006-2100); (3) Abrupt 4 x CO₂ (2006-2300).

The thesis structure presented below follows: Section 2 provides a theoretical background that includes the main concepts and published papers of the major issues addressed in this thesis. Section 3 describes the data source and methodology used to generate the results presented in the follow sections (4 and 5). Section 4 presents the results on Arctic sea ice: Decadal simulations and future scenarios using BESM-OA and CMIP5 models. Section 5 presents the study of Polar Amplification using abrupt 4 x CO₂ numerical experiment. Finally, the final remarks are given in Section 6, that concluded and summarizes the work, including proposes for futures work to extend the knowledge on sea ice modeling and polar amplification of climate change.

At the end of this thesis document (Appendix) is attached the paper published in International Journal as cited: CASAGRANDE, F.; et al. Arctic Sea Ice: Decadal Simulations and Future Scenarios Using BESM-OA. Atmospheric and Climate Sciences, v.6, p.351-366, 2016. <http://dx.doi.org/10.4236/acs.2016.62029>.

2 THEORETICAL BACKGROUND

2.1 Sea ice characteristics

Sea ice formed by freezing of seawater at high latitudes is an important component of the Earth's System. Sea ice covers approximately 5–10 % of world's oceans or about 7–15% of the Earth's surface (SHOKR; SINHA, 2015; WADHAMS et al., 2000).

The formation of sea ice occurs when the temperature of the seawater falls its freezing point, approximately -1.8°C (DAY, 2007; WADHAMS et al., 2000). According Sing et al (2011) there are three physical scales for sea ice: (1) Microscale: that includes crystal structures and impurities and may extending from sub-millimeters size to 0.1 m. (2) Local scale (0.1-10m): it refers to a forms of sea ice (ice, frazil ice and superimposed ice) and consider sea ice as a polycrystalline continuum and (3) Ice floe scale (10 m-10 Km) that includes ice floes and types such as pressure ridges. When the scale exceeds the floe size the sea ice is called drift ice (fields of ice floes). The drift ice speed varies from 1 to 100cm/s. In the Arctic region the Transpolar Drift Stream takes ice across the Eurasian side through the Fram Strait into Greenland Sea, while in the America side sea ice rotates clockwise in the Beaufort Sea Gyre (SING et al., 2011; DAY, 2007; WADHAMS et al., 2000).

When sea ice forms, the salt is excluding from the ice crystal in a procedure called as brine rejection and the surrounding sea water becomes more saline and dense. The salt is excluded because has different crystalline structure. This thin ice floating on the dense water creates a barrier between the ocean and atmosphere that prevents the energy changes across the interface. This is especially important because ocean heat capacity is much greater than that of the atmosphere resulting in a very efficient isolate of the warm ocean from the cold atmosphere.

The physical processes acting on sea ice are divided commonly into two categories that work simultaneously: (1) Thermodynamic processes, controlled by heat exchange or radiation between the ocean and the atmosphere (*e.g* freezing and melting) and (2) Dynamic processes, determined by the ocean and atmosphere patterns (winds and ocean currents), which move and deform sea ice (*e.g* sea ice drift) (HUNKE et al., 2010; FICHEFET; MAQUEDA 1997). The interplay between ice dynamics and thermodynamics determines the Arctic sea ice changes (*e.g.* sea ice advection, sea ice

growth, lateral melting and ridging) and take place at a wide range of spatial and temporal scales in the coupled atmosphere-ocean-sea ice system (BOURASSA et al., 2013; BISHOP et al., 2011; ZHANG et al., 2000).

The presence of sea ice increases surface albedo, insulates the atmosphere from the warmer ocean, reducing heat exchange and thus the vertical mixing in the ocean.

Surface fluxes at high latitudes are important processes in the atmosphere, ocean and cryosphere and have variability associated with a broad range of processes, as shown in **Figure 2.1**. The main difference of surface fluxes between high and mid-latitudes are related to the presence of sea ice, frequently high wind speeds, low temperatures and high variability on local scales (*e.g.* ice margins and sea leads). The air-sea fluxes include fluxes of momentum, energy and freshwater (BOURASSA et al., 2013). The momentum flux is a consequence of the frictional drag exerted by the sea surface and plays an important role in feedback processes, affecting for example, the size of leads and polynyas. The net energy flux is the sum of the sensible and latent heat and the net radiative fluxes (SW radiation from the sun and LW radiation emitted from the surface and by the atmosphere). Freshwater fluxes into the ocean are due to precipitation, runoff and evaporation (P+R-E) (NORTH et al., 2014; BOURASSA et al., 2013).

Figure 2.1 shows a schematic diagram of ocean-atmosphere-sea ice interactions, internal feedback and local effects. The figure reflects the high complex nature of coupled interactions between polar atmosphere, ocean and sea ice. Those interactions involve changes in energy, momentum and freshwater fluxes and implies the needed for integrative and interdisciplinary studies (including research across and among physical, biological and social sciences). Along the chapters we will explore some of those coupled processes and suggest how such processes may impact the Arctic.

According to Carmack et al (2015), advances in our understanding of coupled sea ice-ocean-atmosphere processes and internal feedbacks are required to provide realistic projections of Arctic sea ice in the coming years.

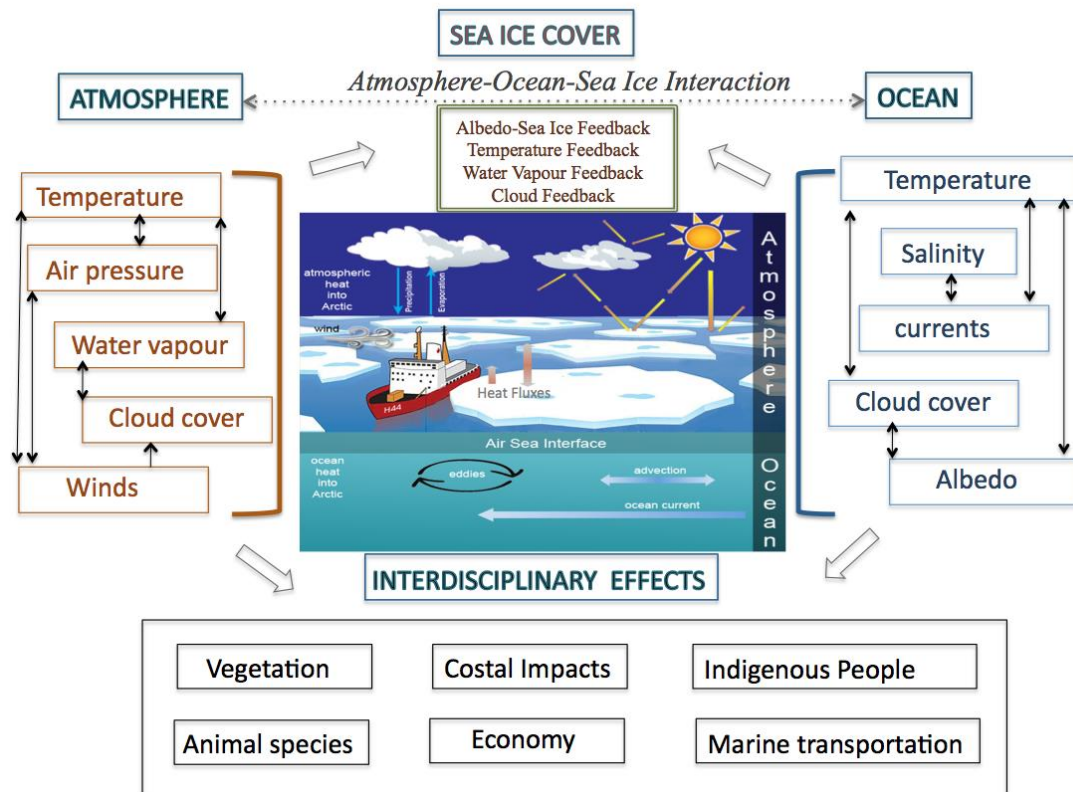


Figure 2.1 Coupled ocean-atmosphere-sea ice interactions scheme, climate feedbacks and local effects in Arctic region.

The main difference between Arctic and Antarctic sea ice is related to geography pattern. In contrast with Antarctica, the Arctic sea ice is a semi-enclosed ocean surrounded by land. Thus, the sea ice formed in the Arctic tends to be thicker (2–5 meters) and may persist for several summers (2–5 years). In Antarctica, the open southern ocean permits a faster drift and almost all sea ice formed melts during summertime, making both the sea ice thickness (1–2 meters) and sea ice age (1–2 years) lower (NSCID, 2016; DOESCHER et al., 2014; PEROVICH, 2011). In relation to the sea ice extent (SIE), both Arctic and Antarctic sea ice show a seasonal cycle quite well defined. The Arctic (Antarctic) sea ice maximum (minimum) occurs in March (September), varying from $16 \times 10^6 \text{ km}^2$ ($4 \times 10^6 \text{ km}^2$) to $4 \times 10^6 \text{ km}^2$ ($21 \times 10^6 \text{ km}^2$) (DOESCHER et al., 2014; BISHOP et al., 2011).

Over the last few decades (since 1980), both observational data and Global Climate Models (CGCM) have shown quite different trends between the Arctic sea ice and the Antarctica sea ice. The Arctic sea ice has decrease faster than expected in both extent

and age, reaching a minimum record extent of $3.4 \times 10^6 \text{ km}^2$ in September of 2012 (STROEVE et al., 2012; KINNARD et al., 2011; PEROVICH, 2011). Conversely, the Antarctica sea ice has been growing reaching a maximum record extent of $20.1 \times 10^6 \text{ km}^2$ in September of 2014 (NSCID, 2016; ZANG, 2007; THOMPSON, 2002).

The reasons for changes in Arctic and Antarctic sea ice are quite different. The retreat of the Arctic sea ice is associated with air temperature rises and polar amplification, while the increase in Antarctic sea ice has been attributed a combination of changes in cyclonic winds around Antarctica and changes in ocean circulation (STROEVE et al., 2012; SERREZE; BARRY 2011; ZANG 2007; THOMPSON 2002).

Melting sea ice affects the ocean circulation through changes in salinity. The brine rejection increases ocean density and consequently may to include changes in the in thermohaline circulation (BISHOP et al., 2011; HUNKE et al., 1997). The **Figure 2.2** shows the complex Arctic Ocean circulation scheme.

The Arctic Ocean is surrounded by the land masses of Eurasia, North America, America, Greenland and several islands. It is connected to the Pacific Ocean by the Bering Strait and to the Atlantic Ocean through the Greenland Sea and Labrador Sea (**Figure 2.2**).

The Bering Strait is narrow (~85 km wide) and shallow (~50 m deep). The fluxes through Bering Strait play an important role regionally and globally. It affects the salt and freshwater cycle of the world oceans, Atlantic Meridional Overtuning Circulation (AMOC), the strength of the deep western boundary currents and the separation of the Gulf Stream from the America coast (WOODGATE; AAGAARD 2005; WADLEY; BIGG, 2002; HUANG; SCHIMITT, 1993).

The Greenland Sea and Labrador Sea are one of the few major areas where convective renewal of intermediate and deep waters contributes significantly to the production and export of North Atlantic Deep Water, thus helping to drive the global thermohaline circulation. The formation and spreading of 18-degree water at shallow-to-intermediate depths off the US eastern seaboard is a major element in the circulation and hydrographic character of the West Atlantic (DICKSON et al., 1996).

The Beaufort Gyre is a clockwise circulation in the Beaufort Sea, north of Alaska. This Circulation results from a high-pressure system that spawns winds over the

region and plays an important role in regulating the Arctic climate variability. According Proshutinsky et al (2002), the Beaufort Gyre accumulates a significant amount of freshwater during one climate regime (anticyclonic) and releases this water to the North Atlantic during another climate regime (cyclonic). This explains the origin of the salinity anomaly periodically found in the North Atlantic as well as its role in the decadal variability in the Arctic.

The North Atlantic Current is a powerful warm ocean that flows north along the east side of the Grand Banks from 40° to 51°N, where it turns sharply to the east and begins its journey across the ocean. The North Atlantic Current originates in the Gulf Stream when the latter curves north around the southeast Newfoundland Rise, a major submarine ridge that stretches southeast from the Grand Banks. A quite well defined front delineates the path of the currents as long as it flows north as a western boundary current. After the current turns east in the north, it broadens into a widening band of eastward drift without a sharp or permanent front in the sense of the eastward flowing Gulf Stream after it separates from Cape Hatteras. The relatively warm water of the North Atlantic current are responsible for moderating Europe subcontinent climate (ROSSBY, 1996; KRAUSS, 1986)

Some publications have shown significant relationships between changes in Arctic sea ice and ocean circulation (JAHN; HOLLAND, 2012, MAHAJAN et al., 2011; LOHMANN; GERDES 1997). According to Jahn and Holland (2012) changes in Arctic sea ice are linked with decreases in AMOC strength and reduction in North Atlantic deep convection due to Arctic Freshwater Export. It is happen because the AMOC is driven by density gradients related to deep-water formation in the high-latitude North Atlantic, a weakening of the AMOC could be caused by a regional reduction in surface ocean density.

According Curry and Mauritzen (2005), the increase in freshwater storage in the Northern Atlantic between 1961 and 1995 (approximately 19,000 km³), and the rapid AMOC weakening in 1970 was precedent by a large-scale freshening. This event was described by Dickson et al (1988) as “one of the most persistent and extreme variations in global ocean climate yet observed in this century” and the source of which has been associated to the Arctic sea ice export. The freshwater volume anomaly has been estimated as 2,000 km³ along the Labrador coast (BELKIN et al.,

1998; DICKSON et al., 1988)

Holland et al (2006) using CMIP numerical models analyzed the Arctic freshwater (sea ice transport and storage, ocean transport and storage and net surface fluxes). They found an increase in the flux of water passing through the hydrological elements. Increased freshwater inputs to the ocean from net precipitation, river runoff and sea ice melt result.

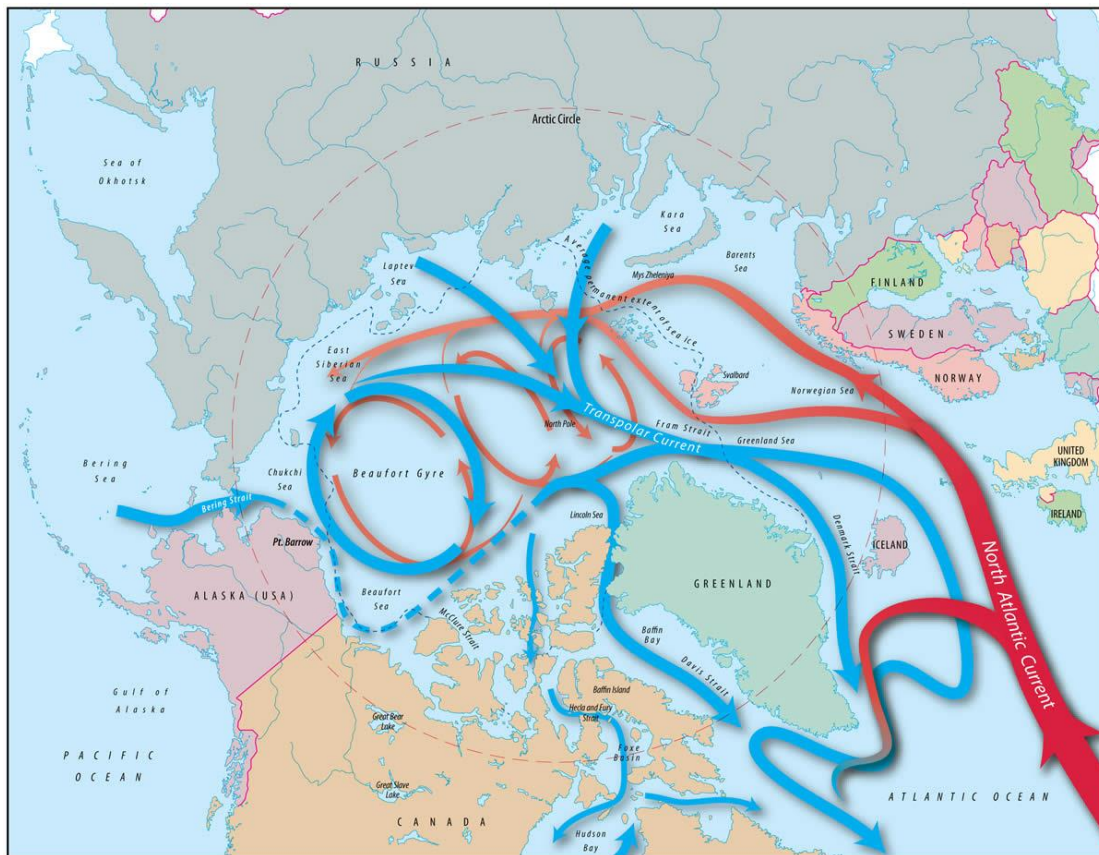


Figure 2.2. Arctic Ocean Circulation Scheme. Blue arrows show cold, relatively fresh water and red arrows show warm, salty water that has entered the system from the North Atlantic.

Source: Woods Hole Oceanographic website

Available in: <http://www.whoi.edu/>

2.2 Polar Amplification and climate feedbacks mechanisms

In 1897, the Swedish scientist Svante Arrhenius suggested that changes in the concentration of carbon dioxide in the atmosphere could modify the surface temperature and this change would be stronger at high latitudes. This seems to be the first formal consideration related to the Polar Amplification concept. In other words, rises in Surface Air Temperature (SAT) as response to increase in atmospheric Greenhouse Gas (GHG) concentration tend to be larger at northern high latitudes than at lower latitude (SERREZE; BARRY, 2011; SERREZE; FRANCIS, 2006; HOLLAND; BITZ, 2003).

Comparing the Polar Regions warming, the southern high latitudes (Peninsula and west Antarctica) increase in SAT has been modest in relation to the Arctic warming (STEIG et al., 2009; MORRIS; VAUGHAN, 2003).

There are many evidences indicating the increase in global SAT as a response to atmospheric GHG forcing (**Figure 2.3**, IPCC AR5 and ACIA 2005). In the Arctic, the SAT is increasing almost twice as fast as the global average over recent decades (NOTZ; MAROTZKE, 2012; STROEVE et al., 2012; SERREZE; BARRY, 2011; HOLLAND; BITZ, 2003).

Bekryaev et al (2010), using an extensive observational dataset (1875-2008), found an exceptional strong Arctic warming over the last decade, reaching to $1.35^{\circ}\text{C decade}^{-1}$. The trend is almost two times stronger than the Northern Hemisphere trend ($0.79^{\circ}\text{C century}^{-1}$), with an accelerated warming rate in the most recent decade.

Figure 2.3 based on HadCRUT4 data shows global, northern and southern hemisphere air surface anomaly temperatures with highest anomalies occurring after 1980 and much more intense at high northern latitudes. The global average (northern hemisphere average) air temperature on Earth has increased by about 0.95°C (1.5°C) in 2015 year (**Figure 2.3**).

Recent release from National Aeronautics and Space Administration (NASA) and National Oceanic and Atmospheric Administration (NOAA) scientists show globally

SAT average from January to December 2015 were 0.87 °C above the climatological value (defined as the 1951-1980 period). According the researchers, global SAT during 2015 were the warmest on record. For the Arctic, the annual average of SAT anomaly, during 2015, was also the highest in the observational record with extensive regions exceeding +3°C relative to the 1981-2010 period (**Figure 2.3**). Conversely, the North Atlantic and south of the Greenland Ocean shows a conspicuous region of cooling.

Recent studies suggested that this persistent cooling may be due to a weakening of the AMOC over the twentieth century. Simulations using Global Climate Models indicate the largest cooling in this region as a response to AMOC weakens during the 21st century (RAHMSTORF et al., 2015; DRIJFHOUT et al., 2012; CHENG et al., 2013). According to Rahmstorf et al (2015), the AMOC is driven by gradients related to deep-water formation in the high-latitudes of the North Atlantic, thus a weakening of the AMOC could be caused by a regional decrease in sea surface density.

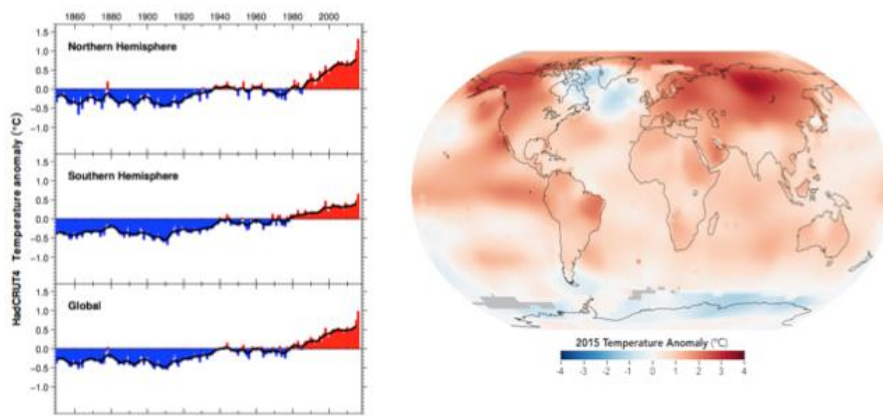


Figure 2.3. (Left) Global, northern and southern hemisphere air surface temperatures anomalies (°C), based on HadCRU¹ data for the period from 1960 to 2015. (Right) Global SAT anomalies in 2015 using observational data set, relative to the 1981-2010 base period.

Source: NASA² (2016)

¹The HadCRU is a data set of monthly instrumental temperature record formed by combining the sea surface temperature and land air temperature compiled by Hadley Centre (UK Met Office) and Climatic Research Unit (CRU). These data are available for download in the following CRU website <https://crudata.uea.ac.uk/cru/data/temperature> and a complete detail about dataset are found in Morice et al., (2012) and Jones et al., (2012).

²Nasa data. Available in: <http://earthobservatory.nasa.gov/IOTD/view.php?id=87359>

This observed Arctic warming as response to GHG forcing (e.g. **Figure 2.3**) is a near universal feature of current CGCM simulations (WINTON 2006, HALL 2004), for both present-day and future scenarios. Holland and Bitz (2003), using 15 state-of-the-art CMIP2 models found that simulated Arctic warming range is from 1.5 to 4.5 times the global mean warming. Winton (2006), using 12 state-of-the-art CMIP3 models found a mean annual Arctic warming rate of 1.9 times greater than the global mean warming in CO₂ doubling forcing. The most recent CMIP5 simulations are in agreement with those results, showing an enhanced Arctic warming linked with changes in sea ice, atmospheric and oceanic heat and moisture transport (PITHAN; MAURITSEN, 2014; BINTANJA; LINDEN, 2013).

Screen and Simmonds (2010) using mean fields from ERA-Interim and reanalysis for the period from 1989 to 2008, found that the maximum Arctic warming happens at the surface and that the warming decrease with height during most of year. The author showed that the Arctic warming, above 700 hPa is confined to winter and is still weaker than surface warming. This vertical structure suggests that changes at the surface, such as decreases in sea ice and snow cover, are the primary causes of recent Arctic amplification.

The enhanced Arctic warming has been attributed to climate feedbacks (PITHAN; MAURITSEN, 2014; SERREZE; BARRY, 2011; HOLLAND; BITZ, 2003; CURRY et al., 1995). Climate feedbacks refer to the amplification or dampening of a process by changes resulting from the initial processes itself. A positive (negative) feedback intensifies (reduces) the initial process in a non-linear response over a wide spectrum of spatial and temporal scales making the quantification further complicated. These Feedback mechanisms depend on integrated coupled processes between ocean-atmosphere-cryosphere and are identified as source of uncertainty around the simulated future Arctic climate (PITHAN; MAURITSEN, 2014; SERREZE; BARRY, 2011; HOLLAND; BITZ 2003).

The mainly intertwined feedbacks involved in the polar amplification process are: albedo-sea ice feedback (CURRY et al., 1995; Hall 2004), Temperature feedback (PITHAN; MAURITSEN, 2014), water vapor and cloud Feedback (LANGEN et al.,

2012; GRAVERSEN; WANG, 2009; VAVRUS, 2004) and lapse rate feedback (PITHAN; MAURITSEN, 2014).

The albedo-sea ice feedback is often cited as the major contributor of polar amplification. As temperature rises, sea ice is reduced, decreasing the surface albedo and increasing the amount of sunlight absorbed by the upper ocean. This increase in absorbed solar radiation contributes with continued and accelerated warming - positive albedo-sea ice feedback. In the opposite way, a decrease in temperature induces to increase in sea ice and surface albedo, thus reinforcing the cooling (SCREEN; SIMMONDS, 2010; SERREZE; FRANCIS, 2006; CURRY et al., 1995). The high albedo of sea ice (>0.6), in contrast with low albedo of open waters (~ 0.07) is responsible for a reflection of most solar radiation, thus regulating the amount of solar energy absorbed by the upper Arctic ocean (DOESCHER et al., 2014; FRANCIS et al., 2009). The melting of sea ices affect the ocean density by the decrease in salinity and changes in salinity may affect the ocean density more than changes in temperature in high latitudes (AAGARD; CARMACK, 1989).

However Graversen and Wang (2009) found that albedo-sea ice feedback is a contributing, but not a dominating mechanism underlying the Arctic warming. The authors, using simulations with locked surface albedo suggested that an increase in water vapor and cloud cover lead to a greenhouse effect, which is more intense in northern high latitudes.

Pithan and Mauritsen (2014), using CMIP5 models suggested that the temperature feedback is causing more enhanced Arctic warming than albedo-sea ice feedback. As temperature warms, more energy is radiated back to space in low latitudes, compared with the Arctic. This effect can be attributed to both the different vertical structure of the warming in high and low latitudes, and a smaller increase in emitted blackbody radiation per unit warming at colder temperatures.

Lu and Cai (2009), analyzed the feedback processes acting in polar amplification using global climate model. They found that surface warming due to increase in CO_2 can still be stronger in high latitudes than in low latitudes even without the negative evaporation feedback in low latitudes and positive ice-albedo feedback in high latitudes, as well as

without the poleward latent heat transport. The radiative energy flux due to increase in CO₂ and vapor feedback lead to stronger warming in low latitudes than in high latitudes at the surface and throughout the entire troposphere. In the vertical, the temperature changes due to increase of CO₂ and water vapor feedback are maximum near the surface and decrease with height at all latitudes.

According Graversen et al (2014), the lapse rate feedback is related to a vertically non uniform warming of the troposphere by altering the infrared irradiance to space relative to that of a vertically uniform tropospheric warming. The lapse rate feedback is negative at low latitudes, as a result of moist convective processes, and positive at high latitudes, due to stable stratification conditions that effectively trap warming near the surface. The authors using climate models simulations found that the lapse rate feedback (albedo sea ice feedback) represents approximately 15% (40%) of the Arctic amplification.

The contributions of each climate feedback for enhanced Arctic warming still are a subject of debate due to the complexities of linked physical processes and uncertainties of climate models.

2.3 Coupled Model Intercomparison Project

Global Climate Models are mathematical representation of the Earth's climate system and incorporate the coupled interactions between the atmosphere, land, ocean and ice in order to estimate the state of the climate under a wide variety of conditions. They are currently considered the most powerful tools available for simulating the global climate change as response to GHG forcing.

The CMIP is a standard framework for evaluating and intercomparing climate simulations generated by coupled ocean-atmosphere climate models. This is a key framework for the advancement of our understanding on climate variability and global climate change since it makes available for any researcher or institute a freely accessible state-of-the-art multimodel dataset. The sharing of these extensive outputs date places "side by side" the climate model developers and researchers from different expertise and institutions. Hence enhancing the pace of climate research and resulting in hundreds of publications and a multimodel perspective of climate change with invaluable benefits for communities and governments worldwide (GLECKLER

et al., 2016; TAYLOR et al., 2012).

The latest CMIP phase, called CMIP5 was coordinated by the World Climate Research Program (WRCR) Working Group on Coupled Models (WGCM) in collaboration with the International Geosphere Biosphere Program (IGBP), Analysis Integration and Modeling of the Earth System (AIMES) and many other elements of the climate science community. The Intergovernmental Panel on Climate Change (IPCC) has used CMIP5 set of climate models results as the scientific basis for its 5th Assessment Report (TAYLOR et al., 2012; MEEH; BONY, 2011).

According to Meehl and Bony (2011), CMIP5 is the most ambitious multi-model intercomparison and analysis projected ever attempted, and the scientific impact depends on the contributions of researchers who are analyzing this rich set of climate models simulations (TAYLOR et al., 2012).

CMIP5 build up a standard data set of model simulations in order to accesses the ability of climate model in simulating the recent past and providing projections of future climate change. It is expected to explain some of the factors responsible for differences between model simulations, improving the knowledge of some key feedbacks such as those involving clouds and the carbon cycle.

The CMIP5 experiments designs are divided into three categories: I) Near-term integrations (10-30yr), also called decadal prediction experiments; (II) Long-term integrations (century time scales) and (III) Atmosphere-only (prescribed SST) simulation for especially computationally-demanding models. Both (I) and (II) numerical experiments are integrated using coupled ocean-atmosphere global climate models or Earth System Models. All the CMIP5 numerical experiments are described in detail by Taylor et al (2012) and Taylor et al (2009).

The CMIP5 data is publically available at Earth System Grid Federation (ESGF) portal. The ESGF maintains a global system of federated data centers that allow access to the largest archive of climate date worldwide. ESGF can be accessed via any one of several websites serving as portal to the ESGF archive, *e.g.* **Figure 2.4**, the ESGF node at INPE/CPTEC (Center for Weather Forecasting and Climate Research), available at: <https://dm2.cptec.inpe.br/projects/esgf-inpe/>.



Figure 2.4. The ESGF node at INPE/CPTEC

Source: <https://dm2.cptec.inpe.br/projects/esgf-inpe/>

2.4 Data source

This study uses short-term simulations (decadal hindcasts) and long-term simulations (future scenarios) of 12 state-of-the-art General Circulation Models (GCMs) and Earth System Models (ESMs), seen in Table 3.1. The numerical experiment design follows the CMIP5 protocol, for decadal data and future projections based on the Taylor protocol (TAYLOR et al., 2012; TAYLOR et al., 2009).

The BESM ensemble members of the decadal simulations were integrated for 10 years, each with initial conditions (IC) on 1 - 10 December of the years 1960, 1965, 1970, 1975, 1980, 1985, 1990, 1995, 2000 and 2005. Three of these ensembles (1960, 1990 and 2005) were extended for an extra 20 years for each of the 10 members, completing 30 years long integrations each. These simulations used atmospheric CO₂ concentrations derived from *in situ* air samples collected at Mauna Loa Observatory, Hawaii (NOBRE et al., 2013). The Atmospheric model initial conditions for each ensemble member used the National Centers for Environmental Prediction (NCEP-NCAR) reanalysis fields for the 0000 UTC of each day from 1 to 10 December of the chosen years. The ocean initial states were chosen from the same dates from a *spinup* run of MOM4p1 that used prescribed atmospheric fields of momentum, solar radiation, air temperature, and freshwater described in Nobre et al (2013).

The future scenarios are defined by the Representative Concentration Pathways (RCPs) and each RCP defines a specific emissions trajectory and subsequent radiative forcing. The radiative forcing values in the year 2100 relative to pre-industrial values are $4.5 \text{ W}\cdot\text{m}^{-2}$ and $8.5 \text{ W}\cdot\text{m}^{-2}$ for RCP4.5 and RCP8.5 respectively, which include the period from 2006 to 2100. The CO_2 concentration in the year 2100 for each RCP is approximately 600 ppm and 1300 ppm for RCP4.5 and RCP8.5, respectively.

The abrupt increase in CO_2 simulation uses two CMIP5 numerical experiments: piControl (pre-industrial fully-coupled control, run for hundreds of years) and abrupt quadrupling of atmospheric CO_2 (as piControl but run for 150 years, following an instantaneous quadrupling of atmospheric CO_2). The design of both experiments also follows the CMIP5 protocol (TAYLOR et al., 2012; TAYLOR et al., 2009). We compare the results only for polar amplification (changes in SAT) for the same numerical experiment using: CCSM4 model, GFDL-ESM2M and MPI-ESM-LR.

We compared BESM results with CMIP5 models simulations using the same numerical experiment setup. Still, the models differ in spatial resolution, physical component and parameterizations. For decadal simulations we chose to work with time series from 1980 to 2012 due to the availability of satellite observations for comparison. The SSM/I (Special Sensor Microwave Imager) satellite observations obtained from the National Snow and Ice Data Center (NSIDC) were used to validate the numerical simulations. For all simulations we calculated the SIE, defined as the area where the sea ice concentration is greater than 15% in a grid.

Table 1. CMIP5 main characteristics

Institute / Country	Model	Experiment Design	Reference
National Institute for Space Research (INPE) – Brazil	Brazilian Earth System Model BESM-OAV2.3 BESM-OA-V2.5	Decadal RCP45/RCP85 Abrupt 4xCO ₂	NOBRE et al., 2013
Canadian Centre for Climate Modelling and Analysis (CCCma)- Canada	Canadian Coupled Climate Model, versions 4 and ESM2 CanCM4 CanESM2	Decadal RCP45/RCP85	MERRYFIELD et al., 2013; CHYLEK et al., 2011.
National Oceanic and Atmospheric Administration – Geophysical Fluid Dynamics Laboratory (GFDL-NOAA) -USA	Geophysical Fluid Dynamics Laboratory - Climate Models GFDL-CM2.1 GFDL-CM3 GFDL-ESM2M	Decadal RCP45/RCP85 Abrupt 4xCO ₂	DELWORTH et al., 2006; GRIFFIES et al., 2011.
Met office Hadley Centre (Met Office) United Kingdom	Hadley Centre Coupled Model HadCM3 HadGEM2-ES	Decadal RCP45/RCP85	GORDON et al., 2000; COLLINS et al., 2011.
Atmospheric and Ocean Research Institute- University of Tokyo (AORI) - Japan	Model for Interdisciplinary Research on Climate MIROC 5	RCP45/RCP85	WATANABE et al., 2010.
Max Planck Institute for Meteorology (MPI) –German	Max Planck Institute -Earth System Model MPI-ESM-LR	Decadal RCP45/RCP85 Abrupt 4xCO ₂	MARSLAND et al., 2003.
National Centre for Atmospheric Research (NCAR) – USA	Community Climate System Model Version 4 CCSM4	Decadal RCP45/RCP85 Abrupt 4xCO ₂	GENT et al., 2011.

2.4.1 BESM-OA Model

In this work, we used two versions of the BESM Coupled Ocean Atmosphere (BESM-OA) model: BESM-OA V2.3 for decadal and RCP simulations and BESM-OA V2.5 for RCP and Abrupt 4 x CO₂ simulations. The main differences between these two versions are the microphysics scheme proposed by Ferrier et al. (2002) and a new surface layer scheme based on Jimenez and Dudhia (2012) described by Capistrano et al (2016, 2015).

Both BESM versions used in this research are composed of the INPE/CPTEC Atmospheric General Circulation Model (AGCM) coupled to NOAA/GFDL's Modular Ocean Model version 4p1 (MOM4p1) Oceanic General Circulation Model (OGCM) via GFDL's Flexible Modular System (BOTTINO and NOBRE, 2016; NOBRE et al., 2013; GRIFFIES, 2009). The INPE/CPTEC AGCM has a spectral horizontal resolution truncated at triangular wave number 62, giving an equivalent grid size of 1.8758 degrees of latitude and longitude and 28 sigma levels unevenly spaced in the vertical (i.e., T062L28). The exchanges of heat, moisture and momentum between the surface and atmosphere in INPE/CPTEC AGCM over the

ocean and continents are computed differently by various physical processes that define the surface fluxes.

The ocean model MOM4p1 (GRIFFIES, 2009) from GFDL, includes the Sea Ice Simulator (SIS), described in Winton (2000).

The SIS is a dynamical model with three vertical layers (two ice and one snow), and five ice thickness categories. The elastic-viscous-plastic technique of Hunke and Dukowicz (1997) is used to calculate ice internal stresses, and the thermodynamics is a modified Semtner's three-layer scheme (SEMTNER, 1976). SIS calculates the concentration, thickness; temperature, brine content, and snow cover of an arbitrary number of sea ice thickness categories (including open water) as well the motion of the complete pack. Additionally, the model is responsible for calculating ice/ocean fluxes and communicating fluxes between the ocean and atmosphere models globally (**Figure 2.5**).

According described in Winton (2000), the model consists of a zero-heat-capacity snow layer overlying two equally thick sea ice layers (**Figure 2.5**). The upper ice layer has a variable heat capacity to represent brine pockets. The lower ice layer has a fixed heat capacity. The prognostic variables are: (1) h_s : snow layer thickness; (2) h_i : ice layer thickness; (3) T1 and T2: the upper and lower ice layer temperatures located at the midpoints of the layers $h_i/4$ and $3h_i/4$ below the ice surface, respectively.

Two of the prognostic variables of Semtner's model have been eliminated: the brine content of the upper ice and the snow temperature. A separate brine variable is no longer needed because the brine content in the new model is completely determined by the upper ice temperature and the (predetermined) ice salinity (WINTON 2000).

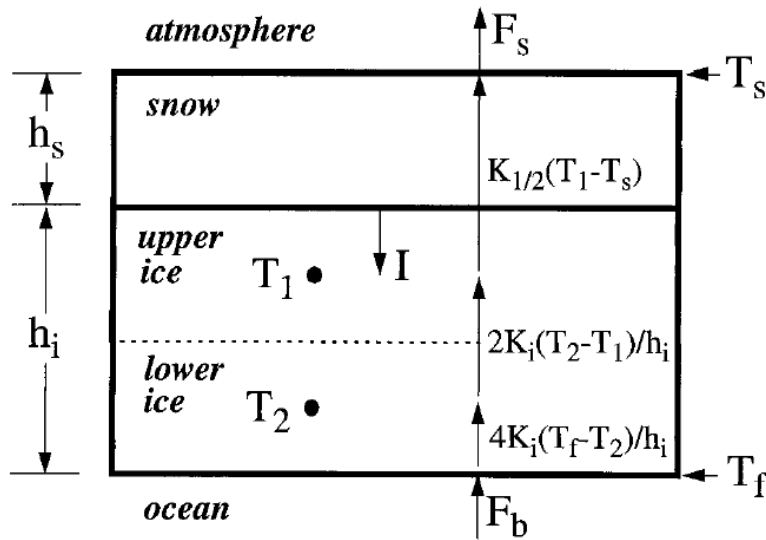


Figure 2.5. Schematic representation of the three-layer sea ice model. The four prognostic variables are: snow layer thickness (h_s), the ice layer thickness (h_i), the upper ice layer Temperatures (T_1) and the lower ice layer Temperatures (T_2). The sea ice bottom temperature is fixed at T_f (freezing temperature of seawater). T_s is the temperature of ice or snow and is determined from the surface energy balance. K_i is the thermal conductivity of sea ice. Source: Winton (2000)

The MOM4p1 horizontal grid resolution is set to 1° in the longitudinal direction, and in the latitudinal direction the grid spacing is $1/4^\circ$ in the tropical region ($10^\circ\text{S} - 10^\circ\text{N}$), decreasing uniformly to 1° at 45° and to 2° at 90° in both hemispheres. For the vertical axis, 50 levels are adopted with a 10 m resolution in the upper 220 m, increasing gradually to about 370 m of grid spacing in deeper layers. We used FMS to couple MOM4p1 and CPTEC/AGCM. Thus, wind stress fields are computed, using Monin-Obukhov scheme within MOM4p1, from the field 10 meters above the ocean surface. Adjustments were done to the Monin-Obukhov boundary layer scheme, whose parameters were tuned according to the wind fields output by the CPTEC AGCM. The AGCM receives the following two fields from the coupler: Sea Surface Temperature (SST) and ocean albedo from ocean and sea ice models at an hourly rate (coupling time step). Adjustments were also made to ocean shortwave penetration parameters due to the CPTEC AGCM supply of visible and infrared short wave radiation. The coupling variables supplied by the AGCM are as follows: freshwater (liquid and solid precipitation), specific humidity, heat, vertical diffusion of velocity components, momentum fluxes, and surface pressure.

The microphysics of Ferrier et al (2002) used in BESM-OA V2.5, replaced the Large Scale Precipitation scheme used in BESM-OA V2.3 (NOBRE et al., 2013). This new microphysics scheme computes changes in water vapor, cloud water, rain, cloud ice and precipitation ice. Also, BESM-OA V2.5 uses a new surface layer scheme based on Jimenez and Dudhia (2012) and described by Capistrano et al. (2016; 2015). In this scheme, the surface and the first AGCM level values are used to assess wind, air temperature and humidity at 10 m. The changes introduced lead to a more consistent surface layer formulation that resulted in a near-surface wind, air temperature and humidity more consistent with observations than previous BESM version. This occurs mainly over the ocean, where those variables are important to compute the heat fluxes at ocean-atmosphere interface.

3 ARCTIC SEA ICE: DECADEAL SIMULATIONS AND FUTURE SCENARIOS USING BESM-OA

3.1 Seasonal Cycle

Seasonal melt-freeze transitions are important to continuously monitor sea ice over the Arctic. Sea ice formation, growth and decay are closely related to air temperature, ocean heat content, albedo and heat fluxes and hence can vary strongly from month to month (DOESCHER et al., 2014; FRANCIS et al., 2009). Thus, we present in this section the Arctic seasonal cycle of sea ice, in order to better understand the differences between the models studied, with a focus on the performance of the BESM-OA V2.3 model.

First, to understand the ability of BESM-OA V2.3 to simulate the seasonal cycle in relation to observation and other CMIP5 models, we present in **Figure 3.1** the seasonal cycle of climatological average of SIE from CMIP5 model and observed values for the period from 1980 to 2010. All of the models were able to represent the seasonal cycle of the Arctic sea ice. Large oscillations between summer and winter are evident, with sea ice growing from autumn and winter reaching a peak in March, and then declining throughout spring and summer as the melting season progresses. However, most models overestimate SIE values in winter (except the MPI-ESM-LR model), and underestimate in summer (except HadCM3 and NCAR-CCSM4). BESM-OA V2.3 ensemble agrees quite well with observations and satisfactorily represents the seasonality of sea ice, although the model's sea ice decays more rapidly than observed in summer and autumn. The observational data (BESM-OA V2.3) shows that Arctic SIE varies between approximately $15 \times 10^6 \text{ km}^2$ ($18 \times 10^6 \text{ km}^2$) at winter maximum and $6 \times 10^6 \text{ km}^2$ ($6 \times 10^6 \text{ km}^2$) at summer minimum. The difference between the model's performance for winter and summer are in agreement with (STROEVE et al., 2012; GORDON et al., 2000; ARZEL et al., 2006; SORTEBERG et al., 2007). It is clear that the BESM-OA V2.3 model, even with an overestimation during winter presents a very good agreement in summer when SIE reaches critical values.

Based on our results, Sortberg et al (2007) and Karlsson and Svensson (2013), we suggest the following scheme to explain the differences between winter and summer model's performance in representing SIE. First, the presence of sea ice affects

strongly the sea ice albedo, which has a key influence on the energy budget and is directly linked to the cloud-albedo effect and cloud-radiation effect. Clouds are linked with the energy budget by reflecting shortwave radiation back to space, trapping Longwave (LW) radiation and radiating it back to the surface, providing one of more the strongest feedbacks in the climate system (LI et al., 2013). Second, in wintertime, the amount of solar radiation is low or non-existent and the ability of the clouds to reemitted LW to the surface presents a positive cloud radiative effect on the surface energy budget. On the other hand, during the seasons with solar radiation, the positive greenhouse effect is competing with a negative cloud albedo effect, because the clouds decrease the amount of incident solar radiation at the surface. Finally, recent publications using CMIP3 and CMIP5 models (KARLSSON; SVENSSON, 2013; SORTEBERG et al., 2007) suggest that models generally have the tendency to underestimate the amount of LW radiation reemitted back to the surface in winter. As a consequence of these processes, the models tend to overestimate SIE in wintertime. Additionally, the annual amplitude of sea ice cover depends inversely on the model's sea ice albedo (KARLSSON; SVENSSON, 2013; SORTEBERG et al., 2007). BESM-OA V2.3 results agree with this scheme, as both downward and upward LW radiation at the surface are underestimated in winter. The ensemble mean is lower than the mean of the observations by approximately $30 \text{ W}\cdot\text{m}^{-2}$ (**Figure 3.2**). Another notable example is related to the MPI-ESM-LR model's performance, which presents a high sea ice albedo and low annual amplitude of sea ice. According to Wild et al (2001), the bias in LW radiation depends on the climate conditions and is not geographically uniform, with higher (smaller) bias in cold and dry climates (warm and humid climates) with low (high) downward LW radiation emission. Knutti and Sedlacek (2013), Li et al (2013) and Stroeve et al (2012), assessed the evolution between CMIP3 and CMIP5 and showed an improvement in the Arctic sea ice prediction and radiation in CMIP5. Nevertheless, a better representation of sea ice depends also on improvements in the representation of the Arctic sea-ice albedo, clouds, cloud-radiation effects and feedback processes.

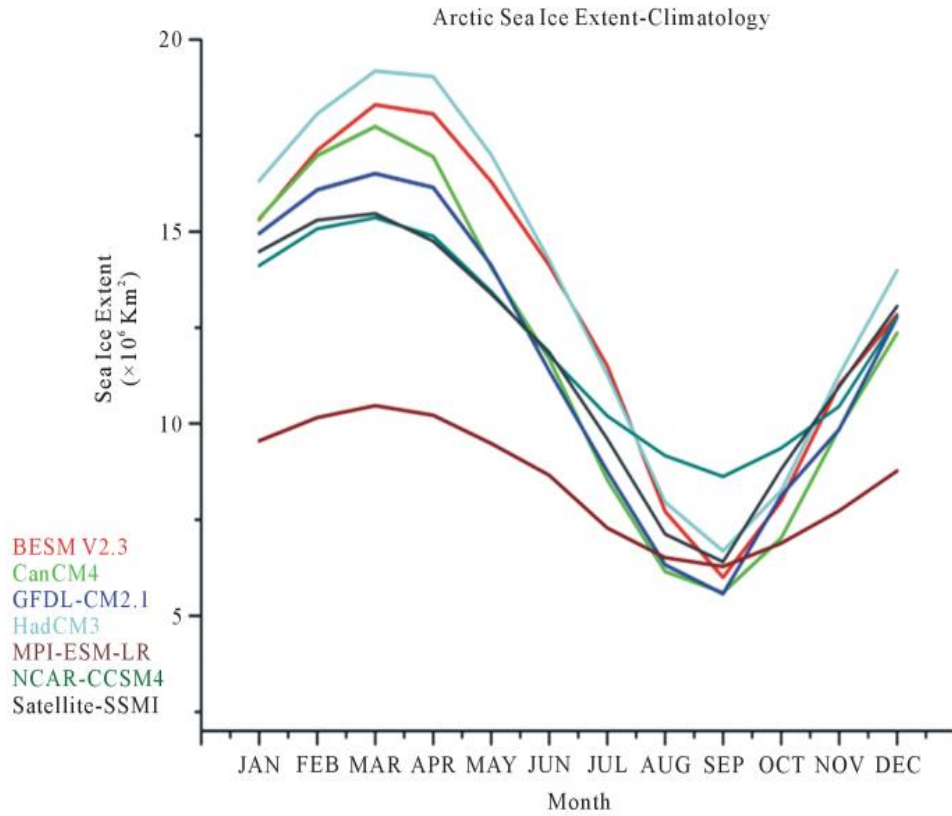


Figure 3.1. Climatology of SIE (1980 to 2010) in the northern hemisphere simulated by BESM-OA V2.3, CMIP5 models and observations.

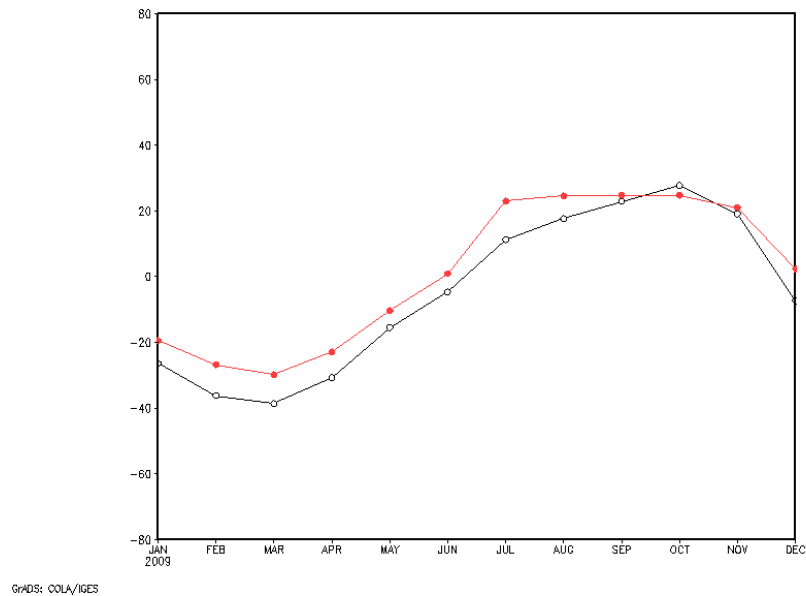


Figure 3.2. Difference between BESM-OA2.3 simulations and observations for LongwaveUp (red line) and LongwaveDown (black line) from 1980 to 2010. The observation data are from International Satellite Cloud Climatology Project (ISCCP) Global Radiative Flux Data Products (ZHANG, 2004). Available in: <http://isccp.giss.nasa.gov/projects/flux.html>

Figure 3.3 shows a Taylor diagram for September, March and annual climatology of SIE. This diagram is a useful tool to compare observed and simulated data in terms of correlation coefficient, RMS and standard deviation. A shorter distance between model and REF (observed) in a Taylor Diagram indicates a better model's performance. For the annual values (black) all the six models have a correlation with the observations higher than 0.96, while for March and September the correlation coefficient presents low values, as expected. For all models (except MPI-ESM-LR) the correlation in March is smaller than 0.6. The annual cycle of SIE is quite well represented because the seasonal cycle of SIE was well represented by all the models as shown in **Figure 3.1**. However, when looking at separate months, the correlation drops, as consequence in the same month time series, only the interannual variability is being evaluated. For the month of March, we suggest the previously described scheme (radiation effect) to explain the low correlation between observation and models. To understand the low correlation in September, we suggest a relation with sea ice thickness. According to Shu and Qiao (2015) and Stroeve et al (2012), the sea ice thickness simulated in the CMIP5 models is too thin, resulting in enhanced sea ice melt and an underestimation for SIE in summertime, as shown in **Figure 3.1**.

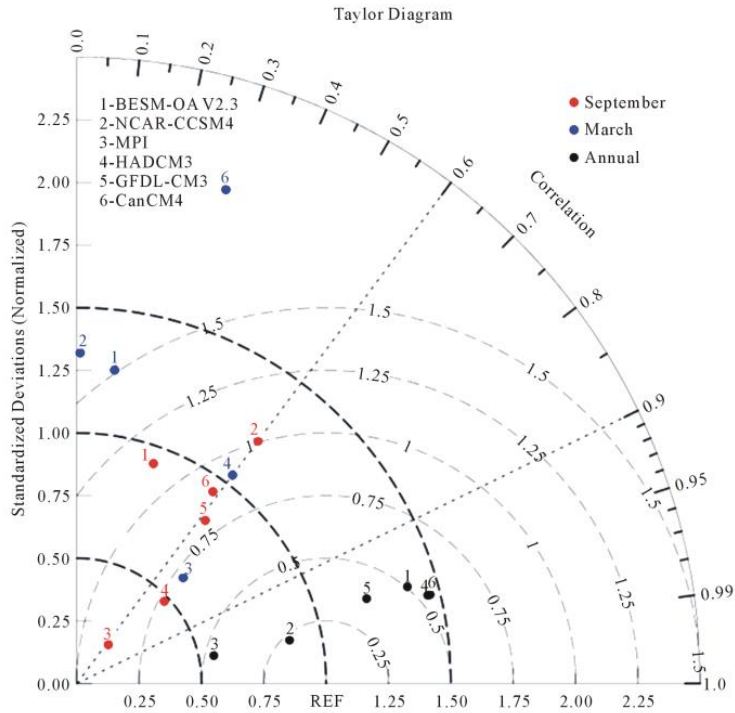


Figure 3.3. Taylor diagram of September, March and climatological annual cycle of SIE for the period 1980-2012. The x-axis and y-axis are the standard deviation normalized. The correlation coefficient between observations and each model is given by the azimuthal position. The centered RMS difference between simulated and observed is proportional to their distance one from another

3.2 Spatial Pattern

Several studies have compared the observed SIE variation using climate models and CMIP data sets in a seasonal cycle or time series approach (STROEVE et al., 2012; STROEVE et al., 2007; ARZEL et al., 2006). This type of analysis is important to know the model’s ability to predict SIE. However, when considering only SIE, the information related to spatial pattern is lost. Analyzing spatial patterns avoids overconfidence in the predictions and excludes compensation of errors of opposite sign in different regions (TIETSCHE et al., 2014).

Cavalieri and Parkinson (2012) also show the importance of evaluating the Arctic Ocean by regions. The authors, using satellite data set to analyze sea ice variability and trends from 1979 to 2010, found that trends for nine distinct regions in the Arctic are not homogeneous and indicated the complex nature of the Arctic climate system by regions.

Figure 3.4 shows September average Sea Ice Cover (SIC) observations over the study area. The spatial difference between modeled and observed SIC in September average

is shown in **Figure 3.5**. September was chosen because commonly is when sea ice reaches its annual minimum over the Arctic.

Despite obvious inter-model differences depicted in **Figure 3.5**, there is a reasonable agreement between all the models. Most models tend to well represent SIC in the central Arctic, whereas the opposite occurs in marginal ice zones. There is a general tendency to underestimate SIC in areas such as the Beaufort Sea and the East Siberian Sea (except for MPI-ESM-LR and HadCM3) suggesting a systematic model error in this region. However, NCAR-CCSM4 overestimates SIC in both Laptev and Kara Sea (**Figure 3.5**). This may reflect the NCAR model's overestimation observed for September and shown in **Figure 3.1**.

The SIC in the region between Canada and Greenland is well represented by BESM-OA V2.3, GFDL-CM2.1 and MPI-ESM-LR models, while SIC between East Siberia and the Barents Seas is only well simulated by MPI-ESM-LR model. Despite a good representation of the spatial pattern of SIC in the MPI-ESM-LR model in September (**Figure 3.5**), it is clear that the amplitude of its annual cycle is smaller than both the others models and satellite observations (**Figure 3.1**). This reveals a certain deficiency in representing physical processes between ocean-atmosphere-sea ice, although the good representation during summer.

The detailed analysis of simulated SIC by regions using Climate Models is justifiable due to both economic and scientific reasons. Economically, as a result of sea ice loss maritime transports may gain two new routes with the opening of the “Northwest Passage” in Northern Canada and Greenland, and the “Northeast Passage” between Northern Russia and Norway (ACIA, 2005). This is considered a hot topic because these passages could lead to fast and cheaper ship transport between Europe and North America. Scientifically, this is relevant because the importance of properly account for the dynamical/thermodynamical processes taking place in shaping SIC over the Arctic region. It is instructive to compare **Figure 3.1** with **Figure 3.5**, analyzing only SIE in September for GFDL-CM2.1 and CanCM4 models (**Figure 3.1**). This can induce overconfidence in how well the models agree (SIE in both models are approximately 5.6×10^6 km²). However, when we look at the spatial patterns in **Figure 3.5**, we find quite different SIE distributions. CanCM4 model shows a large area of high negative values (especially between Greenland and

Canada), whereas GFDL-CM2.1 shows a small area of high negative values only in parts of Beaufort Sea and East Siberian Sea. Thus, even some climate models showing a good performance in simulating SIE during summertime do not necessarily simulate a realistic spatial sea ice distribution.

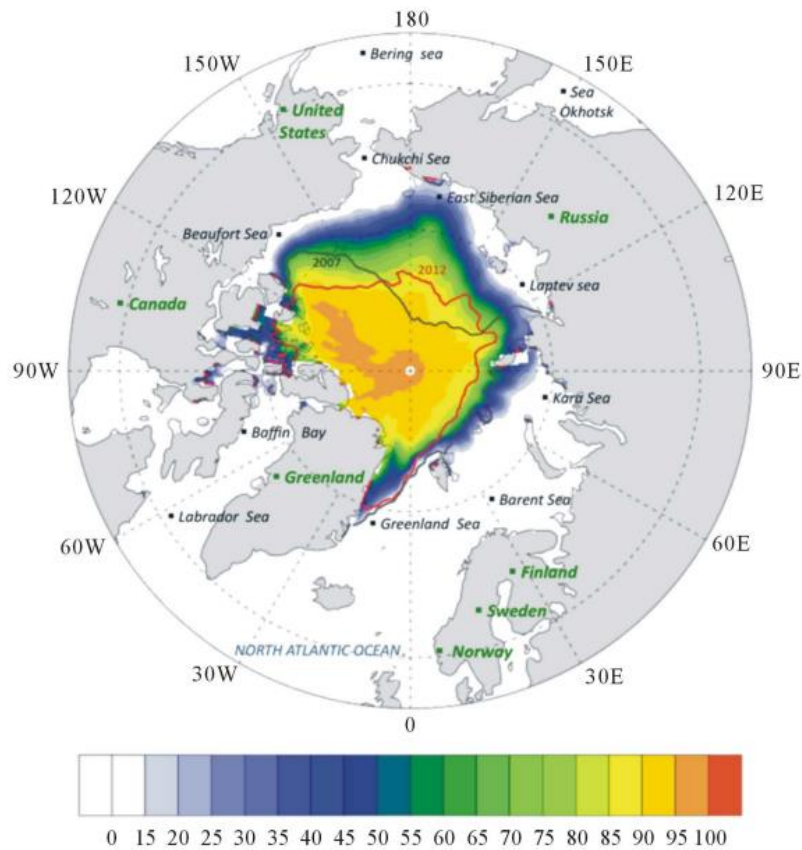


Figure 3.4. Arctic study area and September SIC Climatology (1980-2010) from satellite observations (shaded colors). Dark gray and orange lines refer to the 2007 and 2012 minimum events respectively.

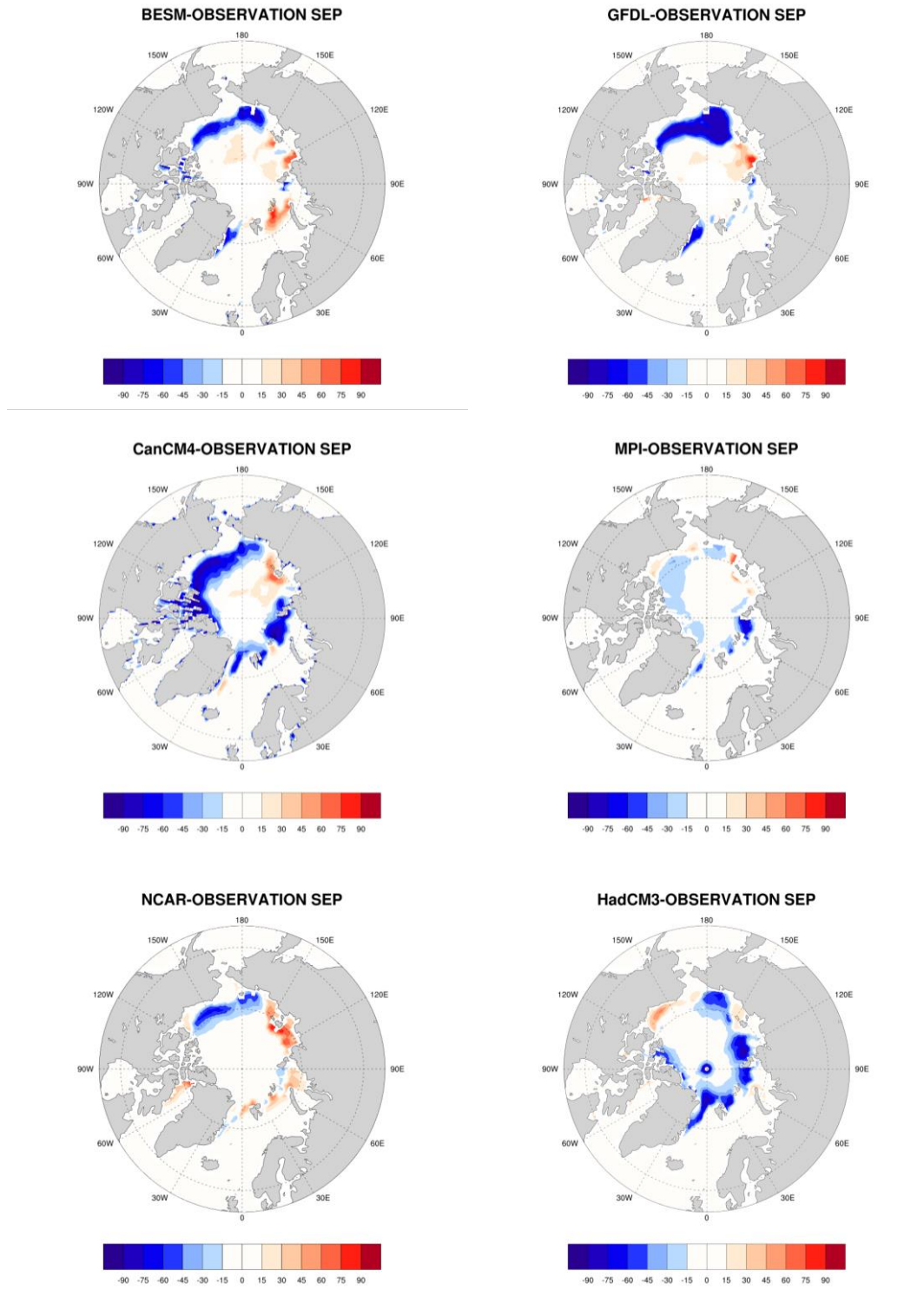


Figure 3.5. Difference between model simulations and observations for September SIC climatologic average from 1980 to 2010. BESM-OA V2.31, GFDL-CM2.1 (upper), CanCM4 and MPI-ESM-LR (middle), HadCM3 and NCAR-CCSM4 (bottom). Positive (negative) value depicted in red (blue) represent areas where the model overestimates (underestimates) sea ice concentration values.

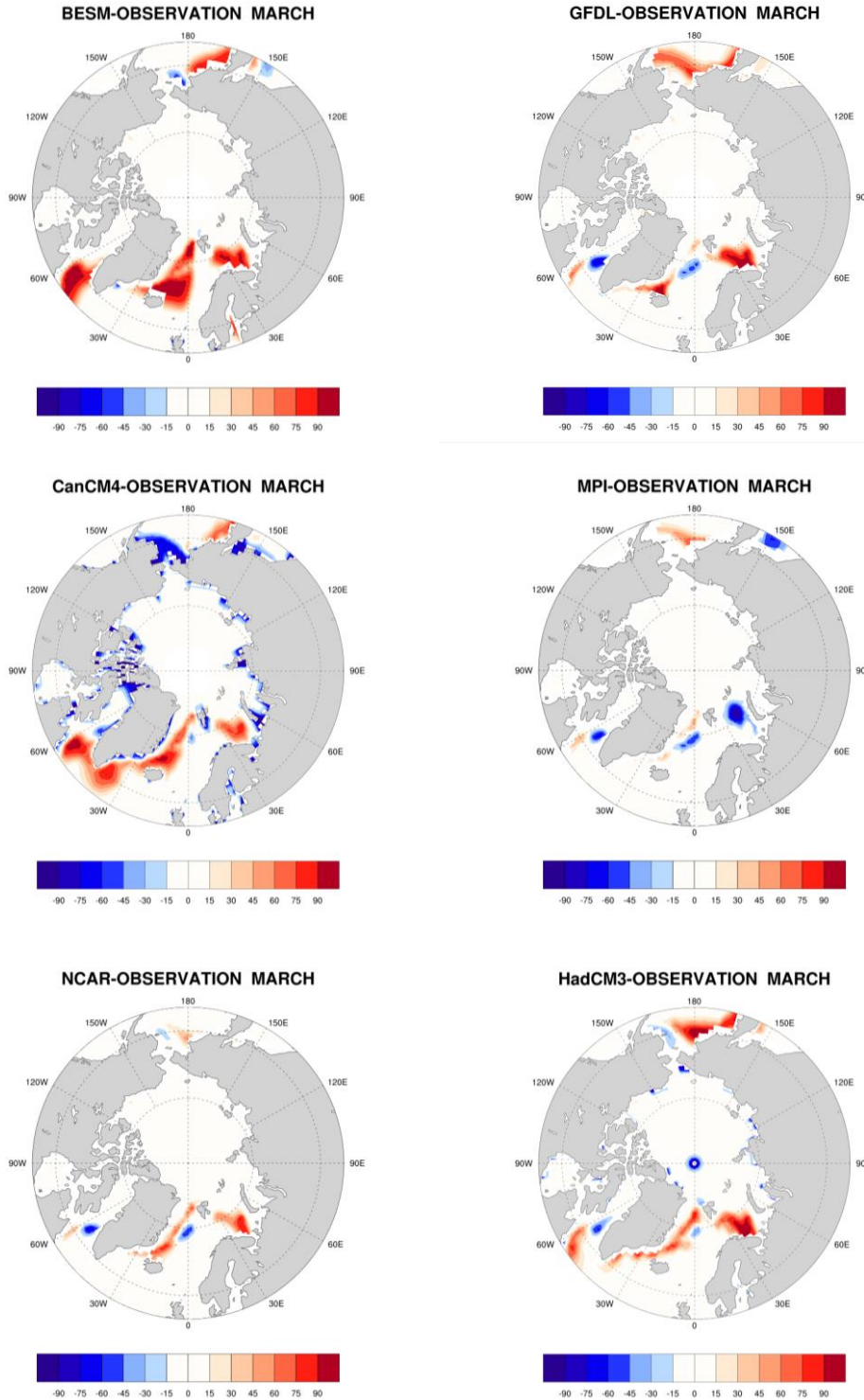


Figure 3.6. Difference between model simulations and observations for March SIC climatologic average from 1980 to 2010. BESM-OA V2.31, GFDL-CM2.1 (upper), CanCM4 and MPI-ESM-LR (middle), HadCM3 and NCAR-CCSM4 (bottom). Positive (negative) value depicted in red (blue) represent areas where the model overestimates (underestimates) sea ice concentration values.

3.3 Minimum of Sea Ice Extent

Changes in ice extent due to the seasonal cycle are so large that they tend to obscure any signal related to interannual variability. To remove the strong seasonal cycle, we again specifically focus on September since it shows the minimum annual of SIE. According to Doescher et al (2014), the ability to identify real changes in the Arctic Climate System increases when we focus on individual seasons. In this context, **Figure 3.7** shows the SIE time series of September averages from 1982 to 2014.

Arctic sea ice has declined sharply during the last three decades, with record low summer ice cover in September 2007 and 2012 as illustrated in **Figure 3.7**. Here, we show the time series of SIE and analyze the ability of the models to represent recent changes.

Arctic SIE averages from 1980 to 2010 (**Figure 3.7**) show a noticeable decrease in Arctic SIE. September SIE simulated by BESM-OA V2.3 (satellite observations) between 2000 and 2010 was $4.2 \times 10^6 \text{ km}^2$ ($5.7 \times 10^6 \text{ km}^2$), while between 1980 and 1990 it was $6 \times 10^6 \text{ km}^2$ ($7.1 \times 10^6 \text{ km}^2$), showing a reduction of approximately 30% (19.8%) in SIE.

The minimum satellite record of SIE occurred in September 2012, with $3.6 \times 10^6 \text{ km}^2$ against $4.5 \times 10^6 \text{ km}^2$ in BESM-OA V2.3. In 2012, satellite observations (GFDL-CM2.1) presented a decrease of 50.4% (42.3%) of SIE in relation to the 1980s decade. Except for the GFDL-CM2.1 model, no other model was able to represent the observed 2012 minimum. However, BESM-OA V2.3 and CanCM4, generated episodes of low SIE in September with a magnitude and behavior comparable with the low observed in 2012. These episodes of minimum SIE occurred in 2006 and 2002 for the BESM-OA V2.3 and CanCM4 models, respectively. According to Doescher et al (2014) and Holland et al (2006), such abrupt sea ice loss resulted from a complex interplay between the thermodynamics and dynamics of sea ice, ocean and atmosphere and successful prediction requires careful initialization with ocean and sea ice conditions.

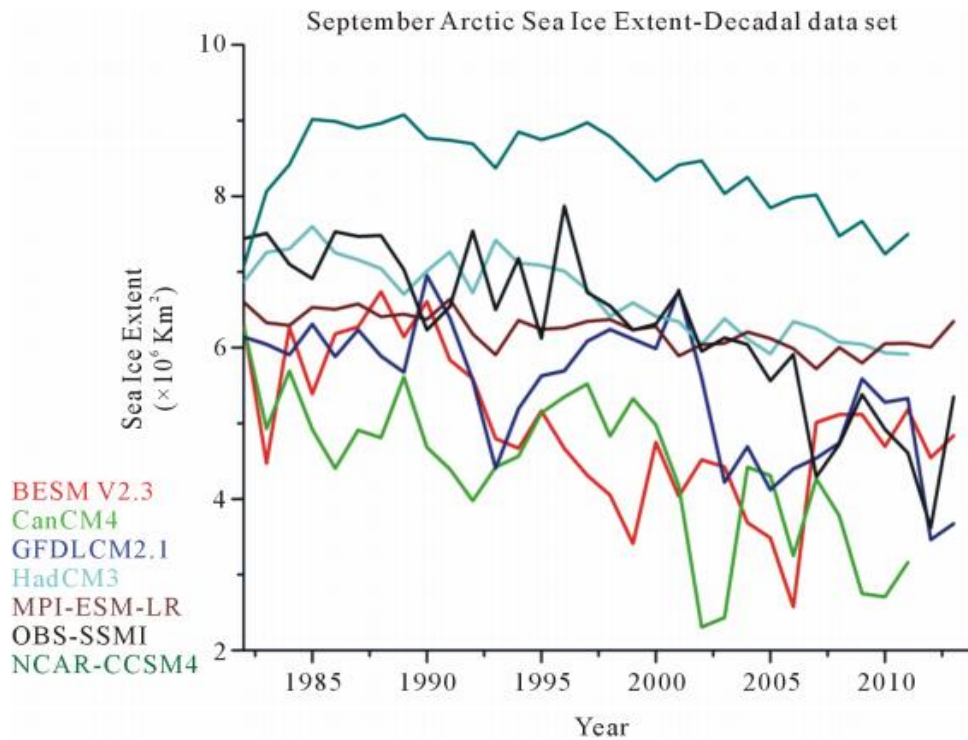


Figure 3.7. Arctic sea ice extent time series of September from 1980 to 2014 for CMIP5 models and observational data.

Figure 3.8 illustrates the spatial distribution of average September SIE (left) and minima of September SIE value found between 1980 and 2010 (right) for all the models evaluated in this work. This figure aimed to show the model's performance to represent the spatial pattern in episodes of low SIE, regardless of year.

Looking at the spatial patterns of the SIE climatological mean and minimum record, it is clear that the climate models are able to reproduce the seasonal cycle of the SIE (**Figure 3.1** and **Figure 3.3**) better than they represent the minimum records. Only GFDL-CM2.1 model presents a good spatial agreement of minimum records with observation. This could be explained by two main reasons. First, it was the only one that matched the spatial pattern of the observed minimum, which may lead to a better agreement with observed meteo-oceanographic patterns. Second, it may be related to a better representation of the sea ice and feedbacks processes in the parameterizations of the GFDL-CM2.1 model. Two other models (BESM-OA V2.3 and CanCM4) also show a reasonable spatial agreement with observations, although not as well as

GFDL-CM2.1. These two models presented an underestimation of SIE, but presented a very good representation of the SIE in the central Arctic region (**Figure 3.8**).

The minimum record for the BESM-OA V2.3 shows a deficiency near Greenland and at the north of Canada. Although BESM-OA V2.3 and CanCM4 were capable to capture the correct signature of the SIE minimum record with a decrease in SIE followed by an increase in the following year (**Figure 3.7**), the correct estimation of minimum SIE, in time, spatial, area and processes signatures remains a challenge for the modeling community.

Due to the sea ice retreat in recent Septembers months, ice cover in the following spring tends to be thinner, thus vulnerable to melting in summer. According to Doscher et al (2014), each record of low SIE is followed by a partial recovery. Additionally, Tietsche et al (2014) suggest that the minimum record of SIE during a single September is reversible, as the albedo sea ice mechanism is compensated by large scale recovery mechanisms. According to Vihma (2014) the sea ice loss increases the heat flux from the ocean to the atmosphere in early winter and autumn. As result of this, a local increase of air temperature, humidity and cloud cover is expected thus reducing the stability of the atmospheric boundary layer.

Hunke et al (2010) evaluated the retrospective and new directions of sea ice models. The authors indicated some deficiencies in the dynamics (*e.g.* transport processes, dynamic coupling and mechanical redistribution) and thermodynamics (*e.g.* feedback processes and melt ponds) and suggested that improvements in the sea ice prediction dependent on improvements in the descriptions of the physical processes and characteristics, as well as, extending the models for Earth System Model simulations including biogeochemistry. According to Flocco et al (2012) and Roeckner et al (2012), one of the processes, poorly represented in sea ice models, is the formation and evolution of melt ponds. Melt ponds affect the heat and mass balances of SIC, mainly by reducing albedo by up to 20%. Consequentially, a reduction of the sea ice volume can reach 40%, leading to further sea ice melt. At the end of the melting season, melt ponds cover up to 50% of the sea ice surface. A better representation of the melt pond scheme will improve the sea ice simulation and is essential for accurate future sea ice projections.

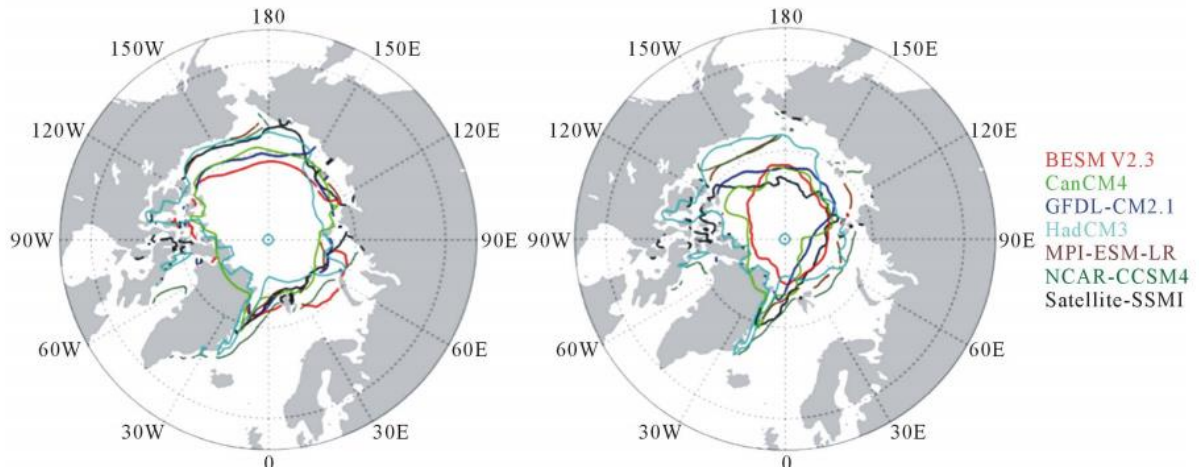


Figure 3.8. Spatial distribution of SIE average (left) and lowest values of September SIE found between 1980 to 2010, (right), for all CMIP5 models evaluated in this work.

3.4 Future Projection of Arctic Sea Ice

The long-term evolution of SIE in the northern hemisphere as simulated by BESM and CMIP5 models, using RCP4.5 and RCP8.5 is shown in **Figure 3.9**. The simulations clearly show a decrease in SIE up to 2100, for all simulations and both RCPs. Arctic SIE decline with the increase of the radiative forcing in all models. The BESM-OA V2.3 control experiment (gray lines in **Figure 3.9**) reinforce that ice-free conditions only happen when external forcing from anthropogenic sources are included in climate model simulations. These results are in agreement with Stroeve et al. (2012).

For September, at the beginning of the series (2006 to present-day), the HadGEM2 model SIE values are close to satellite observations. During March the best representation of the observed data was obtained by MIROC5 and BESM-OA V2.5 models.

During the first 30 years of the series, values from both RCPs are very similar in March and September months. For March, the SIE in the first years of the 21st century ranges from $11.8 \times 10^6 \text{ km}^2$ (MPI-ESM-LR) to $18.8 \times 10^6 \text{ km}^2$ (BESM-OA V2.3) in the RCP45 simulation. For the RCP8.5 simulation they vary between $11.7 \times 10^6 \text{ km}^2$ (MPI-ESM-LR) and $18.4 \times 10^6 \text{ km}^2$ (BESM-OA V2.3). For September SIE values

vary from approximately $2 \times 10^6 \text{ km}^2$ (BESM-OA V2.3) to $6.7 \times 10^6 \text{ km}^2$ (MIROC 5). Already during these early years, it is possible to observe the discrepancy between the two different BESM configurations.

For all RCP simulations, BESM-OA V2.3 and BESM-OA V2.5 show higher (lower) values in SIE during March (September) when compared to other models used in this work. The models reveal strong amplitudes in SIE between different seasons. Both BESM simulations clearly present the higher values in March for all years. However, for September the higher SIE was found in MIROC5 model (similar amplitude was observed in MPI-ESM-LR model).

It is possible to observe a higher inter-annual variability in September than in March for all models, as well as for the early period's satellite observations. The changes in inter-annual variability are important for sea ice prediction and frequency and for assessing the frequency of occurrence of extreme SIE anomalies.

It is noteworthy that the models comparatively show different tendencies for the months of maximum and minimum SIE. For the month of March, the MPI-ESM-LR model presented the lowest values compared to the other models used here, whereas for the month of September the lowest values encountered are those of the BESM-OA V2.5 model. In general, when compared to the other CMIP5 models, the BESM-OA V2.3 model tends to overestimate SIE in March and September, for both RCP simulations.

From the year 2040 onward, all models show a dramatic shrinking in SIE in the RCP 8.5 scenario. This indicates a high sensitivity of sea ice cover in response to an increase in the atmospheric carbon dioxide. The GFDL-CM3 model clearly shows this abrupt decrease in SIE with the RCP8.5 scenario when compared to the RCP4.5 one. In this case, the decline is so strong that at the end of the 21st century the SIE maximum (in March) is similar to the minimum SIE (in September) found in the beginning of the 21st century. If the GFDL-CM3 model is reasonably correct, it means that the Arctic can be ice-free also during the coldest season of the year just after 2100.

For September, ice-free conditions (defined as less than $0.5 \times 10^6 \text{ km}^2$) are obtained from 2020 in Can-ESM2 model, BESM-OA V2.5 and HAGEM2-2S with the RCP8.5

scenario. According to Chylek et al (2011) the addition of the land-vegetation model and terrestrial oceanic interactive carbon cycle to the coupled atmosphere-ocean in the Can-ESM2 model improved the simulations, although increased the overestimation of atmospheric warming after 1970. That explains the minimum values found here for CAN-ESM2 sea ice projections.

Also focusing on the RCP8.5 scenario, most of the models show ice-free situations, or episodes, after 2045 for the month of September. The exceptions are BESM-OA V2.3 and NCAR-CCSM4. These two models are a bit more conservative than the others, pointing out to ice free situations to starting after 2060. It is expected that ice-free conditions will have strong effects on the global climate system though changes in both ocean and atmospheric circulations. It is known that sea ice loss amplifies the effects of radiative forcing by the albedo-sea ice feedback mechanism and cloud effects. It also, affects the meridional and inter-hemispheric temperature gradients that can affect mid-latitude circulation. However the quantification of these effects remains unclear requiring improvements in the global climate models.

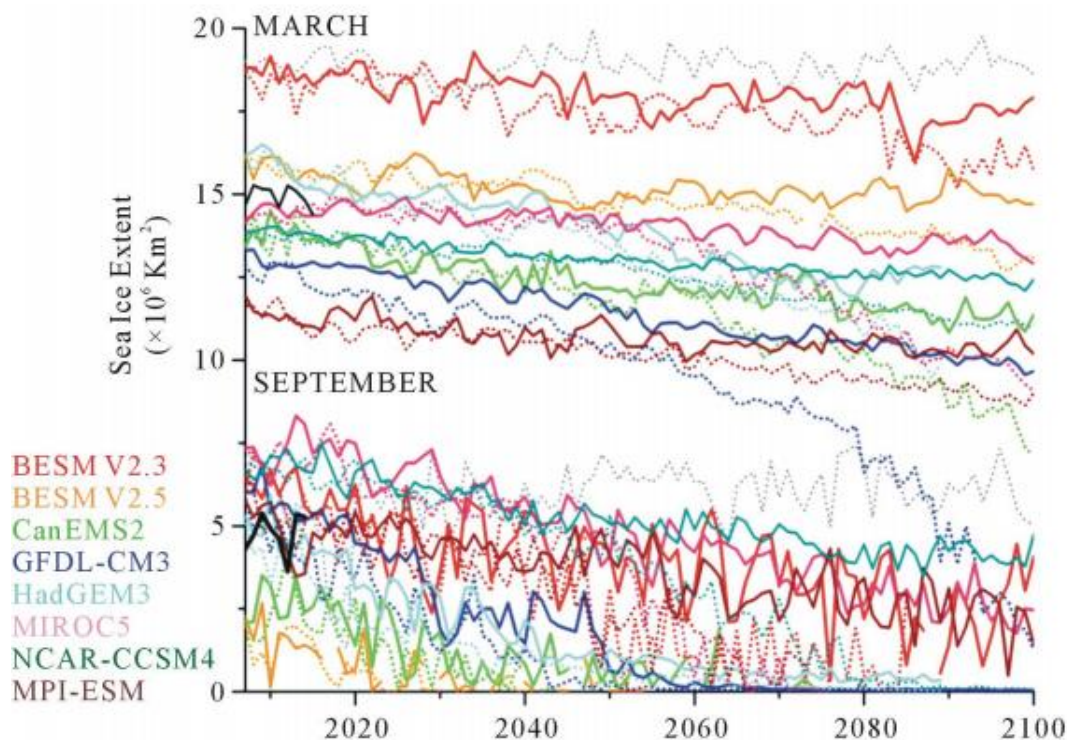


Figure 3.9. Time series of modeled Arctic SIE in September and March from 2006 to 2100, using Representative Concentration Pathways RCP4.5 (solid lines) and RCP8.5 (dash lines). Black lines are the satellite observations and gray lines refer to the control run of the BESM-OA V2.3.

3.5 Surface Anomalies Temperatures

In this section, we compare Surface Anomalies of Temperatures (SAT) for BESM-OA V2.3 and BESM-OA V2.5 to explain the differences between those versions in SIE presented in **Figure 3.9**.

Figure 3.10 shows SAT and Total Cloud Cover for BESM-OA 2.3 and BESM-OA 2.5 using future scenarios, relative to the period from 2006 to 2100. A marked warming in the northern high-latitudes is observed in both BESM versions, being notably stronger in the RCP8.5 simulation. This warming called Polar Amplification occurs due to the increase in the atmospheric greenhouse gas concentration, and is accompanied by an expressive reduction in SIE in both simulations (**Figure 3.9**). The relationship among air temperature rises and sea ice loss is evident and underpinned statistically (DOESCHER et al., 2014). Polar Amplification is associated with several feedback processes as the ice-albedo feedback, temperature, water vapor and clouds. Most of studies indicate that the ice-albedo feedback is the main contributor for enhanced Arctic warming (SERREZE; BARRY, 2011; HOLLAND; BITZ, 2003; CURRY et al., 1995). However Pithan and Maurtsen (2014), using CMIP5 simulations found that, the major contributor to the Arctic polar amplification comes from air temperature feedbacks (as the surface warms, more energy is radiated into space in lower latitudes compared with the Arctic region).

When comparing the warming between the two BESM versions, we observe that higher amplitude values are observed in BESM-OA V2.5, particularly in high latitudes between 75°N to 90°N. As a result of these warming discrepancies the SIE is lower in BESM-OA V2.5 than in BESM-OA V2.3 (**Figure 3.9**).

The microphysics of Ferrier et al (2002) and the new surface scheme based on Jimenez and Dudhia (2012) used in BESM-OA V2.5 produced an improvement in the representation of precipitation, wind, air temperature, humidity, and energy balance at the top of the atmosphere (CAPISTRANO et al., 2016). A better representation of these variables exerts strong influences in coupling ocean-atmosphere-sea ice simulations and teleconnections with higher latitudes. However, the microphysics adopted in BESM-OA V2.5 produced a decrease in the total cloud cover in the Arctic region (**Figure 3.10**). This allows the ocean to absorb more heat from incident shortwave radiation and then contribute to a greater melting of the sea ice. The

decrease in total cloud cover and consequent strong increase in SAT is consistent with the SIE reduction showed in **Figure 3.9**.

According to Jiang et al (2012), Clouds (in both ice and liquid forms) are important modulators of the climate system and are involved in several feedback processes that affect the global atmospheric circulation and the energy budget. Improving the cloud microphysics in Coupled Climate Models result in an advance in climate prediction and reduce the uncertainties in future projections. As recently pointed out by Eyring et al (2015), the understanding of the role of the clouds in the general atmospheric circulation, climate sensitivity and assessing the response of the cryosphere system to a warming climate, are among the greatest challenges for CMIP6.

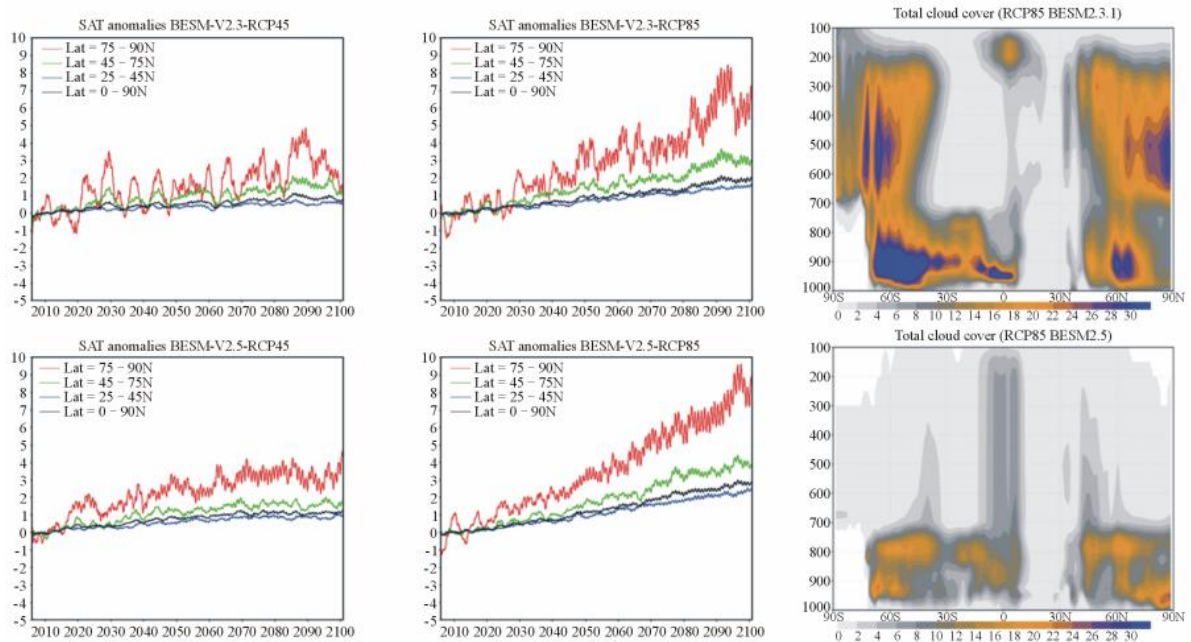


Figure 3.10. Surface Anomalies Temperature (SAT) and Total Cloud Cover (right) from January 2006 to December 2100 for BESM-OA V2.3 and BESM-OA V2.5 For SAT, the red lines represent the average for latitudes between 75°N to 90°N. Green and blue lines are for latitudes between 45°N to 75°N and 25°N to 45°N, respectively. Latitudes between 0°N to 90°N are represented by the black lines.

4 POLAR AMPLIFICATION OF CLIMATE CHANGE

4.1 Polar amplification

Here we present results from BESM-OA V2.5 compared with three state-of-the-art CMIP5 models, using an abrupt 4 x CO₂ numerical experiment to access the seasonality of polar amplification and the coupled processes involved. The main processes linked to the polar amplification are related to changes in SAT, sea ice, ocean heat content and surface energy budget and are closely associated with feedback processes (PITHAN; MAURITSEN, 2014; SCREEN; SIMMONDS, 2010; SERREZE; FRANCIS, 2006).

Figure 4.1 shows the seasonality of Arctic amplification (change in zonally SAT average) simulated by BESM-AO V2.5 and three other CMIP5 models. This gives us a measure of the warming difference between low and high latitudes.

An increase in the zonal mean surface temperature at high latitudes is evident with strongest warming in winter (DJF) and Autumn (SON), which exceeds the summer warming (JJA). These results are in agreement with observational and model simulations for both present-day and abrupt 4 x CO₂ numerical experiment (PITHAN and MAURITSEN 2014; BINTANJA; LINDEN, 2013; SERREZE et al., 2009; SERREZE; FRANCIS, 2006).

BESM-OA V2.5 and MPI-ESM-LR models show enhanced warming in both winter and summer, compared to the GFDL-ESM-LR and NCAR-CCSM4 models. The comparative simulated values in winter for zonal mean temperature are close to 30 K (BESM-OA V2.5 and MPI-ESM-LR) and 20 K (GFDL-ESM-LR and NCAR-CCSM4). For summer the values of zonal mean temperature are close to 7 K (BESM-OA V2.5) and 3 K (NCAR-CCSM4).

In CMIP5 abrupt 4 x CO₂ ensemble mean simulations presented by Pithan and Mauritsen (2014), the arctic warming for winter (summer) is close to 16 K (6.5 K). Which indicates that all of the models overestimate the Arctic winter warming in relation to the CMIP5 ensemble mean, with a more pronounced warming for both BESM-OA V2.5 and MPI-ESM-LR. Holland and Bitz (2003), using CMIP2

simulations included the NCAR model (NCAR-CCSM2) in a separated group of models with “high” Arctic warming.

According to Bintanja and Linden (2013), the CMIP5 models outputs tend to underestimate Arctic winter warming and overestimate summer warming over the last decades when compared to observational data. For long-term simulations the magnitude of simulated Arctic warming winter varies considerably among CMIP5 simulations (BINTANJA; LINDEN, 2013). The differences are in part related to feedback mechanisms, parameterizations, ocean heat uptake and sea ice conditions (BINTANJA; LINDEN, 2013; HOLLAND; BITZ, 2003).

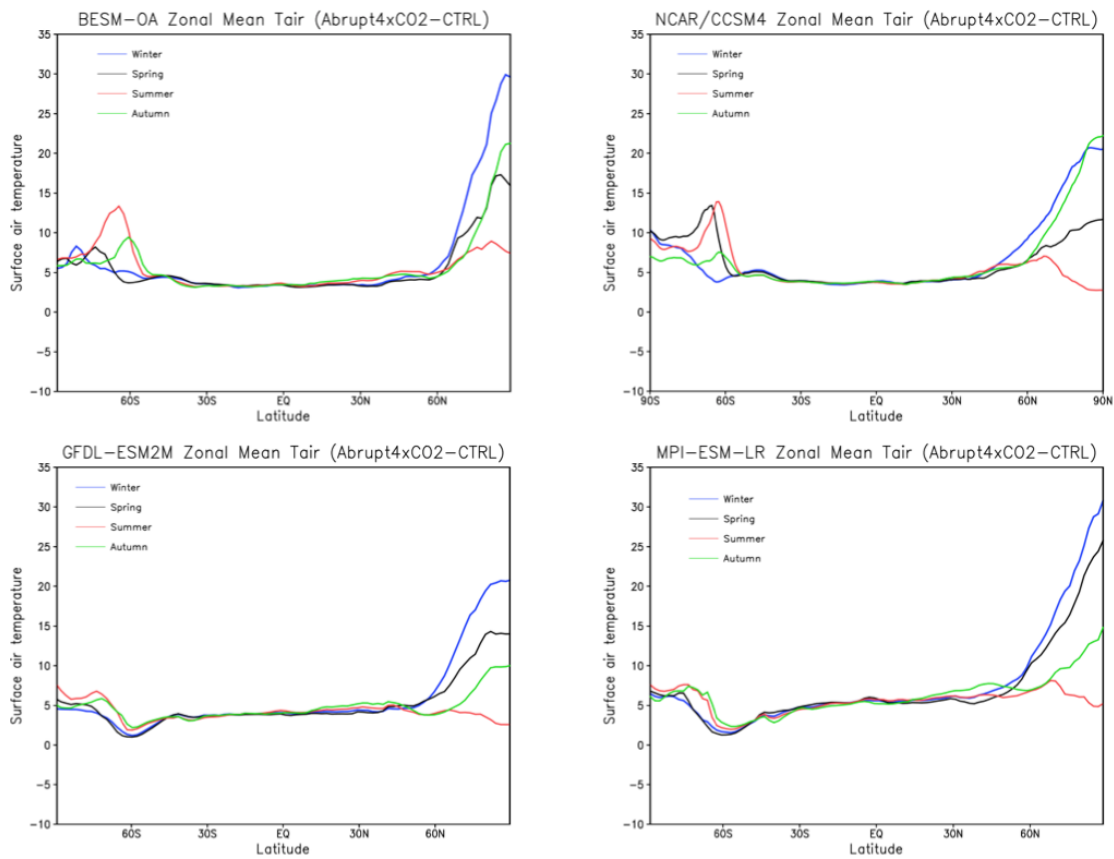


Figure 4.1. Zonal mean surface temperature (K) for the last 30 years of quadrupling atmospheric CO₂ numerical experiment compared to the last 30 years of the piControl run for the following models: BESM-OA V2.5 (top left), NCAR-CCSM4 (top right), GFDL-ESM-LR (bottom left) and MPI-ESM-LR (bottom right) in winter (DJF) represented by blue lines, spring (MAM) represented by black lines, summer (JJA) represented by red lines and autumn (SON) represented by green lines.

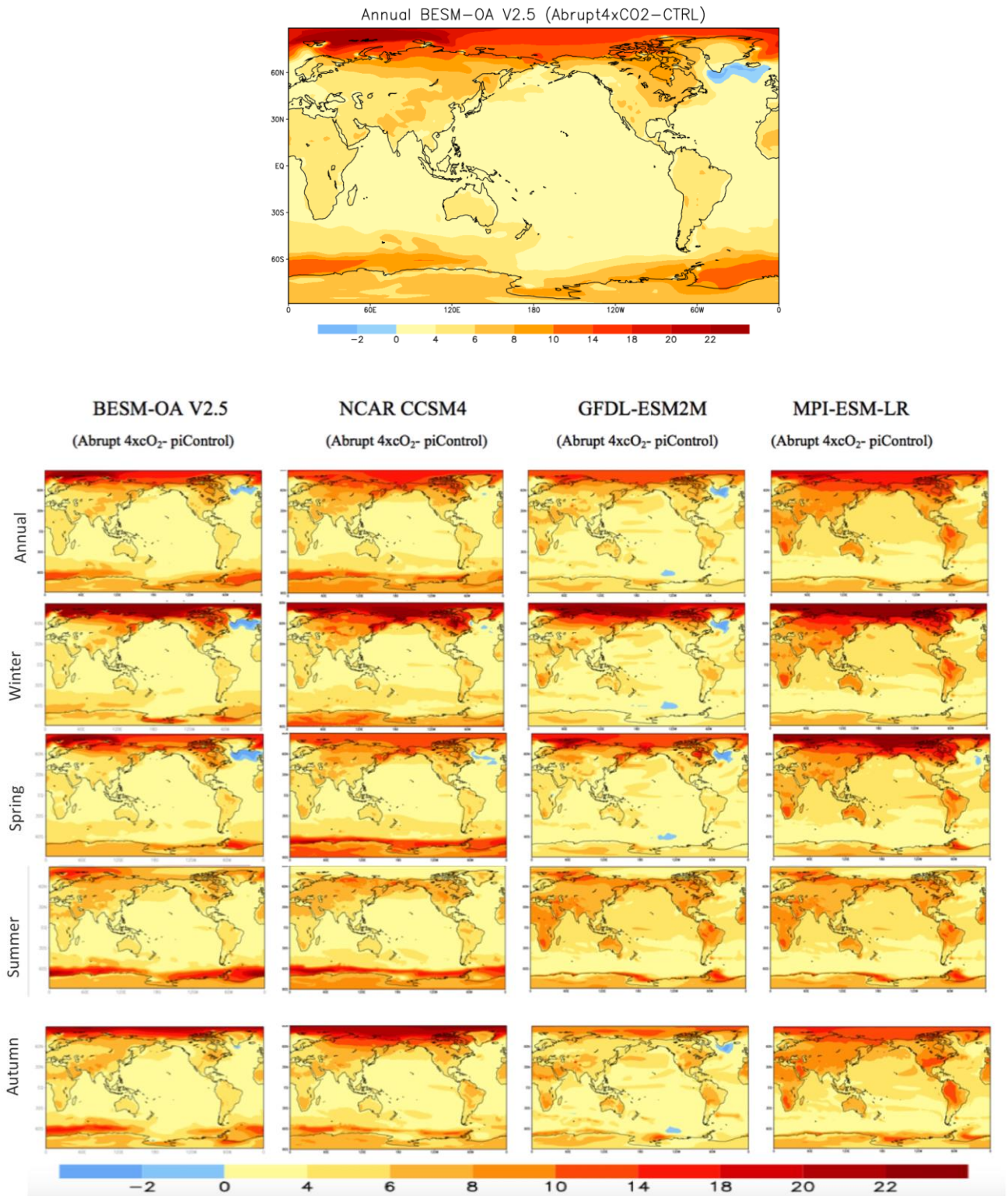


Figure 4.2. Spatial differences of surface temperature between 4 X CO₂ and piControl numerical experiments, considering only the last 30 years of each simulation in BESM-OA V2.5 annual (top) and for seasonal cycle (below) in the BESM-OA V2.5, NCAR-CCSM4, GFDL-ESM-LR and MPI-ESM-LR for winter (DJF), spring (MAM), summer (JJA) and autumn (SON).

Figure 4.2 shows the spatial differences of surface temperature between 4 X CO₂ and piControl numerical experiments, considering only the last 30 years of each simulation in BESM V2.5 and three other CMIP5 models. This allows the comparison of the spatial response of CO₂ forcing in surface temperature from different regions of the world.

The amplified winter warming at high latitudes appears as an inherent characteristic of climate models. Assessing the response of quadrupling atmospheric CO₂ in polar regions, the high southern latitudes warming is modest in relation to Arctic warming and is most pronounced in summer (JJA), with higher values found in the BESM-OA V2.5 and GFDL-ESM-LR simulations. The delayed (accelerated) warming in the Antarctic (Arctic) as a response to an increase in GHG forcing is a consequence of anomalous advection of heat out of (into) the region by the ocean (MARSHALL et al., 2014).

According Marshall et al (2014), the differences in ocean circulations asymmetries between Arctic and Antarctic, with sinking in the North Atlantic and upwelling around Antarctica affect strongly the SST response to increase in GHG concentration, accelerating (delaying) the warming in Arctic (Antarctic) region. Additionally, considering that CO₂ forcing is the same for both poles, large ozone depletion only occurs in Antarctica. Marshall et al (2014) suggest that the initial response of SST around southern high latitudes to ozone depletion is one of cooling and only later contribute to the radiative forcing warming trend as upwelling of sub-surface warm water linked with stronger surface westerlies impacts surface properties.

The main reason for enhanced winter warming at northern high latitudes pointed by Serreze et al (2009) is related to sea ice loss. During summer the energy is used to melt sea ice and increase the sensible heat content of the upper ocean (warming the upper ocean). The atmosphere loses heat to the ocean during summer whereas the flux of heat is reverse in winter. The sea ice loss in summer allows a large warming of the upper ocean but atmospheric warming is modest. The excess heat stored in the upper ocean is subsequently released to the atmosphere during winter (SERREZE et al., 2009).

4.2 Coupled ocean-atmosphere-sea ice processes

The main physical processes underlying Arctic Polar amplification will be discussed below using simulations from BESM-OA V2.5.

One of the main features of the Arctic Ocean is the presence of sea ice cover that isolates the atmosphere from the warmer ocean and is highly sensitive to CO₂ forcing. The Arctic sea ice has decreased dramatically since 1980, faster than forecasted and unprecedented in the past 1.5 millennia (STROEVE et al., 2012; STROEVE et al., 2007; KINNARD et al., 2011). Most of the state-of-the-art global climate models simulations have suggested that the Arctic will become ice-free in summer in approximately 30 years as response to increase in CO₂ concentration (STROEVE et al., 2012). **Figure 4.3** shows the seasonal cycle of SIE and SIT over the area between 70°N and 90°N, considering only the last 30 years of each simulation (piControl and abrupt 4 x CO₂).

For piControl climate simulations, mean of SIE ranges from 3 x 10⁶ km² to 16 x 10⁶ km², and the mean of SIT ranges from 0.2 m to 1.6 m. Previously studies showed that BESM-OA V2.3 represents quite well the seasonal cycle of Arctic SIE even with an overestimation in winter (CASAGRANDE et al., 2016).

The growth and melting of sea ice have an important effect on the heat balance, salinity and ocean heat content. The SIT changes tend to reinforce the warming by altering the transfer of heat and moisture from the ocean to the atmosphere (HOLLAND; BITZ, 2003).

The effect of a quadrupling of CO₂ concentration on Arctic Sea ice is a sharply decrease in SIE and SIT followed by a decrease in annual amplitude, with outstanding ice-free conditions from July to October (**Figure 4.3**). The SIT has the maximum difference between piControl and abrupt 4 x CO₂ in May (approximately 1 m) after the winter Arctic warming. The end of the melting period (when sea ice reaches its minimum annual value) is expected for July instead of September associated to a large winter decrease in SIT and contributing to a delay in sea ice formation (in Autumn). In this scenario the Arctic Ocean will become covered only by first-year-sea ice (sea ice that not survive to summer melt season). This thin sea ice is more vulnerable to melting away making the region more sensitive dynamically and

thermodynamically to temperature changes. Furthermore, we suggest an increase in leads and polynyas (regions of open water surrounding by sea ice) that promotes a very efficient exchange of heat and moisture between the relative warm ocean and cold atmosphere.

The SIT simulated in both BESM-OA V2.5 and the CMIP5 ensemble mean are too thin compared to observational data, resulting in enhanced melt and underestimation of summer SIE (CASAGRANDE et al., 2016; SHU et al., 2015; STROEVE et al., 2012). Thin sea ice conditions in the control climate simulations typically resulted in amplified warming at 4 x CO₂ conditions, given that it is easier for sea ice to melt in a warmer climate (RIND et al., 1997; RIND et al., 1995). According to Rind et al (1997), the climate sensitivity depends more on SIT than SIE from control climate simulations. Thus, we suggest that the enhanced polar warming present in BESM-OA V2.5 and MPI-ESM-LR (**Figure 4.2**) is associated with thin sea ice piControl conditions presented in **Figure 4.3**.

The close relationship between sea ice loss and decrease in albedo results in an increase of heat exchanges between the ocean and the atmosphere. This is because high sea ice albedo (>0.7) reflects most of the incoming solar radiation back to space. When sea ice melts, darker ocean (low albedo, ~0.06) is exposed to solar radiation and absorbs more energy, thus warming the upper ocean.

Winter albedo for piControl (abrupt 4 x CO₂) climate simulations varies from 0.69 to 0.72 (0.1 to 0.52). During summer, the differences between piControl and abrupt 4xCO₂ are lower since the SIE in piControl presents a small area of SIC (approximately 3 x 10⁶ km²).

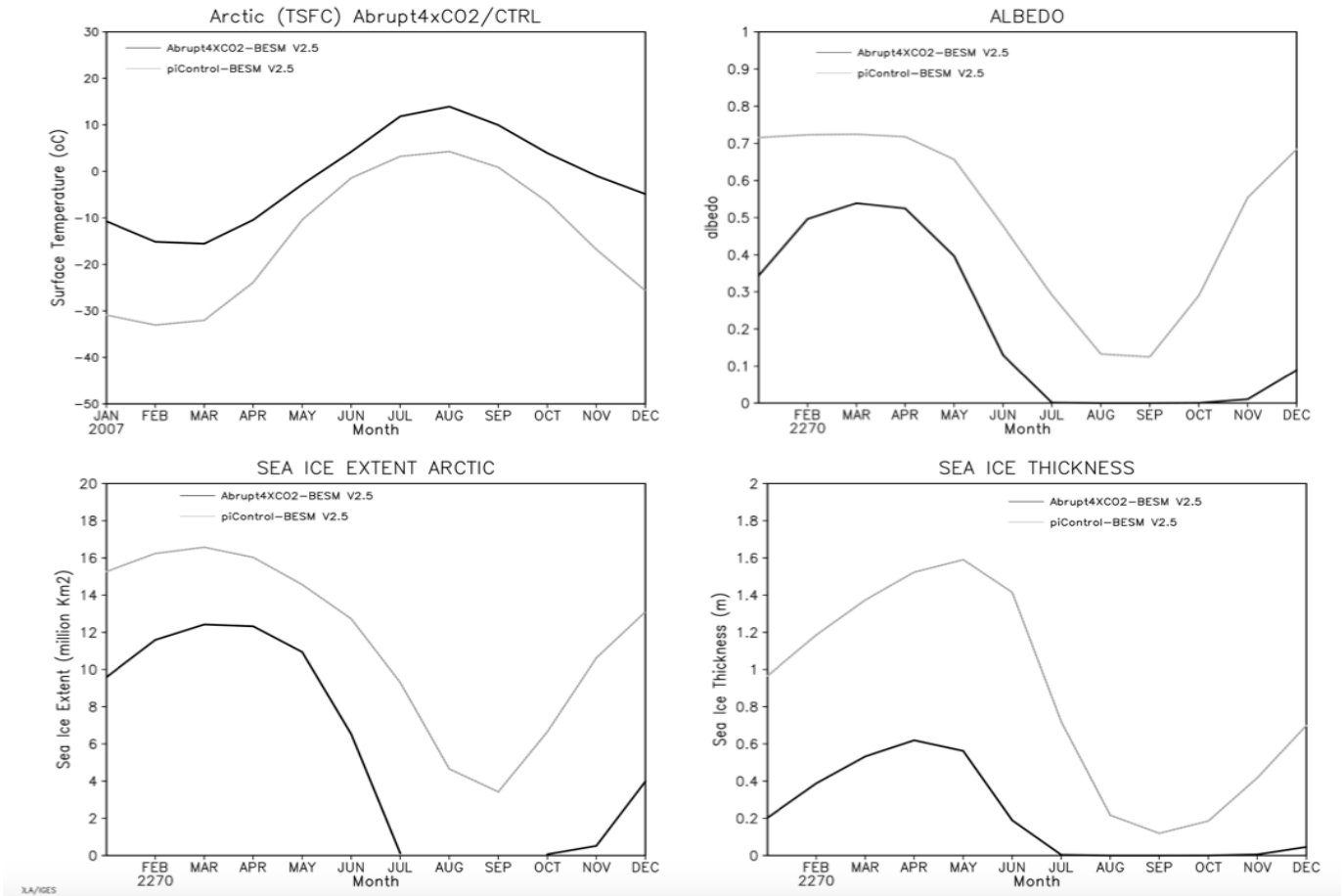


Figure 4.3. Seasonal cycle at northern high latitudes (70°N-90°N) of surface air temperature (°C), Albedo, SIE and SIT for the last 30 years of the quadrupling atmospheric CO₂ numerical experiment compared to the last 30 years of the piControl run, using BESM-OA V2.5.

The net energy fluxes are represented by the sum of net radiative fluxes (SW radiation from the sun and LW radiation emitted from the surface and by the atmosphere), sensible and latent fluxes (BOURASSA et al., 2013). Freshwater fluxes into the ocean are due to precipitation, runoff and evaporation (P+R-E) (NORTH et al., 2014; BOURASSA et al., 2013).

According to Bourassa et al (2013) the latent heat flux is the rate at which energy associated with the phase change of water is transferred from the ocean to the atmosphere, the main terms related are wind speed and humidity. Similarly, the sensible heat flux is the rate at which thermal energy (associated with temperature, but without a phase change) is transferred from the ocean or sea ice to the atmosphere. The main terms are the difference between ocean and atmosphere

temperature and wind speed.

The response of Arctic warming in heat fluxes (Sensible + Latent fluxes) over high northern latitudes is an increase for all seasons, stronger in winter (**Figure 4.4**). The seasonal cycle simulated by piControl (abrupt 4 x CO₂) ranges are from approximately 10 W*m⁻² in winter to 25 W*m⁻² in summer. Large increases are found for the same period of strong Arctic warming (autumn and winter).

The response of Arctic warming on changes in Freshwater fluxes into the ocean (Precipitation – Evaporation) over northern high latitude is an increase for all seasons, meaning that precipitation exceeds evaporation with an accentuated rise in summertime (**Figure 4.4**). The Freshwater fluxes have a quite well defined seasonal cycle. The piControl (Abrupt 4 x CO₂) simulations vary from 10 mm (35 mm) in winter to 45 mm (80 mm) in summer. According to Bintanja and Selten (2014) the projected changes in precipitation over the Arctic Ocean as response to GHG forcing is more than 50 %. Our results agree with Bintanja and Selten (2014) showing a peak of P-E in late autumn and winter associated with strongly intensified local surface evaporation and retreat of sea ice.

According Kug et al (2010) this marked increase is among the highest globally projected precipitation changes and is associated to enhanced poleward moisture transport from the lower latitudes.

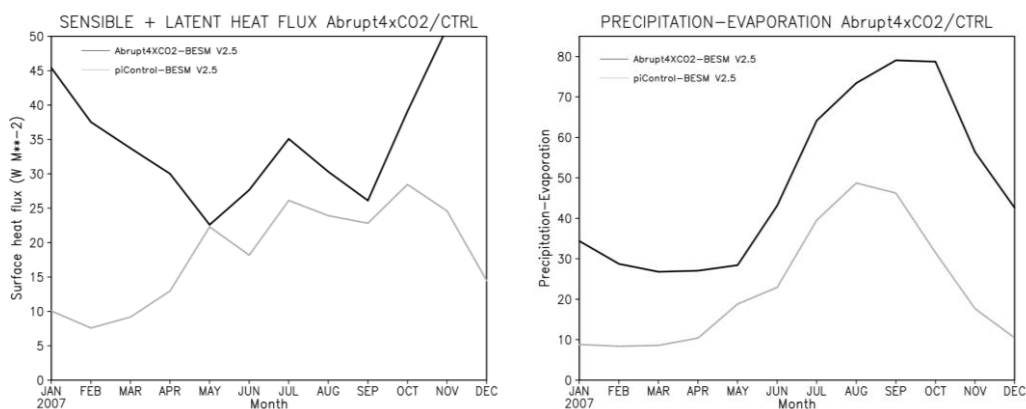


Figure 4.4. Seasonal cycle at northern high latitudes (70°N-90°N) of heat fluxes (sum of sensible and latent fluxes) and Freshwater Fluxes (Precipitation – Evaporation) for the last 30 years of quadrupling atmospheric CO₂ numerical experiment compared to the last 30 years of the piControl run, using BESM-OA V2.5.

Feedback processes in climate system may act to amplify or damp the initial radiative perturbation, such changes in CO₂ concentration. The Radiative Kernel is a powerful technique used for calculate the climate feedbacks in Global Climate Models, allowing a robust analysis of climate sensitivity (JONKO et al., 2012; SODEN et al., 2008). To quantify the feedback, the kernel is multiplied by the change in the variable of interest (e.g albedo, temperature, cloud), typically normalized by the change in global mean surface temperature (SODEN et al., 2008). Capistrano et al (2016) applied the NCAR Radiative Kernel in BESM-OA V2.5 to accesses the seasonal impact from different feedback mechanisms at northern high latitude (The Radiative Kernel NCAR are available in: <https://climatedataguide.ucar.edu/climate-data/radiative-kernels-climate-models>)

The Radiative Kernels presented below were calculated for the water vapor, lapse rate, temperature and albedo feedback for both clear sky and all sky (CAPISTRANO et al., 2016; SHELL et al., 2008). **Figure 4.5** shows the contribution of each feedback mechanism to arctic warming. Positive values are contributing to Arctic warming while negative values are indicating cooling. The surface albedo feedback describes the response of downward shortwave radiation at the Top of the atmosphere TOA to a 1% additive rise in surface albedo (SODEN et al., 2008). The large contribution of albedo feedback is evident from April to August (**Figure 4.5**). This result reinforces the simulated decrease in SIE, SIT and albedo for the same period presented in **Figure 4.3**. The Water vapor feedback is not so evident because BESM-OA V2.5 underestimated atmospheric moisture and total cloud cover for the northern high latitudes (**Figure 3.10**; CAPISTRANO et al., 2016). Even so, water vapor feedback, associated with large changes in clouds is one of the most important climate feedbacks under a global warming. This is considered one of the most important limitations of CGCMs, and is a source of uncertainties in climate simulations, particularly in high latitudes.

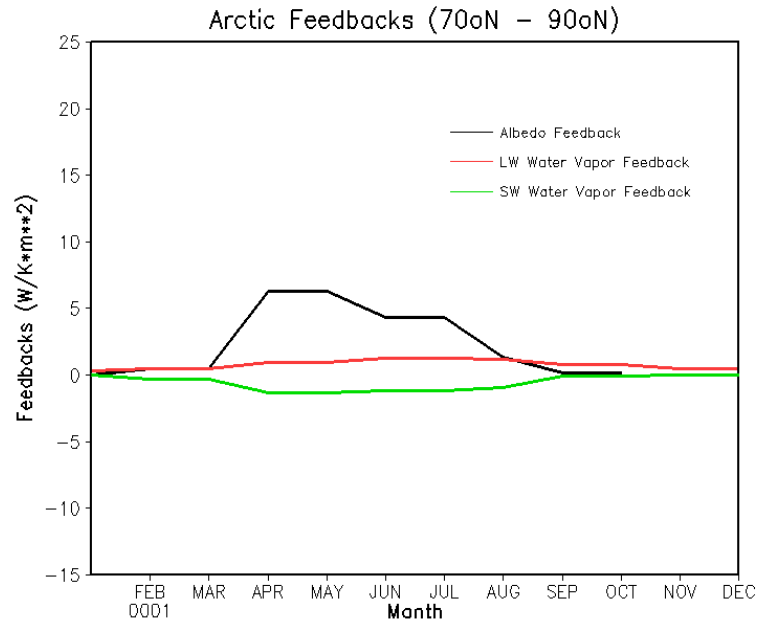


Figure 4.5. Climate feedbacks in BESM V2.5 for northern high latitudes (70°N-90°N). Black line represent albedo feedback while red and green line represent water vapour feedback for LW and SW respectively.

5 FINAL REMARKS

In this work, we evaluated the decadal simulations for the period 1980-2014 and assessed the future climate projections using RCP 4.5 and RCP 8.5 scenarios and abrupt 4 x CO₂ simulation for the period 2006- 2300, using BESM-OA 2.3, BESM-OA 2.5 and CMIP5 simulations to answer two questions.

Our First scientific question: Are Global Climate Models able to reproduce present-day sea ice changes? This was discussed in section 3. BESM-OA V2.3 results for the seasonal cycle are consistent with satellite observations and the other CMIP5 models, however almost all models tend to overestimate SIE in March in relation to observations (Figure 3.1). We suggest that the winter Arctic SIE bias is related to a LW radiation bias in climate models (Figure 3.2). Our results are in agreement with Li et al (2013); Karlsson and Svensson (2013); Sorteberg et al (2007). First, the presence of sea ice affects local albedo, which has a key influence on the energy budget, and is directly linked to the cloud-albedo effect and cloud-radiation effect. Clouds are linked with the energy budget by reflecting shortwave radiation back to space, trapping Longwave (LW) radiation and radiating it back to the surface, providing one of the strongest feedbacks in the climate system (LI et al., 2013). Second, in wintertime, the amount of solar radiation is low or non-existent, and the ability of the clouds to block the loss of reemitted LW to the space presents a positive cloud radiative feedback effect on the surface energy budget. Furthermore, section 3 of this thesis shows that the spatial patterns of climatological averages at the end of the melting season presented a deficiency in capturing the correct signature of the minimum SIE record, as well a model systematic model error between Beaufort Sea and East Siberia (Figures 3.5, 3.7, and 3.8).

Our second scientific question: What are the responses of sea ice and polar amplification to atmospheric CO₂ forcing for the global climate models including BESM? This question was partially answered in section 3, using climate projections RCP 4.5 and RCP 8.5 and partially responded in section 4 using Abrupt 4 x CO₂ simulations.

Future scenarios show an abrupt shrinking of the sea ice, with the presence of ice-free conditions during summer from the year 2045 and onwards, for both RCPs

projections (Figure 3.9). This is a result of the internal climate response to the changing in radiative forcing. Both, the Polar Amplification and feedback processes explain the rapid Arctic sea ice loss, despite the uncertainties and limitations of Global Climate Models (Figures 3.10, 4.1, 4.2, and 4.5). The sea ice responses to increased atmospheric radiative forcing are non homogeneous in CMIP5 models due to differences in the ocean, atmosphere, sea ice conditions, as well the coupling between the components in each model. In relation to Polar amplification, the results showed an enhanced increase in SAT at northern high latitudes with strongest warming in winter and autumn, which exceeds the summer warming (Figure 4.1 and Figure 4.2). These results are in agreement with observational and model simulations for both present-day, RCPs scenarios and abrupt 4 x CO₂ numerical experiments (PITHAN; MAURITSEN, 2014; BINTANJA; LINDEN, 2013; SERREZE et al., 2009; SERREZE; FRANCIS 2006). This enhanced Arctic warming results in decrease of SIE, SIT and albedo surface, causing an increase of heat transfer from the atmosphere to the ocean (Figure 4.3 and 4.4). In the Abrupt 4 x CO₂ scenario, the end of the melting season is expected for July, instead of September, associated to a large winter decrease in SIT and contributing to a delay in sea ice formation (in Autumn). In this scenario the Arctic Ocean will become covered only by first-year-sea ice in the near future. This thin sea ice is more vulnerable to melting away, making the region more sensitive dynamically and thermodynamically to temperature changes.

The way the ongoing Arctic climate change will affect the global climate system is still subject of debate. However, the relatively good representation of the Polar regions on a Earth System model can result in advances in representation of the physical processes in numerical simulations for mid and tropical latitudes. It is due to the several intertwined components of the complex, non linear climate system, which includes the polar regions as a key player. Also, it is of the most importance to stress the relevance of these results using BESM and others CMIP5 simulations for high latitudes, since *in situ* data time series collected from Polar Regions are shorter than those from the rest of the world, inhomogeneous and insufficiently dense to analyze the climate change process as a whole.

Future progress in sea ice modeling is essential for a holistic understanding of the global climate system variability and change, and requires advances in the parameterizations of climate feedback processes. The climate in the Arctic region will

change even more and will induce complex changes in the global climate, thereafter will induce changes in Arctic climate over again. In synthesis, we can say that the Arctic region and its climate are perhaps more complex than it had been foreseen.

REFERENCES

- AAGAARD, K.; CARMACK, E. C. The role of sea ice and other fresh water in the Arctic circulation. **Journal of Geophysical Research: Oceans**, v.94, p.14485-14498, 1989.
- ALEXEEV, V. A.; LANGEN P. L.; BATES, J. R. Polar amplification of surface warming on an aquaplanet in “ghost forcing” experiments without sea ice feedbacks. **Climate Dynamics**, v.24, n.7-8, p.655-666, 2005.
- AMBAUM, M., HOSKINS, B. J., STEPHENSON, D. B. Arctic oscillation or North Atlantic oscillation? **Journal of Climate**, v.14, n.16, p.3495-3507, 2001.
- ARCTIC CLIMATE IMPACT ASSESSMENT (ACIA). Cambridge: University Press, Cambridge, p. 1042, 2005.
- ARZEL, O.; FICHEFET, T.; GOOSSE, H. Sea ice evolution over the 20th and 21st Centuries as Simulated by Current AOGCMs. **Ocean Modelling**, v.12, p.401-415, 2006. Disponível em <<http://dx.doi.org/10.1016/j.ocemod.2005.08.002>>.
- BEKRYAEV, R. V.; POLYAKOV, I. V.; ALEXEEV, V. A. Role of polar amplification in long-term surface air temperature variations and modern Arctic warming. **Journal of Climate**, v.23, n.14, p.3888-3906, 2010.
- BELKIN, I. M.; LEVITUS, S.; ANTONOV, J.; MALMBERG, S-A. Great Salinity Anomalies in the North Atlantic. **Prog. Oceanogr.** **41**, 1_68 (1998).
- BINTANJA, R.; VAN DER LINDEN, E. C. The changing seasonal climate in the Arctic. **Scientific reports**, v.3, n. 1556, 2013. doi:10.1038/srep01556
- BINTANJA, R.; SELTEN, F. M. Future increases in Arctic precipitation linked to local evaporation and sea-ice retreat. **Nature**, v. 509, n. 7501, p. 479-482, 2014.
- BISHOP, M. P.; COLBY, J. D. Topographic Normalization of Multispectral Satellite Imagery. In: SINGH, V. P., SINGH, P., HARITASHYA, U. K., **Encyclopedia of Snow, Ice and Glaciers**. Springer, 2011. ISBN (978-90-481-2641-5).
- BOTTINO, M.; NOBRE, P. **Impacts of cloud cover schemes on the Atlantic Climate in the Brazilian Climate Model—BESM**. São José dos Campos: Inpe, 2015. “unpublished”.

BOURASSA, M. A.; GILLE, S. T.; BITZ, C.; CEROVECKI, I. et al. High-latitude ocean and sea ice surface fluxes: challenges for climate research. **American Meteorological Society**, v.94, p.403-423, 2013. Disponível em: <<http://dx.doi.org/10.1175/BAMS-D-11-00244.1>>.

CAI, M. Dynamical amplification of polar warming. **Geophysical Research Letters**, v.22, 2005. Disponível em: <<http://dx.doi.org/10.1029/2005GL024481>>.

CAPISTRANO, V.B.; FIGUEROA, S.N.; FERNANDEZ, J.P.R.; NOBRE, P. The new surface layer scheme of the Brazilian Earth system model. The surface ocean-lower atmosphere study. **Open Science Conference SOLAS**, Kiel, 2015

CAPISTRANO, V.B.; TEDESCHI, R.; SILVA, J.; NOBRE, P.; NETO, O.; CASAGRANDE, F.; LANFER, A.; BAPTISTA, M.; FIGUEROA, S.; VIAL, J. **Climate sensitivity of the Brazilian earth system model**. São José dos Campos: Inpe, 2016. Version 2.5. unpublished,

CARMACK, E.; POLYAKOV, I.; PADMAN, L., FER, I.; HUNKE, E. et al. Toward quantifying the increasing role of oceanic heat in sea ice loss in the New Arctic. **American Meteorological Society**, v.96, n.12, p.2079-2105, 2015.

CASAGRANDE, F.; et al. Arctic sea ice: decadal simulations and future scenarios using BESM-OA. **Atmospheric and Climate Sciences**, v.6, p.351-366, 2016.

CAVALIERI, D.J.; PARKINSON, C.L. Arctic sea ice variability and trends, 1979-2010. **The Cryosphere**, v. 6, p. 881-889, 2012. Disponível em <<http://dx.doi.org/10.5194/tc-6-881-2012>>.

CHENG, W.; CHIANG, J.; ZHANG, D. Atlantic Meridional Overturning Circulation (AMOC) in CMIP5 models: RCP and historical simulations. **Journal of Climate**, v.26, n.18, p.7187-7197, 2013.

CHYLEK, P.; LI, J.; DUBEY, M.K.; WANG, M.; LESINS, G. Observed and model simulated 20th Century Arctic temperature variability: Canadian Earth System Model CanESM2. **Atmospheric Chemistry and Physics Discussions**, v.11, p.22893-22907, 2011. Disponível em <<http://dx.doi.org/10.5194/acpd-11-22893-2011>>.

COCHRAN, P.; HUNTINGTON, O.H.; PUNGOWIYI, C.; TOM, S.; CHAPIN III, F.S.; HUNTINGTON, H.P.; MAYNARD, N.G.; TRAINOR, S.F. Indigenous frameworks for observing and responding to climate change in Alaska. **Climatic**

Change, v.120, p.557-567, 2013. Disponível em <<http://dx.doi.org/10.1007/s10584-013-0735-2>>.

COHEN, J.L.; FURTADO, J.C.; BARLOW, M.A.; ALEXEEV, V.A.; CHERRY, J.E. Arctic warming, increasing snow cover and widespread boreal winter cooling. **Environmental Research Letters**, v. 7, Article ID: 014007, 2012. Disponível em <<http://dx.doi.org/10.1088/1748-9326/7/1/014007>>.

COLLINS, W.J.; BELLOUIN, N.; DOUTRIAUX-BOUCHER, M.; GEDNEY, N.; HALLORAN, P.; HINTON, T. et al. Development and evaluation of an Earth-System Model—HadGEM2. **Geoscientific Model Development**, v.4, p.1051-1075, 2011. Disponível em <<http://dx.doi.org/10.5194/gmd-4-1051-2011>>.

CURRY, J.A.; SCHRAMM, J.L.; EBERT, E.E. Sea Ice Albedo Climate Feedback Mechanism. **Journal of Climate**, v.8, p.240-247, 1995. Disponível em <[http://dx.doi.org/10.1175/1520-0442\(1995\)0082.0.CO;2](http://dx.doi.org/10.1175/1520-0442(1995)0082.0.CO;2)>.

CURRY, R.; MAURITZEN, C. Dilution of the northern North Atlantic Ocean in recent decades. **Science** **308**, 1772_1774 (2005).

DELWORTH, T.L.; BROCCOLI, A.J.; ROSATI, A.; STOUFFER, R.J.; BALAJI, V.; BEESLEY, J.A. et al. GFDL's CM2 global coupled climate models. Part I: Formulation and Simulation Characteristics. **Journal of Climate**, v.19, p.643-674, 2006. Disponível em <<http://dx.doi.org/10.1175/JCLI3629.1>>.

Day, T. The cryosphere and global environmental change. **Polar Research**, v. 26, . 2, p. 207-208, 2007.

DICKSON, ROBERT, et al. Long-term coordinated changes in the convective activity of the North Atlantic. **Decadal Climate Variability**. Springer Berlin Heidelberg, 1996. p. 211-261

DICKSON, R. R.; MEINCKE, J.; MALMBERG, S. A.; LEE, A. J. The great salinity anomaly in the northern North Atlantic, 1968_82. **Prog. Oceanogr**, v. 20, n. 2, p.103_151, 1988.

DOESCHER, R.; VIHMA, T.; MAKSIMOVICH, E. Recent advances in understanding the Arctic climate system state and change from a sea ice perspective: a review. **Atmospheric Chemistry And Physics**, v.14, p.13571-13600, 2014. Disponível em <<http://dx.doi.org/10.5194/acp-14-13571-2014>>.

DRIJFHOUT, S.; OLDENBORGH, G. J. V.; CIMATORIBUS, A. Is a decline of AMOC causing the warming hole above the North Atlantic in observed and modeled warming patterns?. **Journal of Climate**, v.25, p.8373-8379, 2012.

GLECKLER, P. J.; DOUTRIAUX, C.; DURACK, P. J.; TAYLOR, K.E.; ZHANG, Y.; WILLIAMS, D.N; MASON, E.; SERVONNAT, J. A more powerful reality test for climate models. **Earth & Space Science News (EOS)**. v. 97, 2016. Doi: 10.1029/2016EO051663.

EYRING, V.; BONY, S.; MEEHL, G.A.; SENIOR, C.; STEVENS, B.; STOUFFER, R.J.; TAYLOR, K.E. Overview of the Coupled Model Intercomparison Project Phase 6 (CMIP6) Experimental Design and Organisation. **Geoscientific Model Development**, v.8, p.10539-10583, 2015. Disponível em <<http://dx.doi.org/10.5194/gmdd-8-10539-2015>>.

FERRIER, B.S.; JIN, Y.; LIN, Y.; BLACK, T.; ROGERS, E.; DIMEGO, G. Implementation of a New Grid-Scale Cloud and Precipitation Scheme in the NCEP Eta Model. In: CONFERENCE ON NUMERICAL WEATHER PREDICTION, v.15, 2002, San Antonio. **Preprints...** San Antonio, 2002. p. 280-283.

FICHEFET, T.; MAQUEDA, M. A. Sensitivity of a global sea ice model to the treatment of ice thermodynamics and dynamics. **Journal of Geophysical Research: Oceans**, v.102, n.6, p.12609–12646, 1997. Disponível em <<http://dx.doi.org/10.1029/97JC00480>>.

FRANCIS, J.A.; CHAN, W.; LEATHERS, D.J.; MILLER, J.R.; VERON, D.E. Winter Northern Hemisphere weather patterns remember summer Arctic Sea-ice extent. **Geophysical Research Letters**, v.36, L07503, 2009.

FRANCIS, J. A.; HUNTER, E. New insight into the disappearing Arctic sea ice. **Eos, Transactions American Geophysical Union**, v. 87, n. 46, p. 509-511, 2006.

FLOCCO, D.; SCHROEDER, D.; FELTHAM, D.L.; HUNKE, E.C. Impact of melt ponds on Arctic Sea ice simulations from 1990 to 2007. **Journal of Geophysical Research: Oceans**, v.117, C09032, 2012. Disponível em <<http://dx.doi.org/10.1029/2012jc008195>>.

GENT, P.R.; DANABASOGLU, G.; DONNER, L.J.; HOLLAND, M.M.; HUNKE, E.C.; JAYNE, S.R. et al. The community climate system model version 4. **Journal of Climate**, v.24, p.4973-4991, 2011. Disponível em <<http://dx.doi.org/10.1175/2011JCLI4083.1>>.

GORDON, C.; COOPER, C.; SENIOR, C.; BANKS, H.; GREGORY, J.; JOHNS, T.; MITCHELL, J. ; WOOD, R. The simulation of SST, sea ice extents and ocean heat transports in a coupled model without flux adjustments. **Climate Dynamics**, v.16, p.147-168, 2000. Disponível em <<http://dx.doi.org/10.1007/s003820050010>>.

GRAVERSEN, R. G.; WANG, M. Polar amplification in a coupled climate model with locked albedo. **Climate Dynamics**, v.33, n.5, p.629-643, 2009.

GRAVERSEN, R. G.; LANGEN, P. L.; MAURITSEN, T. Polar amplification in CCSM4: Contributions from the lapse rate and surface albedo feedbacks. **Journal of Climate**, v. 27, n. 12, p. 4433-4450, 2014.

GRIFFIES, S.M. **Elements of MOM4p1**. NOAA/geophysical fluid dynamics laboratory, 2009. n. 6, 444p. Ocean Group Technical Report.

GRIFFIES, S.M.; WINTON, M.; DONNER, L.J.; HOROWITZ, L.W.; DOWNES, S.M.; FARNETI, R.; ET AL. The GFDL CM3 coupled climate model: characteristics of the ocean and sea ice simulations. **Journal of Climate**, v.24, p.3520-3544, 2011. Disponível em <<http://dx.doi.org/10.1175/2011JCLI3964.1>>.

HALL, A. The role of surface albedo feedback in climate. **Journal of Climate**, v.17, n.7, p.1550-1568, 2004.

HOLLAND, M.M.; BITZ, C.M. Polar amplification of climate change in the coupled model intercomparison project. **Climate Dynamics**, v.21, p.221-232, 2003. Disponível em <<http://dx.doi.org/10.1007/s00382-003-0332-6>>.

HOLLAND, M.M.; BITZ, C.M.; TREMBLAY, B. Future abrupt reductions in the summer arctic sea ice. **Geophysical Research Letters**, v.33, L23503, 2006. Disponível em <<http://dx.doi.org/10.1029/2006gl028024>>.

HUANG, R. X.; SCHMITT, R. W. The Goldsbrough-Stommel circulation of the world oceans. **Journal of Physical Oceanography** 23.6 (1993): 1277-1284.

HUNKE, E.C.; DUKOWICZ, J.K. An elastic-viscous-plastic model for sea ice dynamics. **Journal of Physical Oceanography**, v.27, p.1849-1867, 1997. Disponível em <[http://dx.doi.org/10.1175/1520-0485\(1997\)0272.0.CO;2](http://dx.doi.org/10.1175/1520-0485(1997)0272.0.CO;2)>.

HUNKE, E.C.; LIPSCOMB, W.H.; TURNER, A.K. Sea-ice models for climate study: retrospective and new directions. **Journal of Glaciology**, v.56, p.1162-1172, 2010. Disponível em <<http://dx.doi.org/10.3189/002214311796406095>>.

JAHN, A.; STERLING, K.; HOLLAND, M. M.; KAY, J. E.; MASLANIK, J. A. et al. Late-twentieth-century simulation of Arctic Sea ice and ocean properties in the CCSM4. **Journal of Climate**, v.25, n.5, p.1431-1452, 2012.

JIANG, J.H.; SU, H.; ZHAI, C.; PERUN, V.S.; DEL GENIO, A.; NAZARENKO, L.S. et al. Evaluation of cloud and water vapor simulations in cmip5 climate models using NASA "A-Train" satellite observations. **Journal of Geophysical Research: Atmospheres**, v.117, D14105, 2012. Disponível em <<http://dx.doi.org/10.1029/2011jd017237>>.

JIMÉNEZ, P.A.; DUDHIA, J. Improving the representation of resolved and unresolved topographic effects on surface wind in the WRF Model. **Journal of Applied Meteorology and Climatology**, v.51, p. 300-316, 2012. Disponível em <<http://dx.doi.org/10.1175/JAMC-D-11-084.1>>.

JONES, P.D.; LISTER, D.H.; OSBORN, T.J.; HARPHAM, C.; SALMON, M.; MORICE, C.P. Hemispheric and large-scale land surface air temperature variations: an extensive revision and an update to 2010. **Journal of Geophysical Research**, v.117, D05127, 2012. Disponível em: <<http://dx.doi.org/10.1029/2011JD017139>>.

JONKO, A. K. et al. Climate feedbacks in CCSM3 under changing CO2 forcing. Part I: adapting the linear radiative kernel technique to feedback calculations for a broad range of forcings. **Journal of Climate**, v.25, n.15, p.5260-5272, 2012.

KAREN, M.; SHIELDS, C. A. Using the "radiative kernel" technique to calculate climate feedbacks in NCAR's community atmospheric model. In: CONFERENCE ON CLIMATE VARIABILITY AND CHANGE, 20., 2008, New Orleans, USA. **Proceedings...** New Orleans, 2008.

KARLSSON, J.; SVENSSON, G. Consequences of poor representation of Arctic Sea-Ice Albedo and cloud-radiation interactions in the CMIP5 model ensemble. **Geophysical Research Letters**, v.40, p.4374-4379, 2013. Disponível em <<http://dx.doi.org/10.1002/grl.50768>>.

KINNARD, C.; ZDANOWICZ, C.M.; FISHER, D.A.; ISAKSSON, E.; DE VERNAL, A.; THOMPSON, L.G. Reconstructed changes in Arctic Sea Ice over the Past 1450 Years. **Nature**, v.479, p.509-512, 2011. Disponível em <<http://dx.doi.org/10.1038/nature10581>>.

KNUTTI, R.; SEDLÁČEK, J. Robustness and uncertainties in the new CMIP5 climate model projections. **Nature Climate Change**, v.3, p.369-373, 2013. Disponível em <<http://dx.doi.org/10.1038/nclimate1716>>.

KUG, J.-S. et al. Role of synoptic eddy feedback on polar climate responses to the anthropogenic forcing. **Geophysical Research Letters**, v.37, n.14, 2010.

KRAUSS, W. The north Atlantic current. **Journal of Geophysical Research: Oceans**, v. 91, n.C4, p. 5061-5074, 1986.

LANGEN, P. L.; GRAVERSEN, R. G.; MAURITSEN, T. Separation of contributions from radiative feedbacks to polar amplification on an aquaplanet. **Journal of Climate**, v.25, n.8, p.3010-3024, 2012.

KWOK, R.; ROTHROCK, D. A. Decline in Arctic sea ice thickness from submarine and ICESat records: 1958–2008. **Geophysical Research Letters**, v. 36, n. 15, 2009.

LI, J.L.; WALISER, D.E.; STEPHENS, G.; LEE, S.; L'ECUYER, T.; KATO, S.; LOEB, N.; MA, H.Y. Characterizing and Understanding Radiation Budget Biases in CMIP3/CMIP5 GCMs, contemporary GCM, and Reanalysis. **Journal of Geophysical Research: Atmospheres**, v.118, p.8166-8184, 2013. Disponível em <<http://dx.doi.org/10.1002/jgrd.50378>>.

LIU, Y. et al. A cloudier Arctic expected with diminishing sea ice. **Geophysical Research Letters**, v.39, n.5, 2012.

LU, J.; CAI, M. Seasonality of polar surface warming amplification in climate simulations. **Geophysical Research Letters**, v. 36, n. 16, 2009.

LOHMANN, G.; GERDES, R. Sea ice effects on the sensitivity of the thermohaline circulation. **Journal of Climate**, v.11, p.2789-2803, 1998.

MAHAJAN, S.; ZHANG, R.; DELWORTH, T. L. Impact of the Atlantic Meridional Overturning Circulation (AMOC) on Arctic surface air temperature and sea ice variability. **Journal of Climate**, v.24, n.24, p.6573-6581, 2011.

MARSHALL, J.; et al. The ocean's role in polar climate change: asymmetric Arctic and Antarctic responses to greenhouse gas and ozone forcing. **Philosophical Transactions of the Royal Society of London A: Mathematical, Physical and Engineering Sciences**, v.372, n.2019, 2014. Disponível em: <<http://dx.doi.org/10.1098/rsta.2013.0040>>.

MARSLAND, S.J.; HAAK, H.; JUNGCLAUS, J.H.; LATIF, M.; RÖSKE, F. The Max-Planck-Institute Global Ocean/Sea Ice Model with orthogonal curvilinear coordinates. **Ocean Modelling**, v.5, p.91-127, 2003. Disponível em <[http://dx.doi.org/10.1016/S1463-5003\(02\)00015-X](http://dx.doi.org/10.1016/S1463-5003(02)00015-X)>.

MASLANIK, J. A.; FOWLER, C.; STROEVE, J.; DROBOT, S.; ZWALLY, J.; YI, D.; EMERY, W. A younger, thinner Arctic ice cover: Increased potential for rapid, extensive sea-ice loss. **Geophysical Research Letters**, v. 34, n. 24, 2007.

MEEHL G. A.; BONY, S. Introduction to CMIP5. **Clivar Exchanges**, v.16, n.2, p.4–5, 2011.

MEIER, W.N.; HOVELSRUD, G.K.; VAN OORT, B.E.H.; KEY, J.R.; KOVACS, K.M.; MICHEL, C.; HAAS, C.; GRANSKOG, M.A.; GERLAND, S.; PEROVICH, D.K.; MAKSHAS, A.; REIST, J.D. Arctic Sea Ice in Transformation: A Review of Recent Observed Changes and Impacts on Biology and Human Activity. **Reviews of Geophysics**, v.52, p.185-217, 2014. Disponível em <<http://dx.doi.org/10.1002/2013RG000431>>.

MERRYFIELD, W.J.; LEE, W.S.; BOER, G.J.; KHARIN, V.V.; SCINOCCHA, J.F.; FLATO, G.M.; AJAYAMOHAN, R.S.; FYFE, J.C. The Canadian seasonal to interannual prediction system. part i: models and initialization. **Monthly Weather Review**, v.141, p.2910-2945, 2013. Disponível em <<http://dx.doi.org/10.1175/MWR-D-12-00216.1>>.

MORICE, C.P.; KENNEDY, J.J.; RAYNER, N.A.; JONES, P.D. Quantifying uncertainties in global and regional temperature change using an ensemble of observational estimates: the HadCRUT4 dataset. **Journal of Geophysical Research**, v.117, D08101, 2012. Disponível em: <<http://dx.doi.org/10.1029/2011JD017187>>.

MORRIS, E. M.; VAUGHAN, D. G. Spatial and temporal variation of surface temperature on the Antarctic Peninsula and the limit of viability of ice shelves. **American Geophysical Union**, p.61-68, 2003.

NATIONAL SNOW AND ICE DATA CENTER (NSIDC). **Sea ice index**. Boulder, CO: University of Colorado, 2016. Disponível em: <https://nsidc.org/about/contact.html>. Acesso em: 25 jul. 2016.

NOBRE, P.; SIQUEIRA, L.S.; DE ALMEIDA, R.A.; MALAGUTTI, M.; GIAROLLA, E.; CASTELÃO, G.P.; ET AL. Climate Simulation and Change in the Brazilian Climate Model. **Journal of Climate**, v.26, p.6716-6732, 2013. Disponível em <<http://dx.doi.org/10.1175/JCLI-D-12-00580.1>>.

NORTH, G. R.; PYLE, J. A.; ZHANG, F. **Encyclopedia of Atmospheric Sciences**, Segunda Edição. Elsevier. 2014. 2998 p. ISBN (9780123822253).

NOTZ, D.; MAROTZKE, J. Observations reveal external driver for arctic sea-ice retreat. **Geophysical Research Letters**, v.39, L08502, 2012. Disponível em <<http://dx.doi.org/10.1029/2012GL051094>>.

PEROVICH, D.K. The changing arctic sea ice cover. **Oceanography**, v.24, p.162-173, 2011. Disponível em <<http://dx.doi.org/10.5670/oceanog.2011.68>>.

PITHAN, F.; MAURITSEN, T. Arctic amplification dominated by temperature feedbacks in contemporary climate models. **Nature Geoscience**, v.7, p.181-184, 2014. Disponível em <<http://dx.doi.org/10.1038/ngeo2071>>.

PROSHUTINSKY, A., R. H. BOURKE, AND F. A. MCLAUGHLIN. The role of the Beaufort Gyre in Arctic climate variability: Seasonal to decadal climate scales. **Geophysical Research Letters**, v. 29, n. 23, 2002.

RAHMSTORF, S.; FEULNER, G.; MANN, M. E.; ROBINSON, A.; RUTHERFORD, S.; SCHAFFERNICHT, E. J. Exceptional twentieth-century slowdown in Atlantic Ocean overturning circulation. **Nature climate change**, v.5, p.475-480, 2015.

RIGOR, I. G.; COLONY, R. L.; MARTIN, S. Variations in surface air temperature observations in the Arctic, 1979-97. **Journal of Climate**, v.13, p.896-914, 2000.

RIND, D.; HEALY, R.; PARKINSON, C.; MARTINSON, D. The role of sea ice in 2·co2 climate model sensitivity. part i: the total influence of sea ice thickness and extent. **Journal of Climate**, v.8, p.449–463, 1995.

RIND, D.; HEALY, R.; PARKINSON, C.; MARTINSON, D. The role of sea ice in 2·co2 climate model sensitivity. part ii: hemispheric dependencies. **Geophysical Research Letters**, v.21, p.1491–1494, 1997.

ROECKNER, E.; MAURITSEN, T.; ESCH, M.; BROKOPF, R. Impact of melt ponds on arctic sea ice in past and future climates as simulated by MPI-ESM. **Journal of Advances in Modeling Earth Systems**, v.4, M00A02, 2012. Disponível em <<http://dx.doi.org/10.1029/2012ms000157>>.

ROSSBY, T. The North Atlantic current and surrounding waters: at the crossroads. **Reviews of Geophysics**, v. 34, n. 4, p. 463-481, 1996.

SCREEN, J. A.; SIMMONDS, I. The central role of diminishing sea ice in recent Arctic temperature amplification. **Nature**, v.464, n.7293, p.1334-1337, 2010.

SCREEN, J. A.; SIMMONDS, I. Increasing fall-winter energy loss from the Arctic Ocean and its role in Arctic temperature amplification. **Geophysical Research Letters**, v.37, n.16, 2010.

SCREEN, J. A.; Influence of Arctic Sea Ice on European summer precipitation. **Environmental Research Letters**, v.8, Article ID: 044015, 2013. Disponível em <<http://dx.doi.org/10.1088/1748-9326/8/4/044015>>.

SEMTNER, A.J. A Model for the thermodynamic growth of sea ice in numerical investigations of climate. **Journal of Physical Oceanography**, v.6, p.27-37, 1976. Disponível em <[http://dx.doi.org/10.1175/1520-0485\(1976\)0062.0.CO;2](http://dx.doi.org/10.1175/1520-0485(1976)0062.0.CO;2)>.

SERREZE, M. C.; FRANCIS, J. A. The Arctic amplification debate. **Climatic change**, v.76, p.241-264, 2006.

SERREZE, M. C.; et al. The emergence of surface-based arctic amplification. **The Cryosphere**, v.3, p.11-19, 2009.

SERREZE, M. C.; BARRY, R.G. Processes and impacts of arctic amplification: a research synthesis. **Global and Planetary Change**, v.77, p.85-96, 2011. Disponível em <<http://dx.doi.org/10.1016/j.gloplacha.2011.03.004>>.

SHELL, K. M.; KIEHL, J. T.; SHIELDS, C. A. Using the radiative kernel technique to calculate climate feedbacks in NCAR's community atmospheric model. **Journal of Climate**, v.21, n.10, p.2269-2282,2008.

SHOKR, M.; SINHA, N. **Sea ice: physics and remote sensing**. John Wiley & Sons, 2015.

SHOKR, M.; NIRMAL, S. **Sea ice: physics and remote sensing**. American Geophysical Union and John Wiley & Sons, 2015. 600p. ISBN (978-1-119-02789-8).

SHU, Q.; SONG, Z.; QIAO, F. Assessment of sea ice simulations in the CMIP5 models. **The Cryosphere**, v.9, p.399-409, 2015. Disponível em <<http://dx.doi.org/10.5194/tc-9-399-2015>>.

SODEN, B. J. et al. Quantifying climate feedbacks using radiative kernels. **Journal of Climate**, v.21, n.14, p.3504-3520, 2008.

SORTEBERG, A.; KATTSOV, V.; WALSH, J.E.; PAVLOVA, T. The Arctic surface energy budget as simulated with the IPCC AR4 AOGCMs. **Climate Dynamics**, v. 29, p.131-156, 2007. Disponível em <<http://dx.doi.org/10.1007/s00382-006-0222-9>>.

SPIELHAGEN, R. F. et al. Enhanced modern heat transfer to the Arctic by warm Atlantic water. **Science**, v. 331, n.6016, p.450-453, 2011.

STEIG, E. J.; SCHNEIDER, D. P.; RUTHERFORD, S. D.; MANN, M. E.; COMISO, J. C.; SHINDELL, D. T. Warming of the antarctic ice-sheet surface since the 1957 international geophysical year. **Nature**, v.457, p. 459-462, 2009.

STÖSSEL, A.; ZHANG, Z.; VIHMA, T. The effect of alternative realtime wind forcing on Southern Ocean Sea ice simulations. **Journal of Geophysical Research**, v.116, p.1–19, 2011. Disponível em: < <http://dx.doi.org/10.1029/2011JC007328>>.

STROEVE, J.; HOLLAND, M.M.; MEIER, W.; SCAMBOS, T.; SERREZE, M. Arctic Sea ice decline: faster than forecast. **Geophysical Research Letters**, v.34, L09501, 2007. Disponível em <<http://dx.doi.org/10.1029/2007GL029703>>.

STROEVE, J.; KATTSOV, V.; BARRETT, A.; SERREZE, M.; PAVLOVA, T.; HOLLAND, M.; MEIER, W.N. Trends in Arctic Sea ice extent from CMIP5, CMIP3 and observations. **Geophysical Research Letters**, v.39, L16502, 2012. Disponível em <<http://dx.doi.org/10.1029/2012GL052676>>.

TANG, Q.; ZHANG, X.; YANG, X.; FRANCIS, J.A. Cold winter extremes in northern continents linked to Arctic Sea ice loss. **Environmental Research Letters**, v.8, Article ID: 014036, 2013. Disponível em <<http://dx.doi.org/10.1088/1748-9326/8/1/014036>>.

TANG, Q.; ZHANG, X.; FRANCIS, J.A. Extreme summer weather in Northern mid-latitudes linked to a vanishing cryosphere. **Nature Climate Change**, v.4, p.45-50, 2014. Disponível em <<http://dx.doi.org/10.1038/nclimate2065>>.

TAYLOR, K.E.; STOUFFER, R.J.; MEEHL, G.A. **A Summary of the CMIP5 experiment design**. 2009. 30 p. CMIP Report.

TAYLOR, K.E.; STOUFFER, R.J.; MEEHL, G.A. An overview of CMIP5 and the experiment design. **Bulletin of the American Meteorological Society**, v.93, p.485-498, 2012. Disponível em <<http://dx.doi.org/10.1175/BAMS-D-11-00094.1>>.

THOMPSON, D. W.; SOLOMON, S. Interpretation of recent Southern Hemisphere climate change. **Science**, v. 296, n. 5569, p. 895-899, 2002.

TIETSCHKE, S.; DAY, J.J.; GUEMAS, V.; HURLIN, W.J.; KEELEY, S.P.E.; MATEI, D.; MSADEK, R.; COLLINS, M.; HAWKINS, E. Seasonal to Interannual Arctic Sea ice predictability in current global climate models. **Geophysical Research Letters**, v.41, p.1035-1043, 2014. Disponível em <<http://dx.doi.org/10.1002/2013GL058755>>.

VAUGHAN, D.G.; COMISO, J.C.; ALLISON, I.; CARRASCO, J.; KASER, G.; KWOK, R.; MOTE, P.; MURRAY, T.; PAUL, F.; REN, J.; RIGNOT, E.; SOLOMINA, O.; STEFFEN, K.; ZHANG, T. Observations: Cryosphere. In: Stocker, T.F., Qin, D., Plattner, G.-K., Tignor, M., Allen, S.K., Boschung, J., Nauels, A., Xia, Y., Bex, V.; Midgley, P.M.(eds.). **Climate change 2013: The Physical Science Basis**, Contribution of Working Group I to the Fifth Assessment Report of the Intergovernmental Panel on Climate Change. Cambridge, United Kingdom and New York: Cambridge University Press, 2013. p.317-382.

VAVRUS, S. The impact of cloud feedbacks on arctic climate under greenhouse forcing. **Journal of Climate**, v.17, n.3, p.603-615, 2004.

VIHMA, T. Effects of Arctic Sea Ice decline on weather and climate: a review. **Surveys in Geophysics**, v.35, p.1175-1214, 2014. Disponível em <<http://dx.doi.org/10.1007/s10712-014-9284-0>>.

WADLEY, MARTIN R.; GRANT R. BIGG. Impact of flow through the Canadian Archipelago and Bering Strait on the North Atlantic and Arctic circulation: an ocean modelling study. **Quarterly Journal of the Royal Meteorological Society**, v.128, n. 85,p. 2187-2203, 2002.

WADHAMS, P. **Ice in the ocean**. [S.l.]: CRC Press, 2000.

WATANABE, M.; SUZUKI, T.; O'ISHI, R.; KOMURO, Y.; WATANABE, S.; EMORI, S.; TAKEMURA, T.; CHIKIRA, M.; OGURA, T.; SEKIGUCHI, M.; TAKATA, K.; YAMAZAKI, D.; YOKOHATA, T.; NOZAWA, T.; HASUMI, H.; TATEBE, H.; KIMOTO, M. Improved climate simulation by MIROC5 mean states, variability, and climate sensitivity. **Journal of Climate**, v.23, p.6312-6335, 2010. Disponível em <<http://dx.doi.org/10.1175/2010JCLI3679.1>>.

WHITEMAN, G.; HOPE, C.; WADHAMS, P. Climate science: vast costs of Arctic change. **Nature**, v.499, p.401-403, 2013. Disponível em <<http://dx.doi.org/10.1038/499401a>>.

WILD, M.; OHMURA, A.; GILGEN, H.; MORCRETTE, J.J.; SLINGO, A. Evaluation of downward longwave radiation in general circulation models. **Journal of Climate**, v.14, p.3227-3239, 2001. Disponível em <[http://dx.doi.org/10.1175/1520-0442\(2001\)0142.0.CO;2](http://dx.doi.org/10.1175/1520-0442(2001)0142.0.CO;2)>.

WINTON, M. A reformulated three-layer sea ice model. **Journal of Atmospheric and Oceanic Technology**, v.17, p.525-531, 2000. Disponível em <[http://dx.doi.org/10.1175/1520-0426\(2000\)0172.0.CO;2](http://dx.doi.org/10.1175/1520-0426(2000)0172.0.CO;2)>.

_____. Amplified Arctic climate change: what does surface albedo feedback have to do with it? **Geophysical Research Letters**, v.33, n.3, 2006.

WOODGATE, R.; KNUT, A. Revising the Bering Strait freshwater flux into the Arctic Ocean. **Geophysical Research Letters**, v. 32, n.2, 2005.

ZHANG, J. Increasing Antarctic sea ice under warming atmospheric and oceanic conditions. **Journal of Climate**, v. 20, n. 11, p. 2515-2529, 2007.

ZHANG, J; ROTHROCK, D.; STEELE, M. Recent changes in Arctic sea ice: the interplay between ice dynamics and thermodynamics. **Journal of Climate**, v.13, p.3099-3114, 2000.

ZHANG, Y. et al. Calculation of radiative fluxes from the surface to top of atmosphere based on ISCCP and other global data sets: Refinements of the radiative transfer model and the input data. **Journal of Geophysical Research: Atmospheres**, v. 109, n. D19, 2004.

ANEXO A

Arctic Sea Ice: Decadal Simulations and Future Scenarios Using BESM-OA

Fernanda Casagrande¹, Paulo Nobre², Ronald Buss de Souza³, Andre Lanfer Marquez², Etienne Tourigny¹, Vinicius Capistrano², Raquel Leite Mello²

¹National Institute for Space Research, Earth System Science Centre, São José dos Campos, Brazil

²National Institute for Space Research, Centre for Weather Forecasting and Climate Research, Cachoeira Paulista, Brazil

³National Institute for Space Research, Southern Center for Space Research, Santa Maria, Brazil
Email: fernanda.casagrande@inpe.br

Received 26 February 2016; accepted 26 April 2016; published 29 April 2016

Copyright © 2016 by authors and Scientific Research Publishing Inc.

This work is licensed under the Creative Commons Attribution International License (CC BY).

<http://creativecommons.org/licenses/by/4.0/>



Open Access

Abstract

Important international reports and a significant number of scientific publications have reported on the abrupt decline of Arctic sea ice and its impact on the Global Climate System. In this paper, we evaluated the ability of the newly implemented Brazilian Earth System Model (BESM-OA) to represent Arctic sea ice and sensitivity to CO₂ forcing, using decadal simulations (1980-2012) and future scenarios (2006-2100). We validated our results with satellite observations and compared them to Coupled Model Intercomparison Project, Phase 5 (CMIP5) for the same numerical experiment. BESM results for the seasonal cycle are consistent with CMIP5 models and observations. However, almost all models tend to overestimate sea ice extent in March compared to observations. The correct evaluation of minimum record of sea ice, in terms of time, spatial and area remains a limitation in Coupled Global Climate Models. Looking to spatial patterns, we found a systematic model error in September sea ice cover between the Beaufort Sea and East Siberia for most models. Future scenarios show a decrease in sea ice extent in response to an increase in radiative forcing for all models. From the year 2045 onwards, all models show a dramatic shrinking in sea ice and ice free conditions at the end of the melting season. The projected future sea ice loss is explained by the combined effects of the amplified warming in northern hemisphere high latitudes and feedbacks processes.

Keywords

Arctic Sea Ice, Climate Models, Brazilian Earth System Model

1. Introduction

Sea ice is an important and complex component of the global climate system acting both as an indicator as well as an amplifier of climate change [1]-[3]. Notz and Marotzke [4] and Doescher *et al.* [5], indicate that sea ice cover is a more robust indicator of climate change than temperature trends alone, because sea ice changes depend on integrated changes in atmospheric and ocean variables with non linear impacts, on various temporal and spatial scales under global climate forcing.

Over the last 30 years, abrupt changes in sea ice have become evident in the Arctic, especially in the summer months of 2007 and 2012 when Sea Ice Extent (SIE) reached a minimum record extent of 4.2×10^6 km² and 3.4×10^6 km², respectively. Satellite data have shown that the sea-ice loss has happened faster than forecasted and is unprecedented in the past 1.5 millennia [1] [6]-[8].

Sea ice age and sea ice thickness also have decreased rapidly resulting in a sea ice more sensitive to dynamic and thermodynamic forcing [1] [7]. There is an agreement among scientists about the direct relationship between the shrinking of the Arctic sea ice and global warming. According to Holland and Bitz [3] and Curry *et al.* [9], the range of simulated polar warming is from 1.5 to 4.5 times the global mean warming and is widely related to the sea ice-albedo feedback mechanism. Most of the climate models agree that the global air temperature will continue to rise, particularly in northern high latitudes and the Arctic will become ice free in the summer in approximately 30 years, as a response to an increase in atmospheric greenhouse gas concentrations [1] [5]. The impacts of melting sea ice in recent and future decades have not yet been fully understood and accurately quantified. Nonetheless, recent studies suggest that sea ice loss is linked to cold winter extremes in the northern continents, hot summer extremes over mid-latitudes continents, as well as wet summers and flooding in Eurasia [10]-[13].

Besides the important role of sea ice in the climate system, knowing the dynamics and geographical sea ice cover is also essential for human activities such as navigation, oil exploration and fishery [14] [15]. According to Cochran *et al.* [16] and Meier *et al.* [15], changes in Arctic threaten the infrastructure, health and safety of the Arctic indigenous people as well as present a significant risk to local marine biodiversity

According to Whiteman *et al.* [17], sea ice changes will affect all nations, not just those in the world's far north, and all should be concerned about changes that are happening in the Arctic region. In that sense, Global Climate Models, even with inherent uncertainties and limitations are powerful tools for better understanding the changes in sea ice as well as providing future scenarios to guide decision markers, governments and local communities among others.

The recent development of the Brazilian Earth System Model (BESM) is an effort of several institutions and researchers lead by the Brazilian National Institute for Space Research (INPE) to build a multidisciplinary research framework with the intent to understand the causes of global climate change, its effects and its impacts on society. The BESM model, also aims to contribute to Program for Climate Model Diagnostics and Intercomparison (PCMDI) with short-term and long-term simulations, as well as to provide futures scenarios of climate change [18]. Based on several studies and reports [5] [14] [17] [19] and understanding the importance of sea ice in the global climate system and the global economy, BESM simulations are expected to contribute with, among other variables, sea ice short and long-term simulations. BESM simulations can also be useful for future studies on ocean-atmosphere-sea ice coupling processes and impacts of sea ice loss around the world.

In this paper, we evaluated decadal simulations (1980-2012) and future scenarios (2006-2100) of SIE as simulated by two versions of the BESM and by other Coupled General Circulation Models participating in the Coupled Model Intercomparison Project, Phase 5 (CMIP5). Our goal is to evaluate the first results on the ability of BESM to represent past and future sea ice changes and sensitivity of the sea ice to the radiative forcing, using the Taylor protocol [20] [21]. The paper is structured as follows: first, we present the data sources in Section 2. Then, in Section 3, we examine the seasonal cycle, the spatial pattern and the minimum records of the Arctic sea ice, comparing the BESM decadal simulations to satellite observations and other CMIP5 models. In Section 4, we investigate the future scenarios for two different versions of BESM and the CMIP5 models, using two different scenarios, the Representative Concentration Pathway RCP4.5 and RCP8.5. We discuss the results and also indicate possible causes to explain the differences between the sea ice variation using BESM versions 2.3 and 2.5. Finally, in Section 5 we present our conclusions and lay out our recommendations for future work.

2. Data Sources

This study uses short-term simulations (decadal hindcasts) and long-term simulations (future scenarios) of 11

state-of-the-art General Circulation Models (GCMs) and Earth System Models (ESMs), seen in **Table 1**. The numerical experiment design follows the CMIP5 protocol, for decadal data and future projections based on the Taylor protocol [20] [21]. CMIP is an international effort of the scientific community to provide simulations of many different climate models in order to better understand past and future climate changes as well to provide a scientific data set for the Intergovernmental Panel on Climate Change (IPCC).

The BESM ensemble members of the decadal simulations were integrated for 10 years, each with initial conditions (IC) on 1 - 10 December of the years 1960, 1965, 1970, 1975, 1980, 1985, 1990, 1995, 2000 and 2005. Three of these ensembles (1960, 1990 and 2005) were extended for an extra 20 years for each of the 10 members, completing 30 years long integrations each. These simulations used atmospheric CO₂ concentrations derived from *in situ* air samples collected at Mauna Loa Observatory, Hawaii [18]. The Atmospheric model initial conditions for each ensemble member used the National Centers for Environmental Prediction (NCEP-NCAR) reanalysis fields for the 0000 UTC of each day from 1 to 10 December of the chosen years. The ocean initial states were chosen from the same dates from a spinup run of MOM4p1 that used prescribed atmospheric fields of momentum, solar radiation, air temperature, and freshwater described in Nobre *et al.* [18].

The future scenarios are defined by the Representative Concentration Pathways (RCPs) and each RCP defines a specific emissions trajectory and subsequent radiative forcing. The radiative forcing values in the year 2100 relative to pre-industrial values are $4.5 \text{ W}\cdot\text{m}^{-2}$ and $8.5 \text{ W}\cdot\text{m}^{-2}$ for RCP4.5 and RCP8.5 respectively, which include the period from 2006 to 2100. The CO₂ concentration in the year 2100 for each RCP is approximately 600 ppm and 1300 ppm for RCP4.5 and RCP8.5, respectively.

We compared BESM results with CMIP5 models simulations using the same numerical experiment setup. Still, the models differ in spatial resolution, physical component and parameterizations. For decadal simulations we chose to work with time series from 1980 to 2012 due to the availability of satellite observations for comparison. The SSM/I (Special Sensor Microwave Imager) satellite observations obtained from the National Snow and Ice Data Center (NSIDC) were used to validate the numerical simulations. For all simulations we calculated the SIE, defined as the area where the sea ice concentration is greater than 15% in a grid.

Table 1. CMIP5 main characteristics.

Institute/Country	Model	Experiment Design	Reference
National Institute for Space Research (INPE)-Brazil	Brazilian Earth System Model BESM-OAV2.3 BESM-OA-V2.5	Decadal RCP45/RCP85	[18]
Canadian Centre for Climate Modelling and Analysis (CCCma)-Canada	Canadian Coupled Climate Model, versions 4 and ESM2 CanCM4 CanESM2	Decadal RCP45/RCP85	[22] [23]
National Oceanic and Atmospheric Administration-Geophysical Fluid Dynamics Laboratory (GFDL-NOAA)-USA	Geophysical Fluid Dynamics Laboratory-Climate Models GFDL-CM2.1 GFDL-CM3	Decadal RCP45/RCP85	[24] [25]
Met office Hadley Centre (Met Office) United Kingdom	Hadley Centre Coupled Model HadCM3 HadGEM2-ES	Decadal RCP45/RCP85	[26] [27]
Atmospheric and Ocean Research Institute-University of Tokyo (AORI)-Japan	Model for Interdisciplinary Research on Climate MIROC 5	RCP45/RCP85	[28]
Max Planck Institute for Meteorology (MPI)-German	Max Planck Institute-Earth System Model MPI-ESM-LR	Decadal RCP45/RCP85	[29]
National Centre for Atmospheric Research (NCAR)-USA	Community Climate System Model Version 4 CCSM4	Decadal RCP45/RCP85	[30]

BESM-OA Model

In this work, we used two versions of the BESM Coupled Ocean Atmosphere (BESM-OA) model: BESM-OA V2.3 for decadal and RCP simulations and BESM-OA V2.5 for RCP simulations only. The main differences between these two versions are the microphysics scheme proposed by Ferrier *et al.* [31] and a new surface layer scheme based on Jimenez and Dudhia [32] described by Capistrano *et al.* [33] [34].

Both BESM versions used in this research are composed of the INPE/CPTEC atmospheric general circulation model (AGCM) coupled to NOAA/GFDL's Modular Ocean Model version 4p1 (MOM4p1) oceanic general circulation model (OGCM) via GFDL's Flexible Modular System [18] [35] [36]. The INPE/CPTEC AGCM has a spectral horizontal resolution truncated at triangular wave number 62, giving an equivalent grid size of 1.8758 degrees of latitude and longitude and 28 sigma levels unevenly spaced in the vertical (*i.e.*, T062L28). The exchanges of heat, moisture and momentum between the surface and atmosphere in INPE/CPTEC AGCM over the ocean and continents are computed differently by various physical processes that define the surface fluxes.

The ocean model MOM4p1 [35] from GFDL, includes the Sea Ice Simulator (SIS), described in Winton [37]. The SIS is a dynamical model with three vertical layers (two ice and one snow), and five ice thickness categories. The elastic-viscous-plastic technique of Hunke and Dukowicz [38] is used to calculate ice internal stresses, and the thermodynamics is a modified Semtner's three-layer scheme [39]. SIS calculates the concentration, thickness, temperature, brine content, and snow cover of an arbitrary number of sea ice thickness categories (including open water) as well the motion of the complete pack. Additionally, the model is responsible for calculating ice/ocean fluxes and communicating fluxes between the ocean and atmosphere models globally.

The MOM4p1 horizontal grid resolution is set to 1° in the longitudinal direction, and in the latitudinal direction the grid spacing is 1/4° in the tropical region (10°S - 10°N), decreasing uniformly to 1° at 45° and to 2° at 90° in both hemispheres. For the vertical axis, 50 levels are adopted with a 10 m resolution in the upper 220 m, increasing gradually to about 370 m of grid spacing in deeper layers. We used FMS to coupling MOM4p1 and CPTEC/AGCM. Thus, wind stress fields are computed, using Monin-Obukhov scheme within MOM4p1, from the field 10 meters above the above the ocean surface. Adjustments were done to the Monin-Obukhov boundary layer scheme, whose parameters were tuned according to the wind fields output by the CPTEC AGCM. The AGCM receives the following two fields from the coupler: sea surface temperature (SST) and ocean albedo from ocean and sea ice models at an hourly rate (coupling time step). Adjustments were also made to ocean shortwave penetration parameters due to the CPTEC AGCM supply of visible and infrared short wave radiation. The coupling variables supplied by the AGCM are as follows: freshwater (liquid and solid precipitation), specific humidity, heat, vertical diffusion of velocity components, momentum fluxes, and surface pressure.

The microphysics of Ferrier *et al.* [31] used in BESM-OA V2.5, replaced the Large Scale Precipitation scheme used in BESM-OA V2.3. This new microphysics scheme computes changes in water vapor, cloud water, rain, cloud ice and precipitation ice. Also, BESM-OA V2.5 uses a new surface layer scheme based on Jimenez and Dudhia [32] and described by Capistrano *et al.* [33] [34]. In this scheme, the surface and the first AGCM level values are used to assess wind, air temperature and humidity at 10 m. The changes introduced lead to a more consistent surface layer formulation that resulted in a near-surface wind, air temperature and humidity more consistent with observations than previous BESM version. This occurs mainly over the ocean, where those variables are important to compute the heat fluxes at ocean-atmosphere interface.

3. Results and Discussion

3.1. Seasonal Cycle

Seasonal melt-freeze transitions are important to continuously monitor sea ice over the Arctic. Sea ice formation, growth and decay are closely related to air temperature, ocean heat content, albedo and heat fluxes and hence can vary strongly from month to month [5] [40].

Thus, we present in this section the Arctic seasonal cycle of sea ice, in order to better understand the differences between the models studied, with a focus on the performance of the BESM-OA V2.3 model.

First, to understand the ability of BESM-OA V2.3 to simulate the seasonal cycle in relation to observation and other CMIP5 models, we present in **Figure 1** the seasonal cycle of climatological average of SIE from CMIP5 model and observed values for the period from 1980 to 2010.

All of the models were able to represent the seasonal cycle of the Arctic sea ice. Large oscillations between

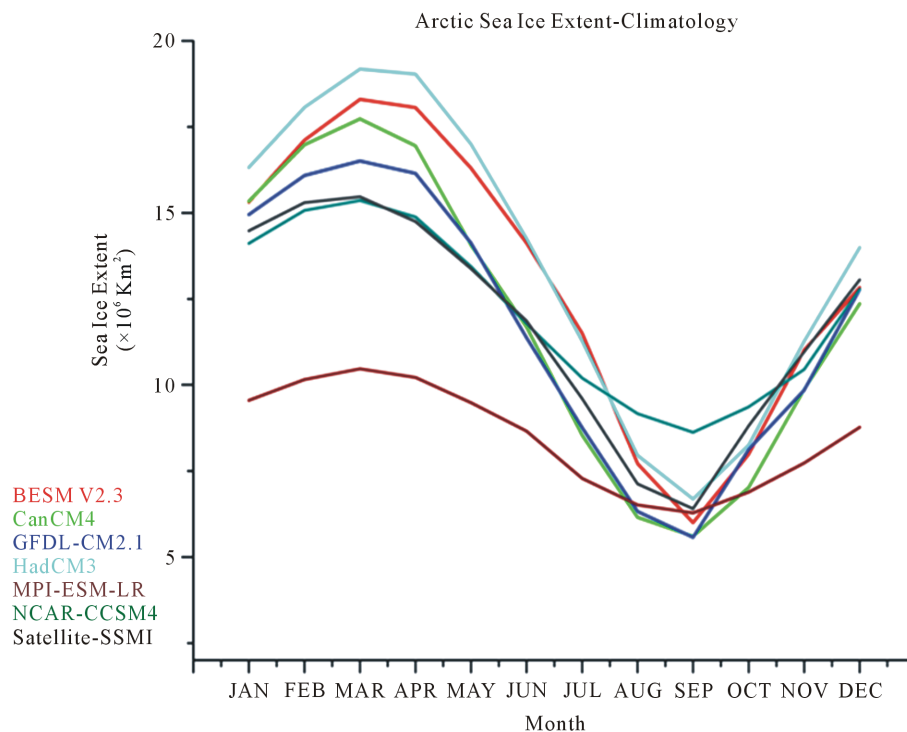


Figure 1. Climatology of SIE (1980 to 2010) in the northern hemisphere simulated by BESM-OA V2.3, CMIP5 models and observations.

summer and winter are evident, with sea ice growing from autumn and winter reaching a peak in March, and then declining throughout spring and summer as the melting season progresses.

However, most models overestimate SIE values in winter (except the MPI-ESM-LR model), and underestimate in summer (except HadCM3 and NCAR-CCSM4). BESM-OA V2.3 ensemble agrees quite well with observations and satisfactorily represents the seasonality of sea ice, although the model's sea ice decays more rapidly than observed in summer and autumn. The observational data (BESM-OA V2.3) shows that Arctic SIE varies between approximately $15 \times 10^6 \text{ km}^2$ ($18 \times 10^6 \text{ km}^2$) at winter maximum and $6 \times 10^6 \text{ km}^2$ ($6 \times 10^6 \text{ km}^2$) at summer minimum.

The difference between the model's performance for winter and summer are in agreement with [1] [26] [41] [42]. It is clear that the BESM-OA V2.3 model, even with an overestimation during winter presents a very good agreement in summer when SIE reaches critical values.

Based on our results, Sortberg *et al.* [42] and Karlsson and Svensson [43], we suggest the following scheme to explain the differences between winter and summer model's performance in representing SIE. First, the presence of sea ice affects strongly the sea ice albedo, which has a key influence on the energy budget and is directly linked to the cloud-albedo effect and cloud-radiation effect. Clouds are linked with the energy budget by reflecting shortwave radiation back to space, trapping Longwave (LW) radiation and radiating it back to the surface, providing one of more the strongest feedbacks in the climate system [44]. Second, in wintertime, the amount of solar radiation is low or non-existent and the ability of the clouds to reemitted LW to the surface presents a positive cloud radiative effect on the surface energy budget. On the other hand, during the seasons with solar radiation, the positive greenhouse effect is competing with a negative cloud albedo effect, because the clouds decrease the amount of incident solar radiation at the surface. Finally, recent publications using CMIP3 and CMIP5 models [42] [43] suggest that models generally have the tendency to underestimate the amount of LW radiation reemitted back to the surface in winter. As a consequence of these processes, the models tend to overestimate SIE in wintertime. Additionally, the annual amplitude of sea ice cover depends inversely on the model's sea ice albedo [42] [43]. BESM-OA V2.3 results agree with this scheme, as both downward and upward LW radiation at the surface are underestimated in winter. The ensemble mean is lower than the mean of the observations by approximately $30 \text{ W}\cdot\text{m}^{-2}$ (not shown). Another notable example is related to the MPI-ESM-LR

model’s performance, which presents a high sea ice albedo and low annual amplitude of sea ice. According to Wild *et al.* [45], the bias in LW radiation depends on the climate conditions and is not geographically uniform, with higher (smaller) bias in cold and dry climates (warm and humid climates) with low (high) downward LW radiation emission.

Stroeve *et al.* [1], Knutti and Sedlacek [46] and Li *et al.* [44], assessed the evolution between CMIP3 and CMIP5 and showed an improvement in the Arctic sea ice prediction and radiation in CMIP5. Nevertheless, a better representation of sea ice depends also on improvements in the representation of the Arctic sea-ice albedo, clouds, cloud-radiation effects and feedback processes.

Figure 2 shows a Taylor diagram for September, March and annual climatology of SIE. This diagram is a useful tool to compare observed and simulated data in terms of correlation coefficient, RMS and standard deviation. A shorter distance between model and REF (observed) in a Taylor Diagram indicates a better model’s performance. For the annual values (black) all the six models have a correlation with the observations higher than 0.96, while for March and September the correlation coefficient presents low values, as expected. For all models (except MPI-ESM-LR) the correlation in March is smaller than 0.6. The annual cycle of SIE is quite well represented because the seasonal cycle of SIE was well represented by all the models as shown in **Figure 1**. However, when looking at separate months, the correlation drops, as consequence in the same month time series, only the interannual variability is being evaluated. For the month of March, we suggest the previously described scheme (radiation effect) to explain the low correlation between observation and models. To understand the low correlation in September, we suggest a relation with sea ice thickness. According to Shu *et al.* [47] and Stroeve [1], the sea ice thickness simulated in the CMIP5 models is too thin, resulting in enhanced sea ice melt and an

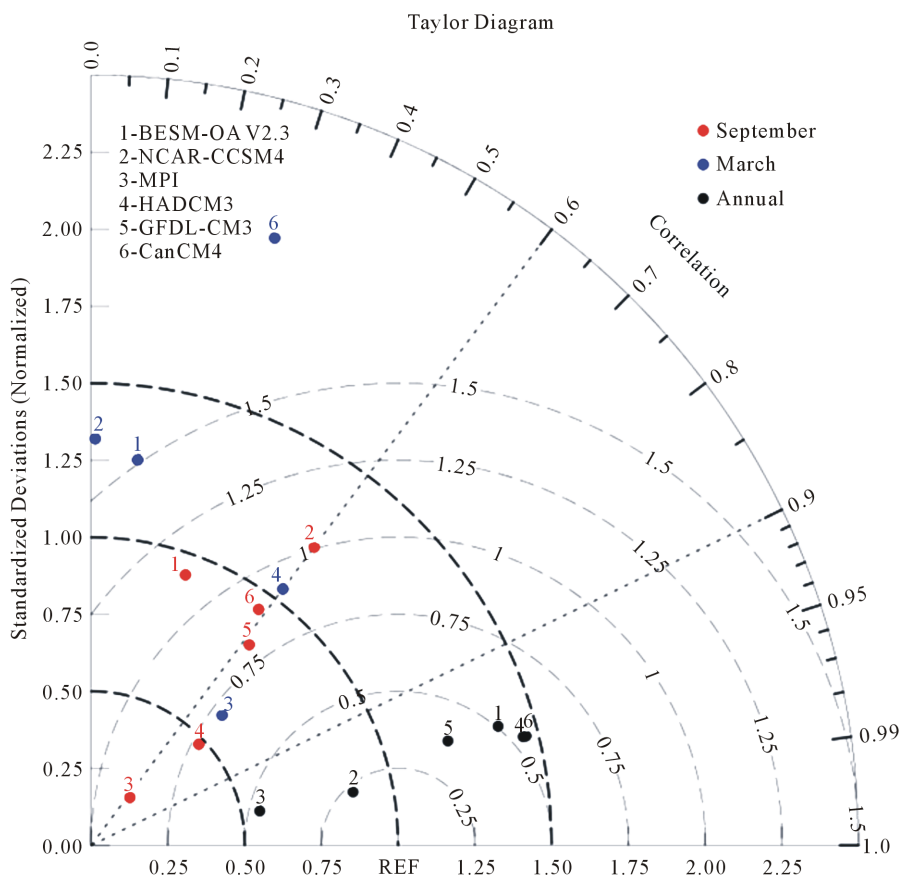


Figure 2. Taylor diagram of September, March and climatological annual cycle of SIE for the period 1980-2012. The x-axis and y-axis is the standard deviation normalized. The correlation coefficient between observations and each model is given by the azimuthal position. The centered RMS difference between simulated and observed is proportional to their distance one from another.

underestimation for SIE in summertime, as shown in **Figure 1**. BESM-OA V2.3 agrees with Shu *et al.* [47], showing an underestimate in sea ice thickness, notably greater in the marginal sea ice zones (not shown).

3.2. Spatial Pattern

Several studies have compared the observed SIE variation using climate models and CMIP data sets in a seasonal cycle or time series approach [1] [6] [41]. This type of analysis is important to know the model's ability to predict SIE. However, when considering only SIE, the information related to spatial pattern is lost. Analyzing spatial patterns avoids overconfidence in the predictions and excludes compensation of errors of opposite sign in different regions [48]. Cavalieri and Parkinson [49] also show the importance of evaluating the Arctic Ocean by regions. The authors, using satellite data set to analyze sea ice variability and trends from 1979 to 2010, found that trends for nine distinct regions in the Arctic are not homogeneous and indicated the complex nature of the Arctic climate system by regions.

Figure 3 shows September average Sea Ice Cover (SIC) observations over the study area. The spatial difference between modeled and observed SIC in September average is shown in **Figure 4**. September was chosen because commonly is when sea ice reaches its annual minimum over the Arctic.

Despite obvious inter-model differences depicted in **Figure 4**, there is a reasonable agreement between all the models. Most models tend to well represent SIC in the central Arctic, whereas the opposite occurs in marginal ice zones. There is a general tendency to underestimate SIC in areas such as the Beaufort Sea and the East Siberian Sea (except for MPI-ESM-LR and HadCM3) suggesting a systematic model error in this region. However, NCAR-CCSM4 overestimates SIC in both Laptev and Kara Sea (**Figure 4**). This may reflect the NCAR model's overestimation observed for September and shown in **Figure 1**.

The SIC in the region between Canada and Greenland is well represented by BESM-OA V2.3, GFDL-CM2.1 and MPI-ESM-LR models, while SIC between East Siberia and the Barents Seas is only well simulated by

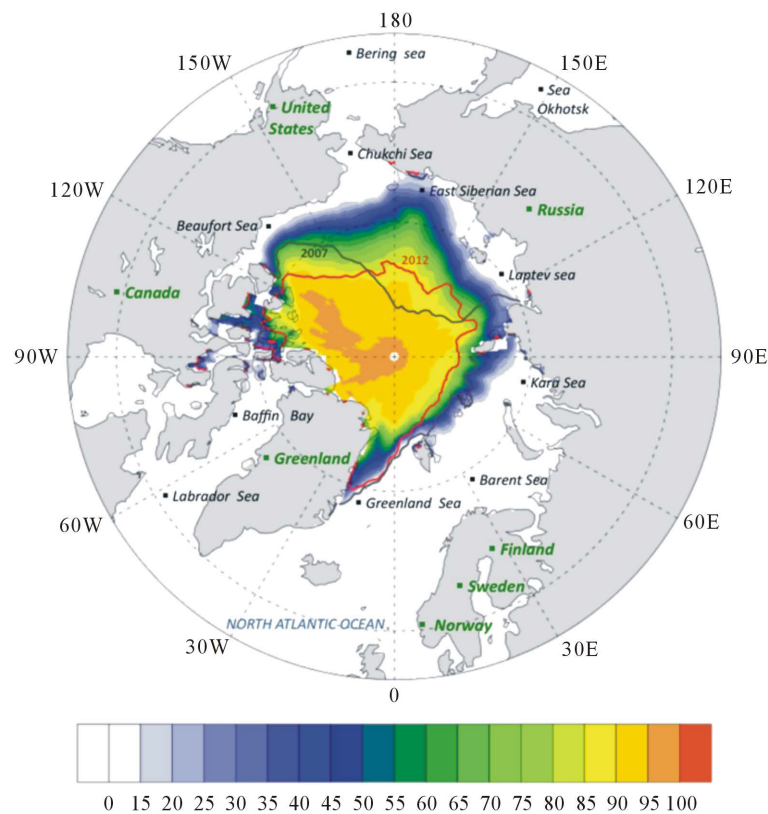


Figure 3. Arctic study area and September SIC Climatology (1980-2010) from satellite observations (shaded colors). Dark gray and orange lines refer to the 2007 and 2012 minimum events respectively.

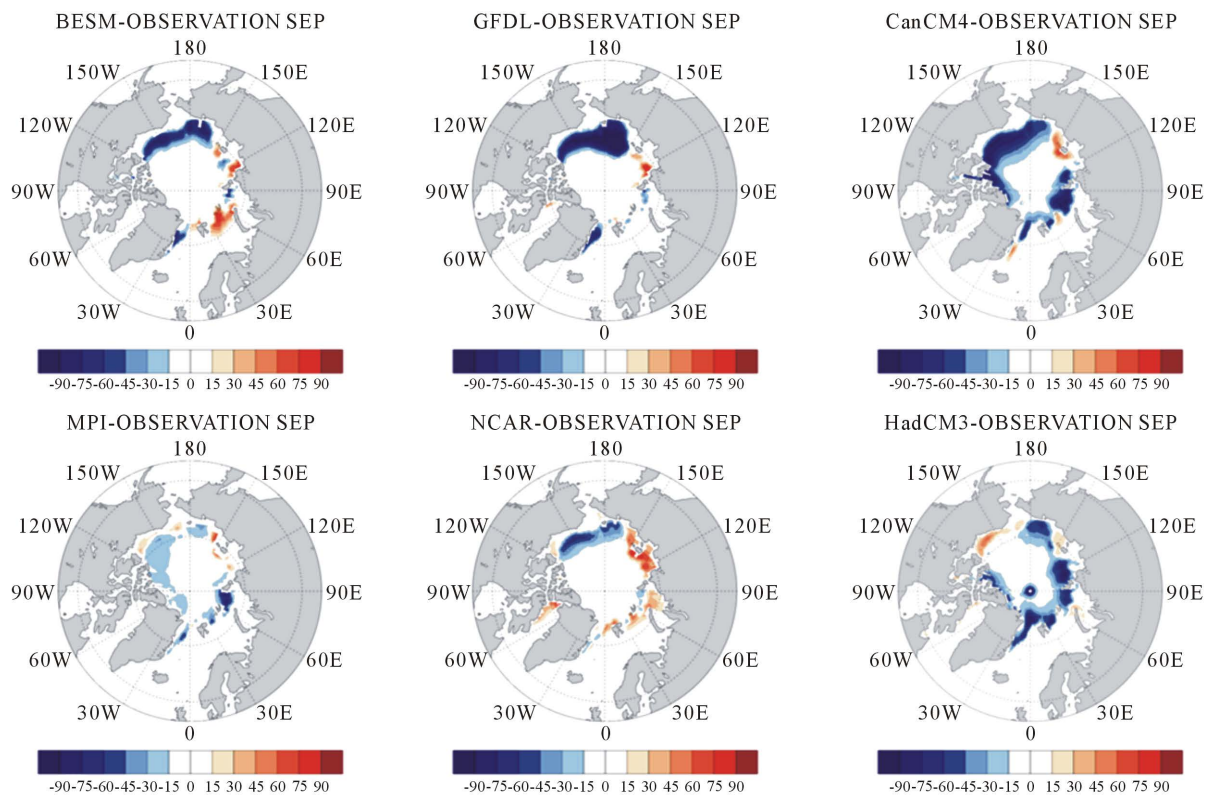


Figure 4. Difference between model simulations and observations for September SIC climatologic average from 1980 to 2010. BESM-OA V2.31, GFDL-CM2.1, CanCM4 (upper) MPI-ESM-LR, HadCM3, NCAR-CCSM4 (bottom). Positive (negative) value depicted in red (blue) represent areas where the model overestimates (underestimates) sea ice concentration values.

MPI-ESM-LR model. Despite a good representation of the spatial pattern of SIC in the MPI-ESM-LR model in September (Figure 4), it is clear that the amplitude of its annual cycle is smaller than both the others models and satellite observations (Figure 1). This reveals a certain deficiency in representing physical processes between ocean-atmosphere-sea ice, although the good representation during summer.

The detailed analysis of simulated SIC by regions using Climate Models is justifiable due to both economic and scientific reasons. Economically, as a result of sea ice loss maritime transports may gain two new routes with the opening of the “Northwest Passage” in Northern Canada and Greenland, and the “Northeast Passage” between Northern Russia and Norway [14]. This is considered a hot topic because these passages could lead to fast and cheaper ship transport between Europe and North America. Scientifically, this is relevant because the importance of properly account for the dynamical/thermodynamical processes taking place in shaping SIC over the Arctic region.

It is instructive to compare Figure 1 with Figure 4, analyzing only SIE in September for GFDL-CM2.1 and CanCM4 models (Figure 1). This can induce overconfidence in how well the models agree (SIE in both models are approximately 5.6×10^6 km²). However, when we look at the spatial patterns in Figure 4, we find quite different SIE distributions. CanCM4 model shows a large area of high negative values (especially between Greenland and Canada), whereas GFDL-CM2.1 shows a small area of high negative values only in parts of Beaufort Sea and East Siberian Sea. Thus, even some climate models showing a good performance in simulating SIE during summertime do not necessarily simulate a realistic spatial sea ice distribution.

3.3. Minimum of Sea Ice Extent

Changes in ice extent due to the seasonal cycle are so large that they tend to obscure any signal related to inter-annual variability. To remove the strong seasonal cycle, we again specifically focus on September since it shows the minimum annual of SIE. According to Doescher *et al.* [5], the ability to identify real changes in the Arctic

Climate System increases when we focus on individual seasons. In this context, **Figure 5** shows the SIE time series of September averages from 1982 to 2014.

Arctic sea ice has declined sharply during the last three decades, with record low summer ice cover in September 2007 and 2012 as illustrated in **Figure 1**. Here, we show the time series of SIE and analyze the ability of the models to represent recent changes.

Arctic SIE averages from 1980 to 2010 (**Figure 5**) show a noticeable decrease in Arctic SIE. September SIE simulated by BESM-OA V2.3 (satellite observations) between 2000 and 2010 was $4.2 \times 10^6 \text{ km}^2$ ($5.7 \times 10^6 \text{ km}^2$), while between 1980 and 1990 it was $6 \times 10^6 \text{ km}^2$ ($7.1 \times 10^6 \text{ km}^2$), showing a reduction of approximately 30% (19.8%) in SIE. March SIE for example (not shown), although at a slower rate in comparison to September, also decreases with time.

The minimum satellite record of SIE occurred in September 2012, with $3.6 \times 10^6 \text{ km}^2$ against $4.5 \times 10^6 \text{ km}^2$ in BESM-OA V2.3. In 2012, satellite observations (GFDL-CM2.1) presented a decrease of 50.4% (42.3%) of SIE in relation to the 1980s decade. Except for the GFDL-CM2.1 model, no other model was able to well represent the observed 2012 minimum. However, BESM-OA V2.3 and CanCM4, generated episodes of low SIE in September with a magnitude and behavior comparable with the low observed in 2012. These episodes of minimum SIE occurred in 2006 and 2002 for the BESM-OA V2.3 and CanCM4 models, respectively. According to Doscher *et al.* [5] and Holland *et al.* [50], such abrupt sea ice loss resulted from a complex interplay between the thermodynamics and dynamics of sea ice, ocean and atmosphere and successful prediction requires careful initialization with ocean and sea ice conditions.

Figure 6 illustrates the spatial distribution of average September SIE (left) and minima of September SIE value found between 1980 and 2010 (right) for all the models evaluated in this work. This figure aimed to show the model's performance to represent the spatial pattern in episodes of low SIE, regardless of year.

Looking at the spatial patterns of the SIE climatological mean and minimum record, it is clear that the climate models are able to reproduce the seasonal cycle of the SIE (**Figure 1** and **Figure 2**) better than they represent the minimum records. Only GFDL-CM2.1 model presents a good spatial agreement of minimum records with observation. This could be explained by two main reasons. First, it was the only one that matched the spatial pattern of the observed minimum, which may lead to a better agreement with observed meteo-oceanographic patterns (not studied here). Second, it may be related to a better representation of the sea ice and feedbacks processes in the parameterizations of the GFDL-CM2.1 model. Two other models (BESM-OA V2.3 and CanCM4) also show a reasonable spatial agreement with observations, although not as well as GFDL-CM2.1. These two models presented an underestimation of SIE, but presented a very good representation of the SIE in

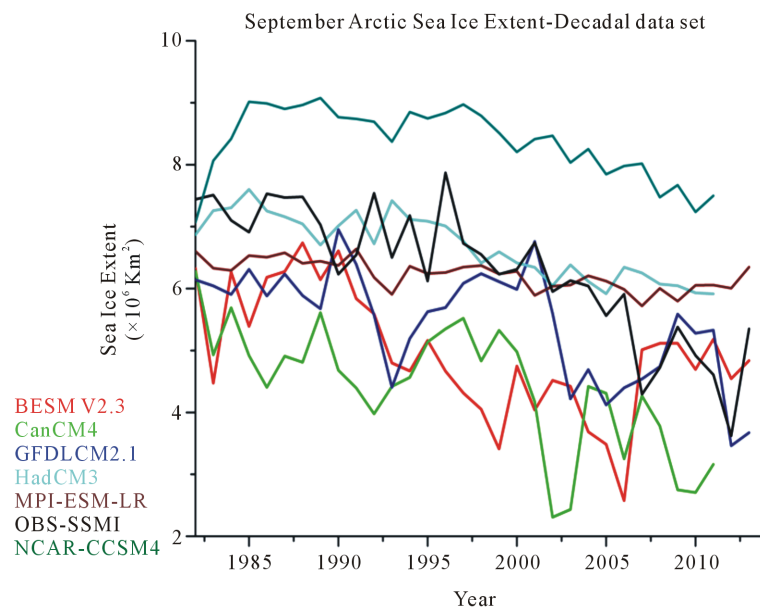


Figure 5. Arctic sea ice extent time series of September from 1980 to 2014 for CMIP5 models and observational data.

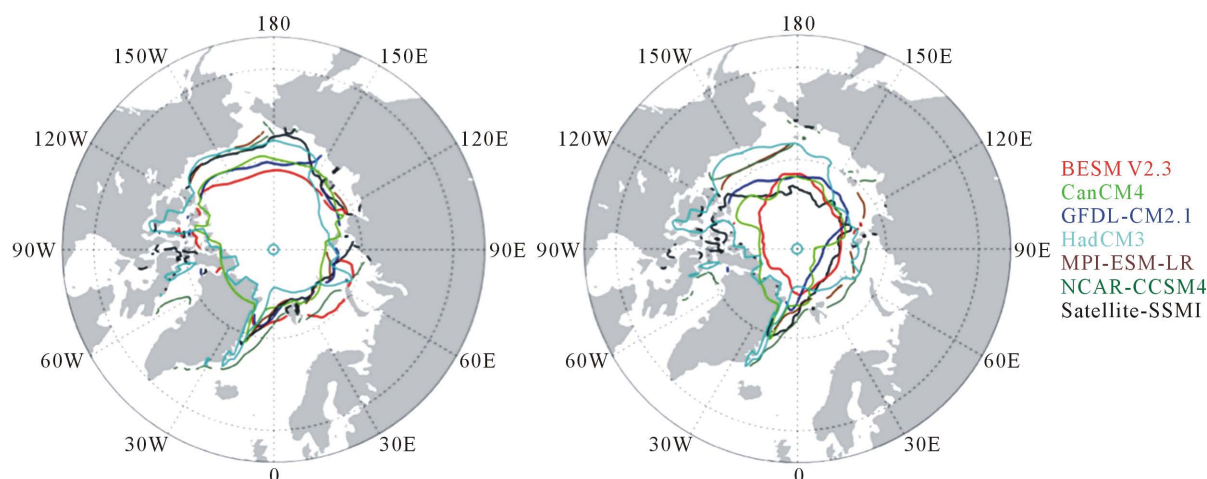


Figure 6. Spatial distribution of SIE average (left) and lowest values of September SIE found between 1980 to 2010, (right), for all CMIP5 models evaluated in this work.

the central Arctic region (**Figure 6**). The minimum record for the BESM-OA V2.3 shows a deficiency near Greenland and at the north of Canada. We understand that this happens because of the overestimation of Sea Surface Temperature (SST) in that region by the BESM-OA V2.3 model (not shown). Although BESM-OA V2.3 and CanCM4 were capable to capture the correct signature of the SIE minimum record with a decrease in SIE followed by an increase in the following year (**Figure 5**), the correct estimation of minimum SIE, in time, spatial, area and processes signatures remains a challenge for the modeling community.

Due to the sea ice retreat in recent Septembers months, ice cover in the following spring tends to be thinner, thus vulnerable to melting in summer. According to Doscher *et al.* [5], each record of low SIE is followed by a partial recovery. Additionally, Tietsche *et al.* [48] suggest that the minimum record of SIE during a single September is reversible, as the albedo sea ice mechanism is compensated by large scale recovery mechanisms. According to Vihma [51] the sea ice loss increases the heat flux from the ocean to the atmosphere in early winter and autumn. As result of this, a local increase of air temperature, humidity and cloud cover is expected thus reducing the stability of the atmospheric boundary layer.

Hunke *et al.* [52] evaluated the retrospective and new directions of sea ice models. The authors indicated some deficiencies in the dynamics (e.g. transport processes, dynamic coupling and mechanical redistribution) and thermodynamics (e.g. feedback processes and melt ponds) and suggested that improvements in the sea ice prediction dependent on improvements in the descriptions of the physical processes and characteristics, as well as, extending the models for Earth System Model simulations including biogeochemistry. According to Flocco *et al.* [53] and Roeckner *et al.* [54], one of the processes, poorly represented in sea ice models, is the formation and evolution of melt ponds. Melt ponds affect the heat and mass balances of SIC, mainly by reducing albedo by up to 20%. Consequentially, a reduction of the sea ice volume can reach 40%, leading to further sea ice melt. At the end of the melting season, melt ponds cover up to 50% of the sea ice surface. A better representation of the melt pond scheme will improve the sea ice simulation and is essential for accurate future sea ice projections.

3.4. Future Projection of Arctic Sea Ice

The long-term evolution of SIE in the northern hemisphere as simulated by BESM and CMIP5 models, using RCP4.5 and RCP8.5 is shown in **Figure 7**. The simulations clearly show a decrease in SIE up to 2100, for all simulations and both RCPs. Arctic SIE decline with the increase of the radiative forcing in all models. The BESM-OA V2.3 control experiment (gray lines in **Figure 7**) reinforce that ice-free conditions only happen when external forcing from anthropogenic sources are include in climate model simulations. These results are in agreement with Stroeve *et al.* [1].

For September, at the beginning of the series (2006 to present-day), the HadGEM2 model SIE values are close to satellite observations. During March the best representation of the observed data was obtained by MIROC5 and BESM-OA V2.5 models.

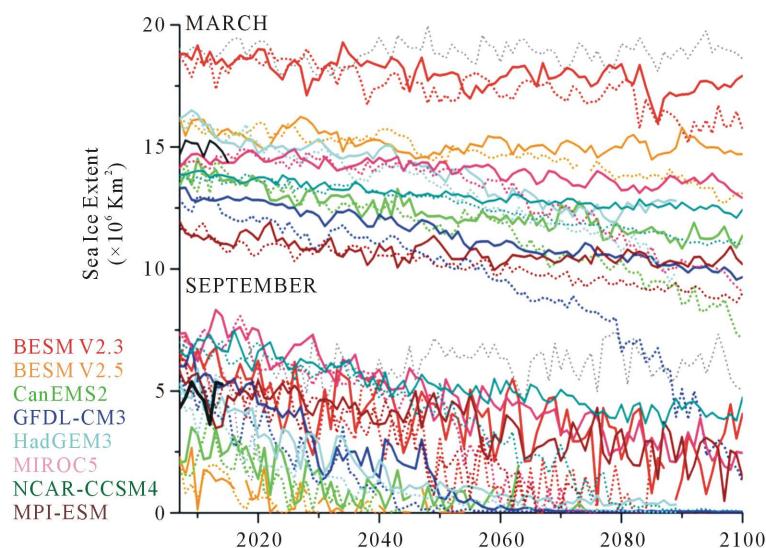


Figure 7. Time series of modeled Arctic SIE in September and March from 2006 to 2100, using Representative Concentration Pathways RCP4.5 (solid lines) and RCP8.5 (dash lines). Black lines are the satellite observations and gray lines refer to the control run of the BESM-OA V2.3.

During the first 30 years of the series, values from both RCPs are very similar in March and September months. For March, the SIE in the first years of the 21st century ranges from $11.8 \times 10^6 \text{ km}^2$ (MPI-ESM-LR) to $18.8 \times 10^6 \text{ km}^2$ (BESM-OA V2.3) in the RCP4.5 simulation. For the RCP8.5 simulation they vary between $11.7 \times 10^6 \text{ km}^2$ (MPI-ESM-LR) and $18.4 \times 10^6 \text{ km}^2$ (BESM-OA V2.3). For September SIE values vary from approximately $2 \times 10^6 \text{ km}^2$ (BESM-OA V2.3) to $6.7 \times 10^6 \text{ km}^2$ (MIROC 5). Already during these early years, it is possible to observe the discrepancy between the two different BESM configurations.

For all RCP simulations, BESM-OA V2.3 and BESM-OA V2.5 show higher (lower) values in SIE during March (September) when compared to other models used in this work. The models reveal strong amplitudes in SIE between different seasons. Both BESM simulations clearly present the higher values in March for all years. However, for September the higher SIE was found in MIROC5 model (similar amplitude was observed in MPI-ESM-LR model).

It is possible to observe a higher inter-annual variability in September than in March for all models, as well as for the early period's satellite observations. The changes in inter-annual variability are important for sea ice prediction and frequency and for assessing the frequency of occurrence of extreme SIE anomalies.

It is noteworthy that the models comparatively show different tendencies for the months of maximum and minimum SIE. For the month of March, the MPI-ESM-LR model presented the lowest values compared to the other models used here, whereas for the month of September the lowest values encountered are those of the BESM-OA V2.5 model. In general, when compared to the other CMIP5 models, the BESM-OA V2.3 model tends to overestimate SIE in March and September, for both RCP simulations.

From the year 2040 onward, all models show a dramatic shrinking in SIE in the RCP 8.5 scenario. This indicates a high sensitivity of sea ice cover in response to an increase in the atmospheric carbon dioxide. The GFDL-CM3 model clearly shows this abrupt decrease in SIE with the RCP8.5 scenario when compared to the RCP4.5 one. In this case, the decline is so strong that at the end of the 21st century the SIE maximum (in March) is similar to the minimum SIE (in September) found in the beginning of the 21st century. If the GFDL-CM3 model is reasonably correct, it means that the Arctic can be ice-free also during the coldest season of the year just after 2100.

For September, ice-free conditions (defined as less than $0.5 \times 10^6 \text{ km}^2$) are obtained from 2020 in Can-ESM2 model, BESM-OA V2.5 and HAGEM2-2S with the RCP8.5 scenario. According to Chylek *et al.* [23] the addition of the land-vegetation model and terrestrial oceanic interactive carbon cycle to the coupled atmosphere-ocean in the Can-ESM2 model improved the simulations, although increased the overestimation of atmospheric warming after 1970. That explains the minimum values found here for CAN-ESM2 sea ice projections.

Also focusing on the RCP8.5 scenario, most of the models show ice free situations, or episodes, after 2045 for the month of September. The exceptions are BESM-OA V2.3 and NCAR-CCSM4. These two models are a bit more conservative than the others, pointing out to ice free situations to starting after 2060.

It is expected that ice-free conditions will have strong effects on the global climate system though changes in both ocean and atmospheric circulations. It is known that sea ice loss amplifies the effects of radiative forcing by the albedo-sea ice feedback mechanism and cloud effects. It also, affects the meridional and inter-hemispheric temperature gradients that can affect mid-latitude circulation. However the quantification of these effects remains unclear requiring improvements in the global climate models.

3.5. Surface Anomalies Temperatures

In this section, we compare Surface Anomalies of Temperatures (SAT) for BESM-OA V2.3 and BESM-OA V2.5 to explain the differences between those versions in SIE presented in Figure 8.

Figure 8 shows SAT and Total Cloud Cover for BESM-OA 2.3 and BESM-OA 2.5 using future scenarios, relative to the period from 2006 to 2100. A marked warming in the northern high-latitudes is observed in both BESM versions, being notably stronger in the RCP8.5 simulation. This warming called Polar Amplification (PA) occurs due to the increase in the atmospheric greenhouse gas concentration, and is accompanied by an expressive reduction in SIE in both simulations (Figure 8). The relationship among air temperature rises and sea ice loss is evident and underpinned statistically [5]. PA is associated with several feedback processes as the ice-albedo feedback, temperature, water vapor and clouds. Most of studies indicate that the ice-albedo feedback is the main contributor for PA [2] [3] [9]. However Pithan and Maurtsen [55], using CMIP5 simulations found that, the major contributor to PA comes from air temperature feedbacks (as the surface warms, more energy is radiated into space in lower latitudes compared with the Arctic region).

When comparing the warming between the two BESM versions, we observe that higher amplitude values are observed in BESM-OA V2.5, particularly in high latitudes between 75°N to 90°N. As a result of these warming discrepancies the SIE is lower in BESM-OA V2.5 than in BESM-OA V2.3 (Figure 7).

The microphysics of Ferrier *et al.* [31] and the new surface scheme based on Jimenez and Dudhia [32] used in BESM-OA V2.5 produced an improved in the representation of precipitation, wind, air temperature, humidity,

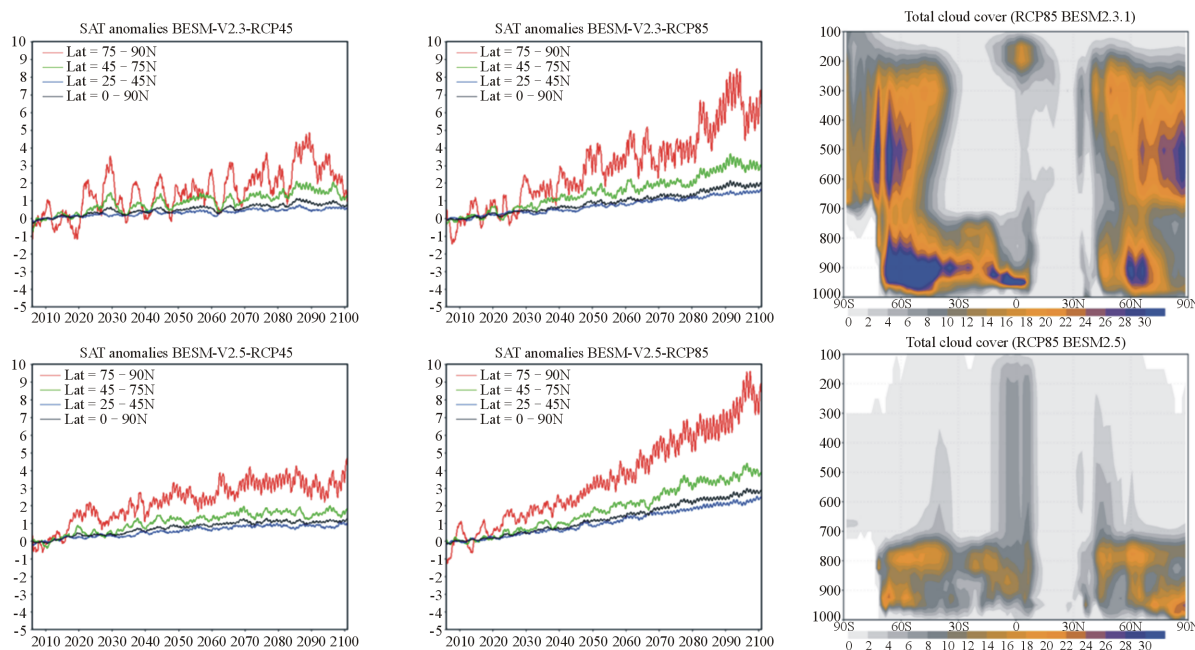


Figure 8. Surface Anomalies Temperature (SAT) and total cloud cover from January 2006 to December 2100 for BESM-OA V2.3 and BESM-OA V2.5. For SAT, the red lines represent the average for latitudes between 75°N to 90°N. Green and blue lines are for latitudes between 45°N to 75°N and 25°N to 45°N, respectively. Latitudes between 0°N to 90°N are represented by the black lines.

and energy balance at the top of the atmosphere (not shown). A better representation of these variables exerts strong influences in coupling ocean-atmosphere-sea ice simulations and teleconnections with higher latitudes. The microphysics adopted in BESM-OA V2.5 produced a decrease in the total cloud cover in the Arctic region (Figure 8). This allows the ocean to absorb more heat from incident shortwave radiation and then contribute to a greater melting of the sea ice. The decrease in total cloud cover and consequent strong increase in SAT is consistent with the SIE reduction showed in Figure 7.

According to Jiang *et al.* [56], Clouds (in both ice and liquid forms) are important modulators of the climate system and are involved in several feedback processes that affect the global atmospheric circulation and the energy budget. Improving the cloud microphysics in Coupled Climate Models result in an advance in climate prediction and reduce the uncertainties in future projections. As recently pointed out by Eyring *et al.* [57], the understanding of the role of the clouds in the general atmospheric circulation, climate sensitivity and assessing the response of the cryosphere system to a warming climate, are among the greatest challenges for CMIP6.

4. Conclusion

In this work, we evaluated the decadal simulation (1980-2014) and assessed the future climate projections (2006-2100) generated by BESM-OA and CMIP5 models. BESM-OA V2.3 results for the seasonal cycle are consistent with satellites observations and the other CMIP5 models, however almost all models tend to overestimate SIE in March in relation to observations. Based on our results and [42] [43] [45], we suggest that the winter Arctic SIE bias is related to a LW radiation bias in climate models. Spatial patterns of climatological averages at the end of the melting season presented a deficiency in capturing the correct signature of the minimum SIE record, as well a model systematic model error between Beaufort Sea and East Siberia (Figure 4 and Figure 6). Future scenarios show an abrupt shrinking of the sea ice and ice-free summer conditions from the year 2045 and onwards, for both RCPs projections. This is a result of the internal climate response to the changing in radiative forcing throughout the years. Polar Amplification and feedback processes explain the rapid Arctic sea ice loss, despite the uncertainties and limitations of Global Climate Models. The sea ice responses are different in CMIP5 models due to differences in the ocean, atmosphere, sea ice conditions, as well the coupling between the components in each model. Future progress in sea ice modeling is essential and requires advances in the parameterizations of climate feedback processes. The climate in the Arctic region will change even more and will induce complex changes in the global climate, thereafter will induce changes in Arctic climate over again. In synthesis, we can say that the Arctic region and its climate are way more complex than forecasted.

Acknowledgements

This research was partially funded by the National Council for Scientific and Technological Development (IBAS/CNPq), Research Program for Global Climate Change/Sao Paulo Research Foundation (PFFMCG/FAPESP), Climate Change Brazilian Network (RedeClima), National Institute for Climate Change (INCT-Clima).

References

- [1] Stroeve, J.C., Kattsov, V., Barrett, A., Serreze, M., Pavlova, T., Holland, M. and Meier, W.N. (2012) Trends in Arctic Sea Ice Extent from CMIP5, CMIP3 and Observations. *Geophysical Research Letters*, **39**, L16502. <http://dx.doi.org/10.1029/2012GL052676>
- [2] Serreze, M.C. and Barry, R.G. (2011) Processes and Impacts of Arctic Amplification: A Research Synthesis. *Global and Planetary Change*, **77**, 85-96. <http://dx.doi.org/10.1016/j.gloplacha.2011.03.004>
- [3] Holland, M.M. and Bitz, C.M. (2003) Polar Amplification of Climate Change in the Coupled Model Intercomparison Project. *Climate Dynamics*, **21**, 221-232. <http://dx.doi.org/10.1007/s00382-003-0332-6>
- [4] Notz, D. and Marotzke, J. (2012) Observations Reveal External Driver for Arctic Sea-Ice Retreat. *Geophysical Research Letters*, **39**, L08502. <http://dx.doi.org/10.1029/2012GL051094>
- [5] Doescher, R., Vihma, T. and Maksimovich, E. (2014) Recent Advances in Understanding the Arctic Climate System State and Change from a Sea Ice Perspective: A Review. *Atmospheric Chemistry And Physics*, **14**, 13571-13600. <http://dx.doi.org/10.5194/acp-14-13571-2014>
- [6] Stroeve, J., Holland, M.M., Meier, W., Scambos, T. and Serreze, M. (2007) Arctic Sea Ice Decline: Faster than Forecast. *Geophysical Research Letters*, **34**, L09501. <http://dx.doi.org/10.1029/2007GL029703>
- [7] Perovich, D.K. (2011) The Changing Arctic Sea Ice Cover. *Oceanography*, **24**, 162-173.

- <http://dx.doi.org/10.5670/oceanog.2011.68>
- [8] Kinnard, C., Zdanowicz, C.M., Fisher, D.A., Isaksson, E., de Vernal, A. and Thompson, L.G. (2011) Reconstructed Changes in Arctic Sea Ice over the Past 1450 Years. *Nature*, **479**, 509-512. <http://dx.doi.org/10.1038/nature10581>
- [9] Curry, J.A., Schramm, J.L. and Ebert, E.E. (1995) Sea Ice Albedo Climate Feedback Mechanism. *Journal of Climate*, **8**, 240-247. [http://dx.doi.org/10.1175/1520-0442\(1995\)008<0240:SIACFM>2.0.CO;2](http://dx.doi.org/10.1175/1520-0442(1995)008<0240:SIACFM>2.0.CO;2)
- [10] Tang, Q., Zhang, X., Yang, X. and Francis, J.A. (2013) Cold Winter Extremes in Northern Continents Linked to Arctic Sea Ice Loss. *Environmental Research Letters*, **8**, Article ID: 014036. <http://dx.doi.org/10.1088/1748-9326/8/1/014036>
- [11] Cohen, J.L., Furtado, J.C., Barlow, M.A., Alexeev, V.A. and Cherry, J.E. (2012) Arctic Warming, Increasing Snow Cover and Widespread Boreal Winter Cooling. *Environmental Research Letters*, **7**, Article ID: 014007. <http://dx.doi.org/10.1088/1748-9326/7/1/014007>
- [12] Tang, Q., Zhang, X. and Francis, J.A. (2014) Extreme Summer Weather in Northern Mid-Latitudes Linked to a Vanishing Cryosphere. *Nature Climate Change*, **4**, 45-50. <http://dx.doi.org/10.1038/nclimate2065>
- [13] Screen, J.A. (2013) Influence of Arctic Sea Ice on European Summer Precipitation. *Environmental Research Letters*, **8**, Article ID: 044015. <http://dx.doi.org/10.1088/1748-9326/8/4/044015>
- [14] ACIA (Arctic Climate Impact Assessment) (2005) Arctic Climate Impact Assessment. Cambridge University Press, Cambridge, 1042 p.
- [15] Meier, W.N., Hovelsrud, G.K., van Oort, B.E.H., Key, J.R., Kovacs, K.M., Michel, C., Haas, C., Granskog, M.A., Gerland, S., Perovich, D.K., Makshtas, A. and Reist, J.D. (2014) Arctic Sea Ice in Transformation: A Review of Recent Observed Changes and Impacts on Biology and Human Activity. *Reviews of Geophysics*, **52**, 185-217. <http://dx.doi.org/10.1002/2013RG000431>
- [16] Cochran, P., Huntington, O.H., Pungowiyi, C., Tom, S., Chapin III, F.S., Huntington, H.P., Maynard, N.G. and Trainor, S.F. (2013) Indigenous Frameworks for Observing and Responding to Climate Change in Alaska. *Climatic Change*, **120**, 557-567. <http://dx.doi.org/10.1007/s10584-013-0735-2>
- [17] Whiteman, G., Hope, C. and Wadhams, P. (2013) Climate Science: Vast Costs of Arctic Change. *Nature*, **499**, 401-403. <http://dx.doi.org/10.1038/499401a>
- [18] Nobre, P., Siqueira, L.S., de Almeida, R.A., Malagutti, M., Giarolla, E., Castelão, G.P., *et al.* (2013) Climate Simulation and Change in the Brazilian Climate Model. *Journal of Climate*, **26**, 6716-6732. <http://dx.doi.org/10.1175/JCLI-D-12-00580.1>
- [19] Vaughan, D.G., Comiso, J.C., Allison, I., Carrasco, J., Kaser, G., Kwok, R., Mote, P., Murray, T., Paul, F., Ren, J., Rignot, E., Solomina, O., Steffen, K. and Zhang, T. (2013) Observations: Cryosphere. In: Stocker, T.F., Qin, D., Plattner, G.-K., Tignor, M., Allen, S.K., Boschung, J., Nauels, A., Xia, Y., Bex, V. and Midgley, P.M., Eds., *Climate Change 2013: The Physical Science Basis, Contribution of Working Group I to the Fifth Assessment Report of the Intergovernmental Panel on Climate Change*, Cambridge University Press, Cambridge, United Kingdom and New York, 317-382.
- [20] Taylor, K.E., Stouffer, R.J. and Meehl, G.A. (2012) An Overview of CMIP5 and the Experiment Design. *Bulletin of the American Meteorological Society*, **93**, 485-498. <http://dx.doi.org/10.1175/BAMS-D-11-00094.1>
- [21] Taylor, K.E., Stouffer, R.J. and Meehl, G.A. (2009) A Summary of the CMIP5 Experiment Design. CMIP Report, 30 p.
- [22] Merryfield, W.J., Lee, W.S., Boer, G.J., Kharin, V.V., Scinocca, J.F., Flato, G.M., Ajayamohan, R.S. and Fyfe, J.C. (2013) The Canadian Seasonal to Interannual Prediction System. Part I: Models and Initialization. *Monthly Weather Review*, **141**, 2910-2945. <http://dx.doi.org/10.1175/MWR-D-12-00216.1>
- [23] Chylek, P., Li, J., Dubey, M.K., Wang, M. and Lesins, G. (2011) Observed and Model Simulated 20th Century Arctic Temperature Variability: Canadian Earth System Model CanESM2. *Atmospheric Chemistry and Physics Discussions*, **11**, 22893-22907. <http://dx.doi.org/10.5194/acpd-11-22893-2011>
- [24] Delworth, T.L., Broccoli, A.J., Rosati, A., Stouffer, R.J., Balaji, V., Beesley, J.A., *et al.* (2006) GFDL's CM2 Global Coupled Climate Models. Part I: Formulation and Simulation Characteristics. *Journal of Climate*, **19**, 643-674. <http://dx.doi.org/10.1175/JCLI3629.1>
- [25] Griffies, S.M., Winton, M., Donner, L.J., Horowitz, L.W., Downes, S.M., Farneti, R., *et al.* (2011) The GFDL CM3 Coupled Climate Model: Characteristics of the Ocean and Sea Ice Simulations. *Journal of Climate*, **24**, 3520-3544. <http://dx.doi.org/10.1175/2011JCLI3964.1>
- [26] Gordon, C., Cooper, C., Senior, C., Banks, H., Gregory, J., Johns, T., Mitchell, J. and Wood, R. (2000) The Simulation of SST, Sea Ice Extents and Ocean Heat Transports in a Coupled Model without Flux Adjustments. *Climate Dynamics*, **16**, 147-168. <http://dx.doi.org/10.1007/s003820050010>
- [27] Collins, W.J., Bellouin, N., Doutriaux-Boucher, M., Gedney, N., Halloran, P., Hinton, T., *et al.* (2011) Development

- and Evaluation of an Earth-System Model—HadGEM2. *Geoscientific Model Development*, **4**, 1051-1075. <http://dx.doi.org/10.5194/gmd-4-1051-2011>
- [28] Watanabe, M., Suzuki, T., Oishi, R., Komuro, Y., Watanabe, S., Emori, S., Takemura, T., Chikira, M., Ogura, T., Sekiguchi, M., Takata, K., Yamazaki, D., Yokohata, T., Nozawa, T., Hasumi, H., Tatebe, H. and Kimoto, M. (2010) Improved Climate Simulation by MIROC5 Mean States, Variability, and Climate Sensitivity. *Journal of Climate*, **23**, 6312-6335. <http://dx.doi.org/10.1175/2010JCLI3679.1>
- [29] Marsland, S.J., Haak, H., Jungclaus, J.H., Latif, M. and Röske, F. (2003) The Max-Planck-Institute Global Ocean/Sea Ice Model with Orthogonal Curvilinear Coordinates. *Ocean Modelling*, **5**, 91-127. [http://dx.doi.org/10.1016/S1463-5003\(02\)00015-X](http://dx.doi.org/10.1016/S1463-5003(02)00015-X)
- [30] Gent, P.R., Danabasoglu, G., Donner, L.J., Holland, M.M., Hunke, E.C., Jayne, S.R., *et al.* (2011) The Community Climate System Model Version 4. *Journal of Climate*, **24**, 4973-4991. <http://dx.doi.org/10.1175/2011JCLI4083.1>
- [31] Ferrier, B.S., Jin, Y., Lin, Y., Black, T., Rogers, E. and DiMego, G. (2002) Implementation of a New Grid-Scale Cloud and Precipitation Scheme in the NCEP Eta Model. Preprints, *15th Conference on Numerical Weather Prediction*, San Antonio, 12-16 August 2002, 280-283.
- [32] Jiménez, P.A. and Dudhia, J. (2012) Improving the Representation of Resolved and Unresolved Topographic Effects on Surface Wind in the WRF Model. *Journal of Applied Meteorology and Climatology*, **51**, 300-316. <http://dx.doi.org/10.1175/JAMC-D-11-084.1>
- [33] Capistrano, V.B., Figueroa, S.N., Fernandez, J.P.R. and Nobre, P. (2015) The New Surface Layer Scheme of the Brazilian Earth System Model. The Surface Ocean-Lower Atmosphere Study (SOLAS), Kiel.
- [34] Capistrano, V., Tedeschi, R., Silva, J., Nobre, P., Neto, O., Casagrande, F., Lanfer, A., Baptista, M., Figueroa, S. and Vial, J. (2016) Climate Sensitivity of the Brazilian Earth System Model. Version 2.5. “unpublished”.
- [35] Griffies, S.M. (2009) Elements of MOM4p1. NOAA/Geophysical Fluid Dynamics Laboratory Ocean Group Technical Report No. 6, 444 p.
- [36] Bottino, M. and Nobre, P. (2015) Impacts of Cloud Cover Schemes on the Atlantic Climate in the Brazilian Climate Model—BESM. “unpublished”.
- [37] Winton, M. (2000) A Reformulated Three-Layer Sea Ice Model. *Journal of Atmospheric and Oceanic Technology*, **17**, 525-531. [http://dx.doi.org/10.1175/1520-0426\(2000\)017<0525:ARTLSI>2.0.CO;2](http://dx.doi.org/10.1175/1520-0426(2000)017<0525:ARTLSI>2.0.CO;2)
- [38] Hunke, E.C. and Dukowicz, J.K. (1997) An Elastic-Viscous-Plastic Model for Sea Ice Dynamics. *Journal of Physical Oceanography*, **27**, 1849-1867. [http://dx.doi.org/10.1175/1520-0485\(1997\)027<1849:AEVPMF>2.0.CO;2](http://dx.doi.org/10.1175/1520-0485(1997)027<1849:AEVPMF>2.0.CO;2)
- [39] Semtner, A.J. (1976) A Model for the Thermodynamic Growth of Sea Ice in Numerical Investigations of Climate. *Journal of Physical Oceanography*, **6**, 27-37. [http://dx.doi.org/10.1175/1520-0485\(1976\)006<0379:AMFTTG>2.0.CO;2](http://dx.doi.org/10.1175/1520-0485(1976)006<0379:AMFTTG>2.0.CO;2)
- [40] Francis, J.A., Chan, W., Leathers, D.J., Miller, J.R. and Veron, D.E. (2009) Winter Northern Hemisphere Weather Patterns Remember Summer Arctic Sea-Ice Extent. *Geophysical Research Letters*, **36**, L07503.
- [41] Arzel, O., Fichefet, T. and Goosse, H. (2006) Sea Ice Evolution over the 20th and 21st Centuries as Simulated by Current AOGCMs. *Ocean Modelling*, **12**, 401-415. <http://dx.doi.org/10.1016/j.ocemod.2005.08.002>
- [42] Sorteberg, A., Kattsov, V., Walsh, J.E. and Pavlova, T. (2007) The Arctic Surface Energy Budget as Simulated with the IPCC AR4 AOGCMs. *Climate Dynamics*, **29**, 131-156. <http://dx.doi.org/10.1007/s00382-006-0222-9>
- [43] Karlsson, J. and Svensson, G. (2013) Consequences of Poor Representation of Arctic Sea-Ice Albedo and Cloud-Radiation Interactions in the CMIP5 Model Ensemble. *Geophysical Research Letters*, **40**, 4374-4379. <http://dx.doi.org/10.1002/grl.50768>
- [44] Li, J.L., Waliser, D.E., Stephens, G., Lee, S., L’Ecuyer, T., Kato, S., Loeb, N. and Ma, H.Y. (2013) Characterizing and Understanding Radiation Budget Biases in CMIP3/CMIP5 GCMs, Contemporary GCM, and Reanalysis. *Journal of Geophysical Research: Atmospheres*, **118**, 8166-8184. <http://dx.doi.org/10.1002/jgrd.50378>
- [45] Wild, M., Ohmura, A., Gilgen, H., Morcrette, J.J. and Slingo, A. (2001) Evaluation of Downward Longwave Radiation in General Circulation Models. *Journal of Climate*, **14**, 3227-3239. [http://dx.doi.org/10.1175/1520-0442\(2001\)014<3227:EODLRI>2.0.CO;2](http://dx.doi.org/10.1175/1520-0442(2001)014<3227:EODLRI>2.0.CO;2)
- [46] Knutti, R. and Sedláček, J. (2013) Robustness and Uncertainties in the New CMIP5 Climate Model Projections. *Nature Climate Change*, **3**, 369-373. <http://dx.doi.org/10.1038/nclimate1716>
- [47] Shu, Q., Song, Z. and Qiao, F. (2015) Assessment of Sea Ice Simulations in the CMIP5 Models. *The Cryosphere*, **9**, 399-409. <http://dx.doi.org/10.5194/tc-9-399-2015>
- [48] Tietsche, S., Day, J.J., Guemas, V., Hurlin, W.J., Keeley, S.P.E., Matei, D., Msadek, R., Collins, M. and Hawkins, E. (2014) Seasonal to Interannual Arctic Sea Ice Predictability in Current Global Climate Models. *Geophysical Research Letters*, **41**, 1035-1043. <http://dx.doi.org/10.1002/2013GL058755>

- [49] Cavalieri, D.J. and Parkinson, C.L. (2012) Arctic Sea Ice Variability and Trends, 1979-2010. *Cryosphere*, **6**, 881-889. <http://dx.doi.org/10.5194/tc-6-881-2012>
- [50] Holland, M.M., Bitz, C.M. and Tremblay, B. (2006) Future Abrupt Reductions in the Summer Arctic Sea Ice. *Geophysical Research Letters*, **33**, L23503. <http://dx.doi.org/10.1029/2006gl028024>
- [51] Vihma, T. (2014) Effects of Arctic Sea Ice Decline on Weather and Climate: A Review. *Surveys in Geophysics*, **35**, 1175-1214. <http://dx.doi.org/10.1007/s10712-014-9284-0>
- [52] Hunke, E.C., Lipscomb, W.H. and Turner, A.K. (2010) Sea-Ice Models for Climate Study: Retrospective and New Directions. *Journal of Glaciology*, **56**, 1162-1172. <http://dx.doi.org/10.3189/002214311796406095>
- [53] Flocco, D., Schroeder, D., Feltham, D.L. and Hunke, E.C. (2012) Impact of Melt Ponds on Arctic Sea Ice Simulations from 1990 to 2007. *Journal of Geophysical Research: Oceans*, **117**, C09032. <http://dx.doi.org/10.1029/2012jc008195>
- [54] Roeckner, E., Mauritsen, T., Esch, M. and Brokopf, R. (2012) Impact of Melt Ponds on Arctic Sea Ice in Past and Future Climates as Simulated by MPI-ESM. *Journal of Advances in Modeling Earth Systems*, **4**, M00A02. <http://dx.doi.org/10.1029/2012ms000157>
- [55] Pithan, F. and Mauritsen, T. (2014) Arctic Amplification Dominated by Temperature Feedbacks in Contemporary Climate Models. *Nature Geoscience*, **7**, 181-184. <http://dx.doi.org/10.1038/ngeo2071>
- [56] Jiang, J.H., Su, H., Zhai, C., Perun, V.S., Del Genio, A., Nazarenko, L.S., *et al.* (2012) Evaluation of Cloud and Water Vapor Simulations in CMIP5 Climate Models Using NASA “A-Train” Satellite Observations. *Journal of Geophysical Research: Atmospheres*, **117**, D14105. <http://dx.doi.org/10.1029/2011jd017237>
- [57] Eyring, V., Bony, S., Meehl, G.A., Senior, C., Stevens, B., Stouffer, R.J. and Taylor, K.E. (2015) Overview of the Coupled Model Intercomparison Project Phase 6 (CMIP6) Experimental Design and Organisation. *Geoscientific Model Development*, **8**, 10539-10583. <http://dx.doi.org/10.5194/gmdd-8-10539-2015>